Experimental Investigation of PCM Integrated Solar Dryer for Fish Drying

By

Dessie Tadele

A Thesis Submitted to Department of Thermal and Aerospace Engineering

School of Mechanical, Chemical and Materials Engineering

Office of Graduate Studies

Adama Science and Technology University

July, 2020

Adama, Ethiopia

Experimental Investigation of PCM Integrated Solar Dryer for Fish Drying

By

Dessie Tadele

Advisor: Dr. Dawit Gudeta

A Thesis Submitted to Department of Thermal and Aerospace Engineering
School of Mechanical, Chemical and Materials Engineering,

Office of Graduate Studies
Adama Science and Technology University

July, 2020
Adama, Ethiopia

DECLARATION

I hereby declare that this M.Sc. thesis entitled "Experimental Investigation of PCM Integrated Solar Dryer for Fish Drying" in partial fulfilment of the requirement of the degree of Master of Science in Thermal Engineering at Adama Science and Technology University is an authentic record of my own work carried out from September 2019 to July 2020 under the supervision of Dr. Dawit Gudeta, Assistant Professor of Thermal and Aerospace Engineering Program.

The matter embedded in this thesis has not been presented for the award of a degree or diploma in any other university. All relevant resources used in this thesis has been duly acknowledged in the text and listed in the reference section.

Dessie Tadele_	___________________	___________________
Candidate	Signature	Date

This is to certify that the above statement made by the candidate is correct to the best of my knowledge and belief. This has been submitted for examination with my approval.

Dr. Dawit Gudeta_	___________________	___________________
Advisor	Signature	Date

APPROVAL PAGE

We, the undersigned, members of the board of examiners of the final open defense by Dessie Tadele have read and evaluated his thesis entitled "*Experimental investigation of PCM integrated solar dryer for fish drying*" and examined the candidate. This is therefore to certify that the thesis has been accepted in partial fulfilment of the requirements of the degree of masters of Science in Thermal Engineering.

Name	Signature	Date
Dessie Tadele______ _	____________________	____________________
Name of student		
_______________________	____________________	____________________
Advisor		
_______________________	____________________	____________________
External examiner		
_______________________	____________________	____________________
Internal Examiner		
_______________________	____________________	____________________
Chair person		
_______________________	____________________	____________________
Head of Department		
_______________________	____________________	____________________
School Dean		
_______________________	____________________	____________________
Post Graduate Dean		

ACKNOWLEDGEMENT

First and foremost, my deepest gratitude goes to the almighty God for being with me in every aspect of my life and for giving me the strength to do this thesis. I would like to thank my advisor Dr. Dawit Gudeta for his continuous encouragement and constructive comments from the beginning of this work up until this thesis is made to the final. He has been guiding me and teaching me valuable lessons. I would also like to thank Dr. Addisu Bekele for his encouragement and suggestion during my master's study.

I would like to express my sincere gratitude to my family and everyone who helped me finish this thesis and finally I would like to thank Adama science and technology university for giving me the chance to join the master's program with full sponsorship.

ABSTRACT

Ethiopia has a huge potential for fish production but loses one third of its annual production due to post-harvest losses. Drying is an effective means of reducing post-harvest losses which increases the shelf life of products by reducing the moisture content to a safe storage level. Solar energy is the most widely used form of energy for drying but the intermittent nature and uncertainty in the availability of solar energy are the major drawbacks. These drawbacks can be eliminated with the integration of thermal energy storages. In this study, an indirect mode solar dryer integrated with a PCM is designed, developed and experimentally tested by drying fish. The dryer is designed based on the daily fish losses from a single fisherman which is determined to be 5 kg. The components of the dryer are a solar air heater (SAH), a paraffin wax-based shell and tube latent heat storage (LHS), drying chamber and a blower. The double pass SAH is used to raise the temperature of the air to the desired level and to reduce the fluctuations in the outlet temperature of the SAH due to the fluctuations and inconsistency in solar radiation, the LHS with a 3 MJ heat storing capacity is integrated between the outlet of the SAH and the inlet of the drying chamber. The blower is used to circulate the air inside the dryer and the performance of the components of the dryer and the drying system is evaluated using energy and exergy analysis. A no-load test is performed to know the trend of the inlet and outlet temperatures of the SAH and the LHS and to evaluate their performance. The drying chamber is loaded with 5 kg fresh fish during the load test to evaluate the performance of the drying system. A maximum temperature of 69 ℃ is obtained at the outlet of the SAH and the energy and exergy efficiencies are 25% and 1.5%, respectively. A temperature of 5 to 10 ℃ higher than the single pass is achieved by circulating the air in the second air channel since the air is further heated as it passes through the second air channel. The LHS reduces the fluctuations in the outlet temperature of the SAH and extends the drying process for two extra hours a day. 5 kg fresh fish is effectively dried in the dryer within 21hrs reducing the moisture content of the fish from 75% to 12.5% by removing 3.57 kg of moisture. The specific energy consumption of the dryer is 7.3 kWh per kilogram of moisture and the power consumed by the blower is 0.6 kWh per kilogram of moisture which is 8.3% of the total energy consumption. The remaining 91.7% energy is harvested from the sun and the overall efficiency of the drying system is 9.4%. Finally, economic analysis is carried out and the payback period is 1.39 years.

Key words: Fish, drying, SAH, LHS, paraffin wax, exergy efficiency.

TABLE OF CONTENTS

Contents **Page**

LIST OF FIGURES

LIST OF TABLES

ABBREVIATIONS

EHC	Effective heat capacity
FAO	Food and agricultural organization
HTF	Heat transfer fluid
LHS	Latent heat storage
PCM	Phase change material
SAH	Solar air heater
db	Dry basis
wb	wet basis

NOMENCLATURE

A	Area (m^2)	**U**	Overall heat loss coefficient (W/m^2. K)
$\mathbf{C_p}$	Specific heat (KJ/kg. K)	**V**	Volume (m^3/s)
D	Diameter (m)	**W**	Width (m)
E	Energy/Exergy (J)	**Z**	Height (m)
$\mathbf{L_f}$	Latent heat of fusion (KJ/kg)	**g**	Gravity (m/s^2)
L	Length (m)	**h**	Enthalpy (KJ/kg.)
M	Moisture content (%)	**h**	Heat transfer coefficient (W/m^2. K)
Nu	Nusselt number	**k**	Thermal conductivity (W/m. K)
Q	Heat (W)	**m**	Mass (kg)
R	Radius (m)	**t**	Time (s)
T	Temperature (℃)	**v**	Velocity (m/s)

GREEK SYMBOLS

$\boldsymbol{\rho}$	Density (kg/m^3)	$\boldsymbol{\varepsilon}$	Emissivity
Φ	Latitude (°)	$\boldsymbol{\sigma}$	Stefan-Boltzmann constant
$\boldsymbol{\theta}$	Angle of incidence (°)	$\boldsymbol{\tau}$	Transmissivity
$\boldsymbol{\beta}$	Tilt angle (°)	$\boldsymbol{\alpha}$	Absorptivity
$\boldsymbol{\omega}$	Hour angle (°)	$\boldsymbol{\zeta}$	Porosity (%)
$\boldsymbol{\gamma}$	Surface azimuth angle (°)	$\boldsymbol{\eta}$	Efficiency (%)
$\boldsymbol{\delta}$	Declination (°)		

SUBSCRIPTS

a	air	**es**	Energy storage
amb	Ambient	**ext**	Extraterrestrial
b	Beam	**G**	Global
c	collector	**i**	Inlet
ch	Charging	**o**	Outlet
d	Diffuse	**p**	Product
dc	Drying chamber	**pf**	Paraffin
dich	discharging		

CHAPTER ONE

INTRODUCTION

1.1 Background of the Study

Drying is one of the methods of food preservation that have been practiced for a long time. The purpose of drying is removing water from the food so that the growth of microorganisms (bacteria, yeasts and molds) can be inhibited. Food scientists have found that reducing the moisture content of food between 10% and 20% prevents microorganisms from spoiling and most of the nutritional value and flavor can also be preserved. Products that can be preserved by drying include agricultural products (cereals), medical plants, fruits, vegetables, fish and meat (Aklilu, 2004).

Ethiopia is a land-locked country and supplies fish for their own population from the inland water bodies. These water bodies have an estimated surface area of 7334 km^2 major lakes and reservoirs, 275 km^2 small water bodies and 7185 km long rivers and the annual fish production potential from those water bodies reaches up to 51,000 tons (FAO, 2015). However, the actual production is much less than the potential that the country has because of the fishery sector is not well developed regarding pre and post-harvest handling practices which leads to losses. The main reasons for post-harvest losses include inadequate handling, poor processing and storing facilities, predators and lack of appropriate fish handling and preserving techniques (Demeke, 2015).

Post-harvest losses in developing countries have estimated to be up to 50% of domestic production and this spoilage is possibly as high as 10% and more. Our country lost almost one-third of its annual production and this was about 10,000 tons of fish per annum among 28,000 tons of production (Demeke, 2015). Generally, 10 to 12 million tons of fish per year is estimated to be lost due to spoilage globally which accounts for 10% of the total production (Getu, 2015).

Fresh fish rapidly deteriorate without external contamination in less than 24 hours. The reason behind this is fish harvesting at an average moisture content of 75% (wet basis) (Gram, 2002). To overcome this problem preservation is mandatory. Fish can be preserved using several techniques including traditional preservation techniques such as freezing, cold storage (chilling), dehydration (salting, drying and smoking) and use of chemical treatment. In freezing, water in fish forms ice crystals and it will break the cell structure of the fish and cause mushiness. The technology of freezing, chilling and chemical treatment is also too expensive and not a common practice for most rural fishery associations. Due to this, the fisheries are forced to use traditional methods like drying, smoking and salting (Solomon, 2017).

Open sun drying is the most widespread method of drying fish and have been practiced since ancient times. However, despite the fact that it is simple and inexpensive, traditional open sun drying has disadvantages (Kituu, 2010).

1. Needs a large area exposed to direct sunlight.
2. Loss of dried products due to rats, cats, dogs, birds and infestation with insects.
3. Wind, rain, moisture and dust spoil the product.
4. Fish drying with unstable moisture content at slow drying process is favorable for microorganism proliferation and becomes a source of food poisoning.
5. Exposing products like fish to direct sunlight destroys light sensitive nutrients present in fish.

Hence to control this problem, other hygienic and environmentally friendly drying technologies must be developed and adopted for the drying of fish with best quality. Renewable energy technologies which include solar, wind, geothermal and bioenergy can be used. From these renewable energy sources, solar energy is cheap, safe, sustainable and abundantly available. The annual average daily solar radiation in Ethiopia reaching the ground is estimated to be 5.2 $kWh/m^2/day$ (REEEP, 2014). Therefore, solar drying is the best alternative that can help for reducing loss and improving the quality of products so that it can be stored for a long time. However, the intermittent nature and uncertainty in the availability of solar energy is the main drawback in solar drying. This drawback can be eliminated with the integration of thermal energy storages. Thermal energy storages have been used either at the bottom of the absorber plate or in the drying chamber. Placing the thermal energy storage at these two sections of the dryers has some disadvantages like the loss of heat from the storage to the sides and top of the absorber and the drying chamber. This heat loss can be minimized by using a separate system of the dryer and the thermal energy storage.

1.2 Solar dryers

In the drying sector, solar drying is an efficient way of utilizing solar energy. In solar drying, products are dried at an elevated temperature using special devices called solar dryers. Based on the mode of solar energy utilization and mode of airflow, the classification of solar dryers is shown in Figure 1.1.

According to the mode of airflow, solar dryers are classified as passive (natural convection or natural circulation) and active (forced convection or forced circulation) solar dryers. Natural convection solar dryers do not require a fan or a blower to pump the air through the dryer which makes them suitable for areas where electricity is not available. The flow of air is mainly due to density differences. However, these dryers have some disadvantages i.e. are not suitable for drying a large number of products due to their low air flow rate, the moisture removal rate is poor, and resulting slow drying rate. Forced convection solar dryers require a blower or fan to pump the air through the dryer therefore electrical power is required for running these devices. The advantage of active solar driers over passive solar dryers is that active solar dryers reduce the drying time by enhancing the rate of heat transfer and temperature and air flow rate can be controlled (Kituu, 2010).

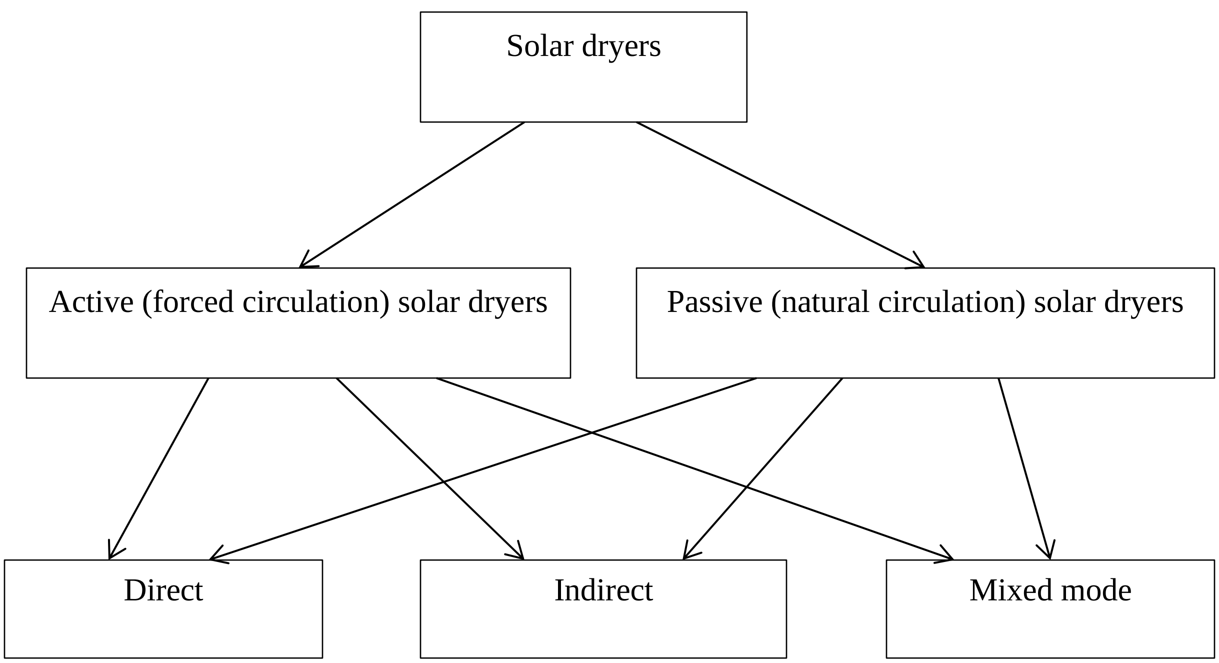

Figure 1.1: Classification of solar dryers.

Based on the mode of solar energy utilization, solar dryers are classified as direct, indirect and mixed mode solar dryers. As shown in Figure 1.1, these dryers can be either natural convection or forced convection solar dryers.

1. Direct solar dryers: in these systems, the substance to be dehydrated is exposed to direct sunlight. The dryer consists of cover material, drying trays and frame as indicated in Figure 1.2. The dryer has inlet and outlet air vents and solar drying is assisted by the movement of the air in and out of the dryer. The products are placed at the drying trays and dried by the incoming solar radiation (Bolaji, 2005).

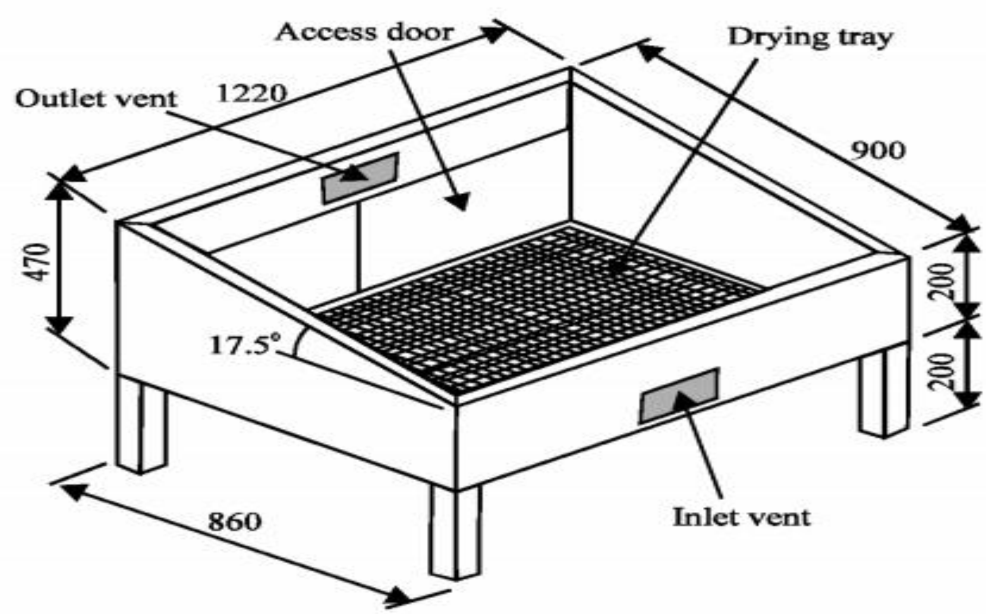

Figure 1.2: Direct solar dryer (Bolaji, 2005).

2. Indirect solar dryers: these dryers consist of a solar air heater with a black absorber plate, a transparent cover plate, insulation and a drying chamber as shown in Figure 1.3. The black surface heats incoming air, rather than directly heating the substance to be dried. This heated air passes through the drying chamber and exits upward often through a chimney, taking moisture released from the substance with it (Bolaji, 2005).

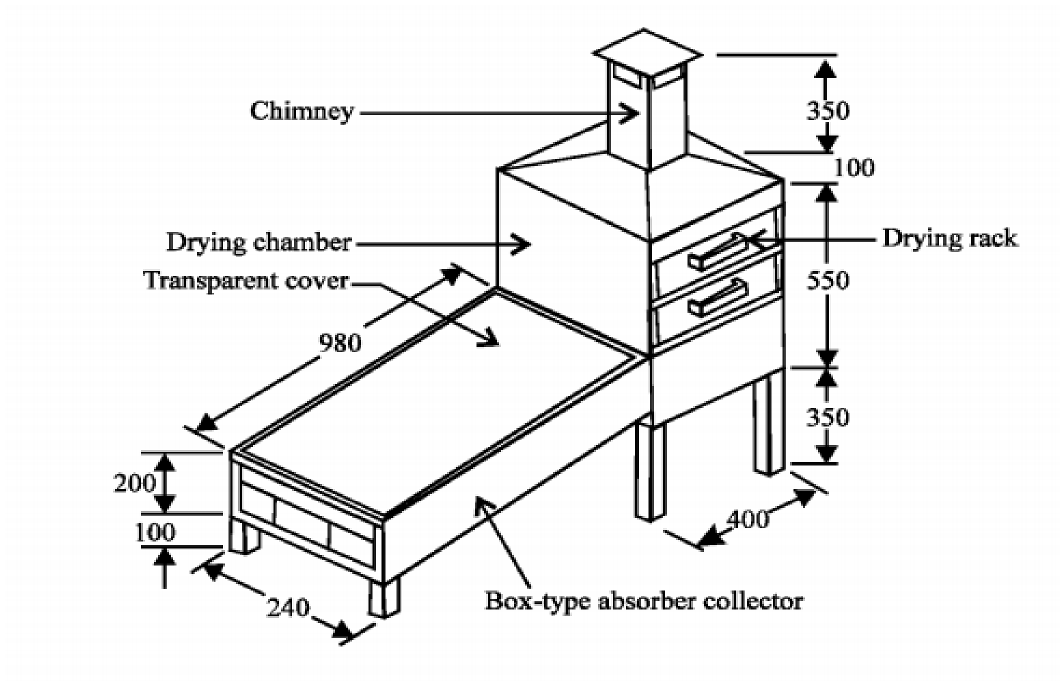

Figure 1.3: Indirect solar dryer (Bolaji, 2005).

3. Mixed mode solar dryers: the structural features of these dryers are the same as indirect type solar dryers except that the drying chamber is made from transparent walls as shown in Figure 1.4. The products are heated with both the solar radiation transmitted through the transparent walls and the hot air from the solar air heater.

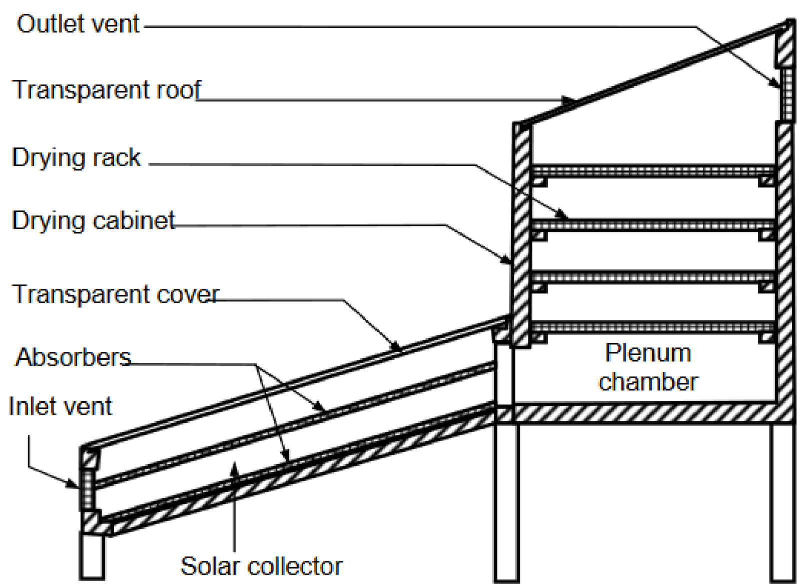

Figure 1.4: Mixed mode solar dryer (Bolaji and Olalusi, 2008).

Solar dryers can also be classified as hybrid solar dryers. Hybrid solar dryers are solar dryers integrated with either auxiliary heating devices or thermal energy storage units. The auxiliary heating devices include biomass backup heaters, electric heaters, wood stoves and liquid or gas fuel burners. The thermal energy storage unit includes sensible heat storages like concrete, rock, sand and bricks and latent heat storages like paraffin wax and salt nitrates.

1.3 Thermal energy storages

A common problem in solar drying is the gap between the period of solar energy availability and its period of usage. The intermittent nature and the uncertainty in the availability of solar radiation are also the concerns associated with solar drying. So, in the drying sector the supply and demand of energy is an important consideration. Thermal energy storage can minimize the gap between supply and demand in this case. These thermal storage systems include sensible and latent heat storage systems as shown in Figure 1.5. In sensible heat storage systems, the energy is stored by changing the temperature of storage material like concrete, sand-rock minerals, ferroalloy materials, bricks, etc. whereas in latent heat storages, the heat transfer occurs when substances like salt nitrates, paraffin wax, etc. change their phase from solid to liquid and vice versa. Latent heat storage systems store higher amounts of energy per unit storage material compared to sensible heat storage systems (Swami *et al*., 2018).

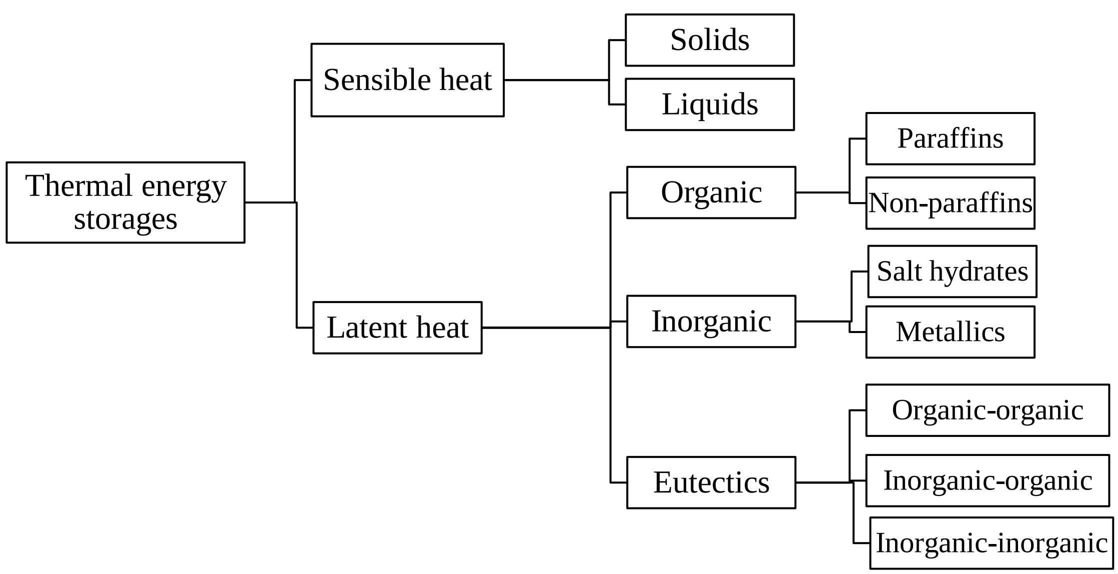

Figure 1.5: Classification of thermal energy storages.

1.4 Statement of the problem

A tremendous quantity of fish is lost due to poor post-harvest handling practices. The reasons for these losses are inadequate handling, poor processing and storing facilities, predators and lack of appropriate handling and preserving techniques. The existing preserving techniques like freezing, cold storage (chilling) and chemical treatment are too expensive and not commonly practiced by rural fishermen. Electrical energy is also required to run the freezer and cold storages. The other preservation technique used by the fishermen is open sun drying of fish and the products dried by this method have poor quality. These factors reduce fishermen income from fish. In order to alleviate these problems, other hygienic, environmentally friendly and economical preservation techniques should be developed. Solar drying technique that uses free energy from the sun can be used. To overcome the problems associated with the intermittent nature and uncertainty in the availability of solar energy, a thermal energy storage system is integrated with the solar dryer and the performance of the dryer is experimentally investigated by drying fish. To reduce the heat losses associated with the location where the thermal energy is used, a separate arrangement of the dryer and the thermal energy storage is used.

1.5 Objective of the study

In this section, the general and specific objectives of the study are briefly indicated.

1.5.1 General objective

The general objective of this thesis is experimentally investigating the performance of a solar dryer integrated with a paraffin wax based thermal energy storage system for fish drying application.

1.5.2 Specific objectives

The specific objectives of this study are:

- ✓ Sizing flat plate solar air heater, the thermal energy storage and the drying chamber suitable for drying 5kg of fish at a time.
- ✓ Conducting energy and exergy analysis of the flat plate solar air heater, the thermal energy storage and the drying chamber.
- ✓ Performing numerical simulation of the solar air heater and thermal energy storage.
- ✓ Fabrication of the solar dryer integrated with thermal energy storage.
- ✓ Evaluating the performance of the dryer experimentally.
- ✓ Validation of the experimental result.

1.6 Significance of the study

The significance of this study is introducing an alternative drying mechanism of fish apart from the traditional open sun drying. The dryer reduces post-harvest losses due to spoilage in which high temperatures within the dryers retard the activities of microorganisms. Compared to open sun drying of fish, the developed solar dryer protects the product from wind, rain, moisture and dust. It also eliminates access to birds, cats and dogs and infestation with insects. Expensive preservation techniques like freezing, cold storage (chilling) and chemical treatment can also be eliminated. The dryer will reduce the monetary loss associated with post-harvest loss.

1.7 Scope and limitation of the study

This thesis focuses on experimental analysis for the performance evaluation of a solar dryer integrated with thermal energy storage for fish drying application. This includes design of the components of the dryer, energy and exergy analysis of each components of the dryer, development of a prototype, performing an experiment on the dryer and validating the experimental result. Numerical simulation of the solar air heater and the thermal energy storage is also performed. Since this study mainly focuses on performance investigation of the dryer, the drying kinetics of the product is not included.

1.8 Organization of the study

This thesis is organized with seven chapters. Chapter one presents introduction of the thesis including background about drying, solar dryers and thermal energy storages, problem statement, objectives, significance and scope of the study. Literatures about solar dryers, solar air heaters and thermal energy storages are reviewed in chapter two. Chapter three elaborates about the methodology of the work including data collection and radiation estimation. The design of the PCM integrated solar dryer, energy and exergy analysis of the components of the dryer and numerical formulation of the solar air heater and thermal energy storage are incorporated in chapter four. The prototype of the dryer is manufactured based on the design on chapter four and the experimental setup and procedure is described in chapter five. The results of the experiment are presented with a discussion in chapter six and finally the thesis is concluded in chapter seven.

CHAPTER TWO

LITERATURE REVIEW

In this chapter, available literatures related to solar dryers with and without thermal energy storage systems, solar air heaters and thermal energy storages are reviewed in-depth.

2.1 Solar dryers

There are several classes of solar dryers. But the major ones are direct solar dryers and indirect solar dryers. Direct solar dryers expose the substance to be dried to direct sunlight and have enclosures; glass covers and/or vents to increase efficiency whereas indirect solar dryers consist of a solar air heater component that heats the air. The heated air then passes to the drying chamber where the product being dried is placed. The heated takes moisture from the product and finally leave the chamber. According to the mode of airflow, solar dryers can also be classified as natural convection and forced convection solar dryers. Natural convection dryers do not require a fan or a blower to pump the air through the dryer. But the low airflow rate and the long drying time results in low drying capacity. Thus, this system is restricted to the processing of small quantities of products. For processing large quantities of products, forced convection dryers should be used. But forced convection solar dryers require electrical power to run the fan or blower. Since the remote areas of many developing countries are not connected to electric grids, these dryers are limited to electrified areas.

In this section existing literatures about solar dryers are reviewed and have been taken for further improvement in this study. The reviewed literatures consist of direct, indirect, natural convection and forced convection solar dryers with and without a thermal energy storage system.

2.1.1 Solar dryers without thermal energy storage

Solar dryers for drying fish and other products were developed and their performance were tested. **Asmare *et al*. (2015)** developed a solar tent dryer to reduce post-harvest losses. The solar tent fish dryer was prepared from readily available materials such as wood, white and black plastic, nail, rope and mesh wire with a size of 2 m height and 1.7 m length. The result indicated that the total moisture loss of 60% was obtained in three days. Similarly, **Komolafe *et al*. (2011)** designed and constructed a simple convective fish dryer to reduce the problems related to fish processing. The components of the dryer are the base frame which is fabricated from angle iron bar, the drying chamber, the drying cage which is constructed with a stainless wire mesh, a fan housing consisting of 3 fan blades and three electric heating elements 3000 W, 6000 W and 9000 W respectively. The result shows that, the no-load evaluation (temperature profile) of the dryer gives the highest temperature of 110 ℃ (drying chamber temperature) in 30 minutes which is expected to give a higher drying rate than the natural sun drying and open–fired drying methods.

Aklilu (2004) performed experimental analysis for the performance evaluation of an indirect free convection solar dryer for drying potato. The components of the dryer were flat plate solar collector, the drying chamber and connecting ducts. The result from this experiment shows that, for airflow rates ranging from 0.00595 to 0.0114 kg/s.m^2 of collector area, temperatures rise of 14-29 ℃ (from 8:30 AM- 4:00 PM) higher than the ambient air temperature in a clear day was observed. The final moisture content of the potato was 2.62-2.93%. Thermal efficiency lies between 14.59% and 29.95%. The drying time required by traditional open sun drying is reduced by 3 h (about 19%). The system drying efficiency (η_s) or system efficiency was about 16% and dryer efficiency (η_d) was about 65%. Later, **Habtamu (2007)** simulated an indirect solar cereal dryer using TRNSYS. The components of the dryer are flat plate solar collector and an integrated dryer chamber. A thermal solar collector model was developed and basic heat transfer equations for single-plate and double glass glazing were derived and techniques for the solution of these equations were presented. Using metrological data and collector parameters as input, a computer program was written to predict the collector outlet temperature, mass flow rate and other engineering variables. The result shows that temperatures rise of 14-28 ℃ (from 8:30 AM- 4:00 PM) higher than the ambient air temperature in a clear day was observed. The final moisture content of the cereal after 13.5-14 sunny hours was observed to be 0.1-0.12%. The initial moisture content of the local cereal ranges from 16 to 30% and the final moisture content of the dried cereals ranges from 10 to 12%.

Sablani *et al*. (2003) investigated the performance of three different solar dryers, namely open rack consisted of perforated rack, convection cabinet made with wooden walls with wire mesh and multi-rack dome dryer consisted of three layers with ten racks per layer. The result shows that, the air temperatures generated and relative humidity within the cabinet unit were 11 to 53 ℃ and 20 to 87% depending upon the time of day respectively. For the multi-rack dome unit, the air temperature and relative humidity varied from 11 to 37 ℃ and 22 to 96% respectively. The initial moisture content of sardine was 2.33 kg water/kg dry solids and at the end of drying the final moisture contents were 0.166 and 0.111 kg water/kg solids for open rack and cabinet dryers, respectively and 0.219 and 0.228 kg water/kg solids at the top and bottom layer of the multi-rack dome dryer respectively. Similarly, **N'Jai (1987)** tested three different types of natural convection solar dryers for drying fermented fish in Gambia. All the dryers were constructed from rhun palm sticks covered with clear polyethylene material. The first was a solar tent dryer, the second dryer was house-shaped solar dryer and the last one was solar dome dryer. It was reported that, well-dried products with reasonably long storage life were successfully produced and the degree of losses due to insect infestation and maggots becomes insignificant. **Sachithananthan *et al.* (1985)** also conducted a study in a solar dome dryer using three fish species (horse mackerel, goatfish and catfish). Hooks and trays were used to place the fish samples in the dome. The result shows that the drying rate was higher in the sun-dried fish during the first two days than that inside the solar dryer. This was attributed to a greater flow of air around the sample. However, the drying rate was better inside the solar dome during the later stage. In this case, the process was internal mass transfer controlled. It was also reported that fish dried in the solar dome dryer has a very good quality in terms of odor, rancidity and microbial or insect attack.

Hubackova *et al*. (2014) developed a solar drying model for selected Cambodian fish species and compared it with the electric oven dryer. The solar dryer consisted of a solar collector, a drying chamber and a blower. The result shows that the average drying temperature and relative humidity in the solar dryer were 55.6 ℃ and 19.9%, respectively. The overall efficiency of the solar dryer corresponding to 15% of final product moisture content was 12.37% and the average evaporative capacity of the dryer is 0.049 kg/h. It was also concluded that, the drying rates were higher in the solar drying process compared to control drying in an electric oven. **Reza *et al*. (2009)** also carried out a study in a solar tunnel dryer to produce safe and high-quality dried fish products. The dryer consists of a flat plate collector, a tunnel drying unit and four small fans. Five fish species such as silver Jewfish, Bombay duck, big-eye tuna, Chinese pomfret and ribbonfish were used. The result shows that, moisture content of the fish samples reached 16% after 36 and 32 h of drying at temperature ranges of 45 to 50 ℃ and 50 to 55 ℃, respectively. Products produced at 45 to 50 ℃ were found to have excellent flavor, color and texture.

Bala and Mondol (2001) experimentally investigated solar drying of fish using a solar tunnel dryer with a capacity of 150 kg. The components of the dryer were a transparent plastic covered flat plate collector, a drying tunnel connected in series to four d.c. fans and two 40 W solar modules to operate the fans. The fish was initially treated with dry salt and stacked for about 16 hours before drying. The result shows that the final moisture content of salted fish reaches 16.78% (w.b.) from 67% (w.b.) in 5 days in a solar tunnel dryer. **Kituu *et al*. (2010)** developed mathematical models for predicting the plenum chamber temperatures and the drying of Tilapia fish (Oreochromis niloticus) in a solar tunnel dryer and simulated in Visual Basic 6 (Microsoft Visual Basic 6.0™). The drying system consisted of a tunnel and chimney section. To enhance natural convection, the drying chamber was lined with acrylic glass to trap solar energy and heat the exhaust air. At the base of the exhaust pipe was a solar-driven 12 V, 0.16 A 1.92 W d.c. suction fan, capable of delivering $1.2m^3/s$ of air. The result shows that using Student's t-test, there was no significant difference between simulated and actual data for plenum chamber temperature (T_{stst} = 0.551, $T_{crit,\ one\text{-}tail}$ = 1.717, $T_{crit,\ two\text{-}tail}$ = 2.074), and moisture ratio (T_{stat} = 0.961, $T_{crit,\ one\text{-}tail}$ = 1.708), at 5% level of significance.

Sengar *et al*. (2009) designed a low-cost solar dryer to dry products under hot and humid conditions. The main parts of the dryer were collector, drying chamber, inlet and outlet openings. UV stabilized 200micron plastic film was used for the collection of solar energy and mosquito net was used as trays with a capacity of 0.6kg. The result from this study shows that, this solar dryer is suitable for domestic drying of prawns' fish up to10 kg capacity. Salted fish inside the dryer required 8h to reach a moisture content of 16.15% whereas unsalted fish required 15 h to reach 15.15% in open conditions. Overall collection efficiency was 70.97% and average drying efficiency was 14% and 11% whereas pickup efficiency was 10 and 9% for salted and unsalted fish respectively.

Bolaji (2005) investigated the performance of an indirect solar dryer using a box type collector. The components of the dryer were a solar air heater, an opaque crop bin and a chimney. The collector was made of a glass cover and black absorber plate and was inclined at an angle of

20° to the horizontal. The result shows that the maximum efficiency of the system was 60.5% and the maximum average temperatures were 64 and 57 ℃ inside the collector and drying chamber, respectively. **Tiris *et al.* (1995)** also constructed and studied the performance of a natural convection indirect solar dryer. The dryer consists of a solar air heater and a drying chamber. The experiment was done for different food products at different airflow rates and the thermal efficiencies of the solar air heater and the drying chamber were discussed. The result shows that thermal efficiencies were between 30% and 80% during drying experiments and the overall drying performance and efficiency increase as the airflow rate increases.

Al-Juamily *et al.* (2007) developed and tested an indirect mode forced convection solar dryer for drying fruit and vegetable. The dryer consisted of a solar collector, blower, and a solar drying cabinet. Two identical solar collectors with V-groove absorber plates and two air passes were used. Grapes, apricots and beans with initial moisture contents of 80%, 80% and 65% respectively, were dried. The result shows that the final moisture content of apricot was 13% within one day and a half of drying, 18% for grapes in two and a half days of drying and 18% for beans in 1 day only. Similarly, **Afriyie *et al.* (2009)** experimentally tested the performance of a solar chimney crop dryer. A cabinet dryer using a normal chimney was tested first and repeated with a solar chimney and the roof of the drying chamber was inclined further to form a tent dryer to carry out the trials. The result shows that the solar chimney dryer can be designed with the appropriate angle of drying chamber roof to increase the airflow rate.

Das and Kumar (1989) designed and studied the performance of a low cost and simple solar dryer. The dryer consists of a vertical flat plate collector and a drying chamber with a capacity of 20 kg of high moisture field harvest (paddy). The experiments were performed during the winter months. The result shows that an average air temperature rise of 21.8 ℃ and 27.1 ℃ with an average air flow rate of 0.6707 m^3/min for the inclined and vertical collectors, respectively, and when the average air temperature rise in the inclined collector was increased to 68.5 ℃, a 33% reduction in airflow rate was observed.

2.1.2 Solar dryers with thermal energy storage

To minimize the problems associated with the uncertainty and intermittent nature of solar radiation, thermal energy storages were developed to improve the solar drying application. The thermal energy storages used were latent and sensible heat storages. In this section solar dryers assisted by thermal energy storage materials (sensible and latent heat storage materials) are reviewed.

2.1.2.1 Solar dryers with latent heat storage

Latent heat storages store energy when they change their phase from solid to liquid and vice versa. So many researches have been conducted on solar dryers with the integration of latent heat storages. **Shalaby *et al.* (2014)** reviewed previous works on solar drying systems which implemented phase change materials as an energy storage medium. It was concluded that recent researches focused on PCMs as energy storage media because of their higher thermal energy storage density compared with sensible heat storage materials. It was also concluded that implementing PCM in solar dryers reduces heat losses and improves efficiency. Similarly, **Swami *et al*. (2018)** experimentally analyzed a solar fish dryer with phase change material. The dryer consisted of a flat plate collector, drying chamber, chimney and air blower. For experimentation, two different PCMs, Paraffin wax C23–24 (melting point 45-48 ℃) and Paraffin wax C31–33 (melting point 68-70 ℃) were used. The result shows that, optimized conditions which are 5 m/s velocity, 0.314 kg/s mass flow rate and 10 cm depth of heating chamber were best suitable for solar fish drying and the drying period is then reduced approximately by 70%. Out of total available heat, 40% of heat was utilized and 60% was found to be exhausted unutilized and the use of PCM is found to be an excellent solution to accumulate this heat. PCM-1 maintains an average temperature higher than the average temperature of the dryer without PCM and the drying period was reduced up to approximately by 80% of the traditional method and by 20% of the solar dryer method. PCM-2 was also tested for load condition and the average temperature maintained was 36.5 °C and it was stated that due to the temperature range of the drying process, PCM-2 was not suitable for this application. It is also indicated that fish can only sustain a maximum temperature of 62 °C. **Bal *et al.* (2011)** also designed and developed a natural circulation solar dryer integrated with a paraffin wax based latent heat storage (LHS) system. Initial measurements of temperature at the inlet, outlet, back and below of solar panel with the free natural circulation of air have been carried out daily. The result shows that the continuous drying of agricultural/food products at a steady and moderate temperature of 40–75 ℃ can be possible. The main drawback of the initial model associated with heat loss was modified by adding a coating of PU foam below the panel.

Shalaby and Bek (2014) experimentally investigated an indirect mode solar dryer integrated with phase change material for drying medical plants. The components of the dryer were two identical flat plate solar collectors, drying chamber, PCM storage and blower. No-load test of the dryer was performed with and without PCM at mass flow rates of 0.0664 to 0.2182 kg/s. The result shows that using the PCM gives a drying air temperature of 2.5 to 7.5 ℃ higher than ambient temperature after sunset for at least 5 hours. It was also concluded that, peak values of the drying temperature were obtained with mass flow rates of 0.1204 kg/s and 0.0894 kg/s when the dryer is operated with and without PCM, respectively. After implementing the PCM, the final moisture content is achieved in 12-18 h. Similarly, **Reyes *et al.* (2014)** developed and tested a solar dryer integrated with a phase change material. The energy storage was basically a solar collector. It consisted of a hundred copper tubes with external aluminum fins. The tubes were filled with 14 kg of paraffin wax having a melting temperature range of 58–60 ℃ and were exposed to the sun rays transmitting through a transparent cover. The air was first preheated by the solar air heater during the daytime and raised to the predetermined value by an auxiliary electric heater. The result shows that a temperature rise of 20 ℃ above the ambient was supplied by the accumulator for about 2 h and around 40–70% electrical energy was saved. The thermal efficiencies of the solar air heater and the accumulator were in the range of 22 to 67% and 10 to 21%, respectively. **Jain and Tewari (2015)** also developed a direct type solar dryer integrated with a paraffin wax based latent heat storage system. The latent heat storage consisted of 48 cylindrical tubes (0.75 m in length and 0.05 m in diameter) filled with 48 kg paraffin wax and placed at the bottom of the drying chamber. A black absorber plate covered with a toughen glass was placed at the top of the drying chamber and a PCM packed bed was placed below it. The result shows that a drying air temperature of 6 ℃ higher than the ambient was supplied by the energy storage system for about 5 to 6 hours after sunset.

Shringi *et al.* (2014) developed a solar dryer integrated with a thermal energy storage system evacuated tube heat pipe collector. The evacuated tube heat pipe collector heated a mixture of

60% propylene glycol and 40% water to 54–118 °C. The heated fluid was then circulated through a heat exchanger coil located in the PCM with a melting temperature of 87 °C. Then the air at the temperature between 39 °C and 69 °C was used in the dryer for drying garlic cloves. The result shows that without recirculation of the exhaust air, the exergy efficiency was in the range of 5 to 55% in the first 3 h of the drying period. Thereafter, the exhaust air was re-circulated and the exergy efficiency was 67 to 88%. **Sain *et al.* (2013)** studied a natural convection mode solar dryer integrated with a paraffin wax based latent heat storage system. The dryer was tested under both full load (with Ginger) and no-load condition. The result from the test shows that the moisture content of Ginger was reduced from 74% to 3% in 24 h and daily drying efficiency was 12.4 %. Collector efficiency during no load test was in the range of 53 to 96% and full load test in the range of 40 to 55%.

Fath (1995) proposed and analyzed a simple design of the solar air heater with a built-in thermal energy storage system. The thermal energy storage system consists of a corrugated set of tubes filled with a PCM. The result shows that, a daily average efficiency of 63.35% was achieved with an airflow rate of 0.02 kg/s, and an outlet temperature of 5°C above ambient was extended for about 16 h, compared to 38.7% and 9 h, respectively, for the conventional flat plate solar air heater. The outlet temperature was extended for about 21 h with an airflow rate of 0.01 kg/s. Similarly, **Fath (1995)** presented the thermal performance of a thermo-siphon solar air heater with a built-in thermal energy storage system. Phase change materials with melting temperatures of 61, 51, 43 and 32 °C were studied. The obtained results were compared with the system without storage material. The result shows that, PCMs with 51 and 43 °C melting temperature were best. The solar air heater with the 43 °C melting temperature PCM can discharge a thermal load of a minimum of 0.01 kg/s air flow rate and a temperature rise of up to 8 °C. Depending on the PCM melting temperature, solar intensity and mass flow rate of the flowing air, the daily average efficiency of the heater varies between 27% and 63.8%. Later, **Enibe (2003)** introduced a transient thermal analysis of a natural convection solar air heater integrated with a thermal energy storage system. PCM with a total mass of 65 kg was prepared in modules and placed evenly across the absorber plate. The predicted results of the solar air heater were compared with the experiment within the limits of experimental error. The predicted result shows that useful and overall efficiencies of the integrated system were 13% and 18%, respectively.

Alkilani *et al.* (2009) predicted the outlet air temperature of a solar air heater integrated with a thermal energy storage system with mass flow rates in the range of 0.05 to 0.19 kg/s. 0.5% mass fraction of aluminum powder was added with paraffin wax to enhance the conduction heat transfer process. The freezing time of the PCM has been predicted for the investigated mass flow rate. The result shows that the freezing time of the PCM is inversely proportional to the mass flow rate; it took approximately 8 h with a flow rate of 0.05 kg/s and the outlet air temperature was predicted as 42 ℃ at this flow rate. Similarly, **Tyagi *et al.* (2012)** presented a comparative experimental study of a solar air heater with and without thermal energy storage material. Paraffin wax and hytherm oil were used as thermal storages and the study was based on energy and exergy analysis. First and second law efficiencies were determined for three different arrangements, one arrangement without thermal energy storage and two arrangements with thermal energy storage. The result shows that both efficiencies were higher for the solar air heater with thermal storage material than those without thermal storage material. It was also revealed that both efficiencies of the solar air heater that uses paraffin wax were higher than that of hytherm oil. Later, **Bouadila *et al.* (2013)** experimentally evaluate the thermal performance of a new solar air heater using a packed bed of PCM spherical capsules. The packed bed absorber was formed of spherical capsules with a black coating and it is fixed with a steel matrix. The result shows that, the daily energy and exergy efficiency of the solar air heater varied between 32% and 45% and 13% and 25%, respectively.

2.1.2.2 Solar dryers with sensible heat storage

Sensible heat is stored by changing the temperature of materials like rock, sand, concrete and brick. These sensible heat storage materials were used to assist solar dryers. A lot of researches were done on the use of sensible heat storages to assist solar dryers. **El-sebaii *et al.* (2001)** designed, constructed and experimentally investigated indirect mode natural convection solar dryer using sand as a thermal storage material. Different fruits (seedless grapes, figs and apples) and vegetables (green peas, tomatoes and onions) were experimented. The result shows that for seedless grapes, equilibrium moisture content was reached after 72 without storage and 60 h with storage material reducing the drying process by 12 h. Similarly, **Mohanraj and Chandrasekar (2009)** experimentally studied an indirect mode forced convection solar dryer with sensible heat storage material for drying chili. Sand mixed with aluminum scraps was placed between the absorber plate and insulation to store the heat. The capacity of the drying chamber was about 50 kg of chili per batch. The result shows that the integration of storage materials increases the drying time by about 4 h per day and maintain consistent air temperature. The initial moisture content of chili was 72.8% and dried to a final moisture content of 9.2% and 9.7% (wet basis) at the bottom and top trays respectively.

Ayyapan and Mayilsamy (2012) tested the performance of a natural convection solar tunnel dryer integrated with rock bed as a sensible heat storage material for drying copra. The result shows that the moisture content of copra was reduced from 52% (w.b.) to 7.1% (w.b.) in 54 h with storage and 60 h without heat storage material. But it took 153 h to reduce the moisture content of copra from 52.3% (w.b.) to 7.1% in open sun drying. The average thermal efficiency of the dryer was 15% and increased by 2% to 3% using the storage. Later, **Ayyappan *et al.* (2015)** conducted an experimental investigation on a natural convection solar greenhouse dryer integrated with sensible heat storage materials for drying coconuts. The result shows that the moisture content of coconuts was reduced from 52 (w.b.) to 7% (w.b.) in 78h, 66 h and 53 h using concrete, sand and rock-bed saving 55%, 62% and 69%, respectively, of drying time compared to open sun drying which takes 174 h to reduce the moisture content to the same level. The efficiency of the dryer was found to be 9.5, 11 and 11.65% when using concrete, sand and rock-bed respectively. **Madhlopa and Ngwalo (2007)** designed and constructed an indirect mode natural convection solar dryer integrated with thermal energy storage and a biomass-backup heater. Simple materials and skills were employed to build it. The dryer was tested with solar, biomass and solar–biomass modes of operation, by drying twelve batches, each batch weighing 20 kg of fresh pineapple. The result shows that the solar–biomass mode of operation reduces the moisture content of pineapple slices from about 66% to 11% (db). The average values of moisture pickup efficiency were 15%, 11% and 13% in the solar, biomass and solar–biomass modes of operation respectively.

Aissa *et al.* (2012) also studied the performance of a forced convection solar dryer with granite stone as a sensible heat storage material. Experiments were conducted at air mass flow rates, varying from 0.016 kg/s to 0.08 kg/s, for five hot summer days of July 2008. The temperature distribution along the air heater was discussed and the result shows that the solar air heater gives an outlet temperature of 10 to 25 ℃ more than the ambient. **Saravanakumar and Mayilsamy**

(2010) developed and tested the thermal performance of a forced convection flat plate solar air heater with sensible heat storage material. A centrifugal blower was used to increase the outlet temperature of the collector and efficiency (10–20%). The result shows that among the sensible heat storages, Gravel with iron scraps has better efficiency. It was also reported that forced convection solar dryers are more suitable for drying high-quality products even in a cloudy climate.

- From the above literature survey, it can be concluded that direct solar dryers overcome the problems associated with open sun drying but compared to indirect solar dryers, direct solar dryers have some drawbacks as the products are subjected to direct sunlight. Indirect solar dryers have the following advantages.
    i. High drying rate. Products are dried within 15–30 h instead of a few days.
    ii. Drying can be controlled scientifically, ensuring the proper moisture content of the final product. Thus, the dried product can be stored for long times.
    iii. No losses at all, as the products are not subject to any natural phenomena.
    iv. Increased productivity, as dryers can be loaded again within a few hours.
    v. No discoloration of the product inside the dryer.
    vi. No moisture condensation inside the glass cover.

These dryers can be constructed from locally available materials like wood and bamboo. It is also observed that solar dryers with thermal energy storage (sensible and latent heat storages) give better drying than dryers without thermal energy storage. Compared to sensible heat storages, latent heat storages have better enhancement on solar dryers.

2.2 Solar air heaters

Solar air heaters are renewable energy solar thermal systems used to heat air by absorbing solar energy using an absorbing medium called absorber plate. They are easy to construct and are the most cost-effective out of all the solar technologies. Flat plate solar air heaters with metal absorber plate and glass cover are the most common collectors used for solar drying applications without affecting the environment. The absorber plate is painted black because black colors absorb a higher percentage of sunlight than light colors. The glass cover which is called glazing has roles of minimizing heat loss from the absorber plate, shielding the absorber plate from direct exposure to weathering and transmitting as much solar radiation as possible. They are simple and are effective means of collecting solar energy for applications that require temperatures below 100 ℃ **(Aldabbagh *et al.*, 2010)**.

2.2.1 Components of flat plate solar air heaters

The major components of a flat plate solar air heater are the absorber plate, glazing (cover) and insulation as represented in Figure 2.1.

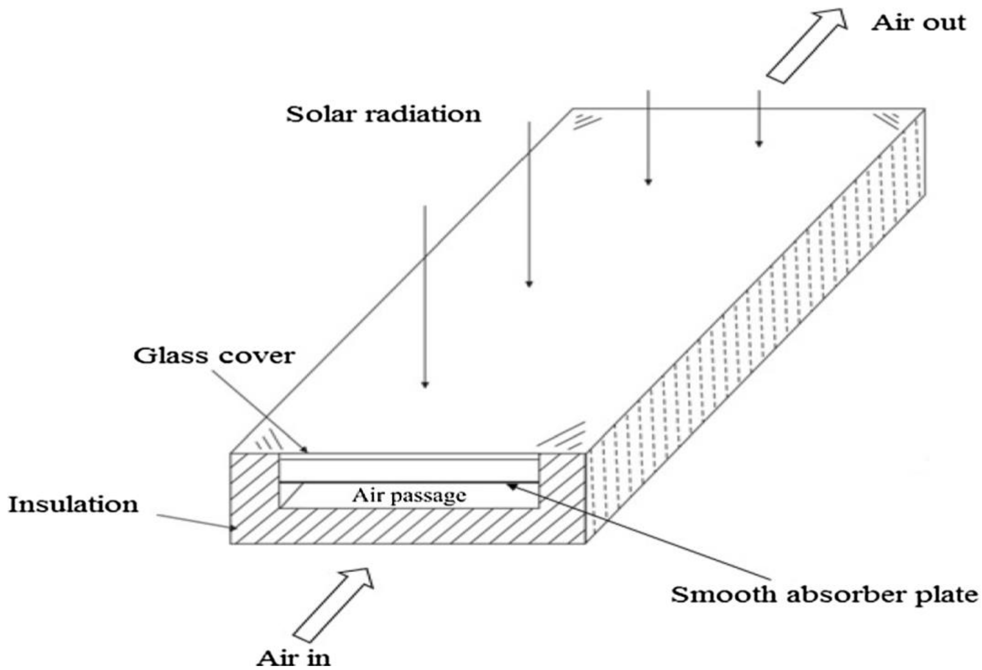

Figure 2.1: Schematic diagram of a solar air heater (Ghritlahre *et al*., 2019).

a. Absorber plate

The function of the absorber plate is absorbing the incident solar radiation and transfers it to the working fluid. It is usually painted black because black colors absorb higher percentage of sunlight than light colors. The absorptance of the collector surface for shortwave solar radiation depends on the nature and color of the coating and on the incident angle. The surfaces of the absorber should have high values of solar radiation absorptance and low values of long wave emittance (**Bakari *et al.*, 2014 and Aldabbagh *et al.*, 2010**).

b. Cover plate

The cover plate also called glazing is the top cover of the solar collector. The major functions of the cover plate are minimizing convective and radiant heat loss from absorber, transmitting the incident solar radiation to the absorber plate with minimum loss, and protecting the absorber plate from outside environment. Other important characteristics of glazing materials are reflection, absorption and transmission. In order to attain maximum efficiency, reflection and absorption should be as low as possible, whilst transmission should be as high as possible. Usually the common materials used as glazing are glass and plastics (Bakari *et al.,* 2014).

c. Insulation

A layer of insulating material can reduce heat losses from the back and edge of an absorber plate and should be able to withstand the collector stagnation temperatures. It should be fire resistant, not subjected to outgoing gassing and not damageable by moisture. Insulating materials are usually fiber glass, mineral wool, thermo foam, Styrofoam and urethanes (Bakari *et al.,* 2014).

2.2.2 Factors that affect the performance of flat plate solar air heaters

The performance of flat plate solar air heaters can be affected by many factors like:

a. Thickness of glazing.
b. Glazing material and number of glazing.
c. Air gap between plate and glazing.
d. Absorber plate coating and emissivity.
e. Ambient temperature.
f. Air flow rate.
g. Collector tilt angle.
h. Transmittance of the glazing.
i. Insulation.
j. Configuration of the collector (double pass or single pass).
k. Air flow arrangement inside the collector (parallel flow or counter flow).

Previous works on the effects of these factors on the performance of flat plate solar air heaters are reviewed and presented as follows.

Many researchers studied the effect of these factors on the performance of solar air heaters. **Smith (2011)** studied the effect of glazing on the performance of flat plate collectors and reported the advantages of glazing of collectors. The advantages are better transmission of solar radiation to the absorber plate, reduction in convection and radiation heat losses from the surface of the absorber plate and reduction in heat loss due to low temperature difference between the ambient and glazing. A comparative study between glazed and unglazed flat plate collector's thermal efficiency was carried out by **Khan *et al.* (2010)**. The result shows that the thermal efficiency was found to be 57.3% for the glazed collector and 33.3% for the unglazed collector.

Bakari *et al.* (2014) investigated the effect of thickness of glazing on the performance of flat plate solar collectors for drying fruits. 3 mm, 4 mm, 5 mm, and 6 mm glass thicknesses were used and compared with a glass of 5 mm thickness. The results showed that 4 mm glass has the highest thermal efficiency of 35.4%, while the 6 mm glass has the lowest performance of 27.8% and efficiency of 3 mm and 5 mm glasses were 32.7% and 30.4%, respectively. However, the use of a glass of 4 mm thick needs precautions in handling and during placement to the collector to avoid extra costs due to breakage. **Ihaddadene *et al.* (2014)** also studied the effect of distance between double glazing's on the performance of solar air heaters. The result shows that the effect of the double glazing depends on the characteristics of the glass added, in this case, a normal glass of 3 mm thick was added, double glazing thus does not improve the performance of the solar collector studied. The efficiency of the double-glazed solar collector decreases with increasing the distance separating the two glasses.

Do Ango *et al.* (2013) numerically studied the effect of design parameters (air gap thickness and collector's length) and operating conditions (mass flow rate, solar radiation and inlet temperature) on the efficiency of solar collectors. The result shows that increasing the mass flow rate and air gap thickness improves performance, an optimal performance being obtained a thickness of 10 mm, whereas increasing collector length does not affect their performance. Finally, the incoming solar radiation has a small effect on the collector's efficiency. Similarly, **Ihaddadene *et al*. (2014)** carried out an investigation on effect of air gap varying in the range from 50 to 60 mm on thermal efficiency. The result shows that the thermal efficiency of flat plate collectors decreases with an increase in the air gap. It was also reported that increasing the distance that separates double glazing decreases the thermal efficiency of flat plate solar collectors. **Njomo and Michel (2006)** also studied sensitivity analysis of thermal performances of flat plate solar air heaters. The analysis has been performed for input parameters such as incident solar irradiation, inlet temperature, mass flow rate, the depth of the fluid channel, the number and nature of the transparent covers. The result shows that, the outlet fluid temperature decreases with increasing mass flow rate. The outlet fluid temperature decreases with increasing air channel depth and collectors working with low air mass flow rates show high temperature differences between the inlet and outlet air temperatures and low thermal efficiencies.

Prakash *et al.* (2013) studied both theoretical and experimental investigation on the effect of nanocoating of absorber plate material on absorptance and emittance. The result shows that due to the presence of nanocoating, the absorptance is high and the emittance is low.

He *et al.* (2016) did a parametric study on the effect of ambient temperature on the efficiency of flat plate collectors. The result shows that the thermal efficiency of flat plate collectors increases from 48% to74% when the ambient temperature was increased from 5 ℃ to 40 ℃.

Matuska *et al*. (2009) predicted the thermal efficiency of a solar collector for various insulation thicknesses. The result shows that there is a radical increase in thermal efficiency when the insulation thickness increases from 20 to 50 mm. It was also concluded that the thermal efficiency of the collector remained constant beyond 50 mm thickness of insulation. **Madhusudan *et al.* (1981)** also studied the effect of insulation on the performance of flat plate collectors. The result shows that, from the 33-50% heat loss, 22-30% happen due to convection, 5-7% due to radiation from the front surface of the absorber and 5-10% from the back surface. And it was concluded that insulation of solar collectors is mandatory to ensure reduction in heat losses from the different sections of the collector.

Ahmad and Tiwari (2009) investigated the effect of tilt angle on the performance of flat plate collectors. The result shows that the collector energy loss is almost 1% when the collector tilt angle was adjusted seasonally instead of adjusting each month. Similarly, **Wang and Hong (2015)** studied the effect of collector tilt angle on the thermal performance of a solar collector.

It was reported that solar energy reaching the solar collector surface changes with the tilt angle and orientation of the collector. Collector installed at an optimum tilt angle and with proper orientation resulted in maximum radiation on the surface of the collector. It was also reported that collectors installed in the northern hemisphere oriented to the south and are tilted at a certain angle.

Bekele *et al.*, (2019) designed and experimentally investigated the heat transfer and fluid flow characteristics of a solar dryer with delta shaped turbulators fitted on the absorber plate. The absorber plate is subjected to a uniform heat flux of 800 W/m^2 and the experiment was performed with Reynolds number ranging from 3000 to 30,000. Correlations for Nusselt number and friction factor were developed as a function of angle of attack, Reynolds number, relative turbulator height, transvers pitch and longitudinal pitch. It was concluded that the developed correlations predicted the values with in an error limit of ±12% to ±14% and can be directly used to develop and predict the performance of SAH with delta shaped turbulators. Better performance of these solar air heaters but with high pressure drop for the same operating conditions compared with the smooth ones.

Dhiman *et al.* (2012) theoretically and experimentally investigated counter and parallel flow packed bed solar air heaters. The analytical model for these air heaters was presented. Effects of air mass flow rates and bed porosities on thermal efficiencies of counter and parallel flow solar air heaters were investigated. The result shows that the thermal efficiency of the counter flow solar air heater was 11 to 17% higher compared to parallel flow solar air heaters. **Bhargava *et al.* (1983)** also studied the various configurations of air heaters based on air flow passages. The types considered were: Type-I (air flowing between the cover and absorber plate), Type-II (air flowing between absorber plate and bottom plate) and Type-III (air flowing between cover and absorber as well as between absorber and bottom plate). It was found that Type-III was most efficient than other configurations, but the average outlet air temperature was less than Type-II. A fourth type was also compared with others and it was similar to two-pass air heaters, i.e. Type-III, but instead of air exiting after flowing between cover and absorber, it was made to flow between absorber and bottom plate but in opposite direction. It was found that the outlet air temperature for Type IV was greater than the outlet air temperature for Type-II for a plate length of up to 5 m. But, if the length is greater than 5 m, the outlet temperature was greater for Type-II.

- From the literature survey, it is observed that the performance of flat plate solar air heaters increases with increasing airflow rate, ambient temperature and insulation thickness. It also increases with the presence of glazing and absorber plate coating. However, increasing the thickness of glazing and the air gap between the absorber plate and glazing decreases their performance. It is also observed that the double pass configuration of flat plate solar air heaters is more efficient than the single pass and the counterflow arrangement of the double pass configuration has a higher thermal efficiency than the parallel flow.

2.3 Thermal energy storages

Solar energy technologies become widely accepted since they use the free energy of the sun and are environmentally friendly. But the uncertainty and inconsistent nature of the solar radiation is the main drawback of these technologies and creates an imbalance in the demand and supply of energy. Thermal energy storages play a great role in minimizing the gap between supply and demand of energy. Apart from minimizing the gap between the supply and demand for energy, thermal energy storages improve the performance of the energy systems and playas an important role in conserving energy (Lingayat and Suple, 2013). Thermal energy storages can be sensible or latent heat storages.

Thermal energy is stored as sensible heat by rising the temperature of a solid or a liquid by using its heat capacity. The amount of heat stored depends on the temperature change, the amount of storage material and the specific heat of the storage medium. Sensible heat storage materials include rock, brick, concrete, sand, soil, water, engine oil, ethanol etc. If m is the mass in kg, T_1 and T_2 are the initial and final temperatures in ℃ and C_p is the specific heat of the storage material in KJ/kg. ℃, the amount of thermal energy stored or released as sensible is (Lingayat and Suple, 2013),

$$Q = mC_p(T_2 - T_1) \quad \text{...} \quad (2.1)$$

Latent heat storages store thermal energy when a material changes from one phase to another. The amount of heat stored or released when a material changes from solid to liquid or vice versa is called latent heat of fusion and from liquid to vapour or vice versa is called latent heat of vaporization. If m is the mass in kg and L_H is the latent heat of fusion or vaporization in kJ/kg of the material, the amount of thermal energy stored or released as latent heat is (Lingayat and Suple, 2013),

$$Q = mL_H \quad (2.2)$$

Compared to sensible heat storages, latent heat storages are attractive since they provide a high energy storage density and can store energy at a constant temperature which is the phase transition temperature of the material.

2.3.1 Latent heat storages

Latent heat storages are also called phase change materials (PCMs). PCMs can be classified as organic, inorganic and eutectics.

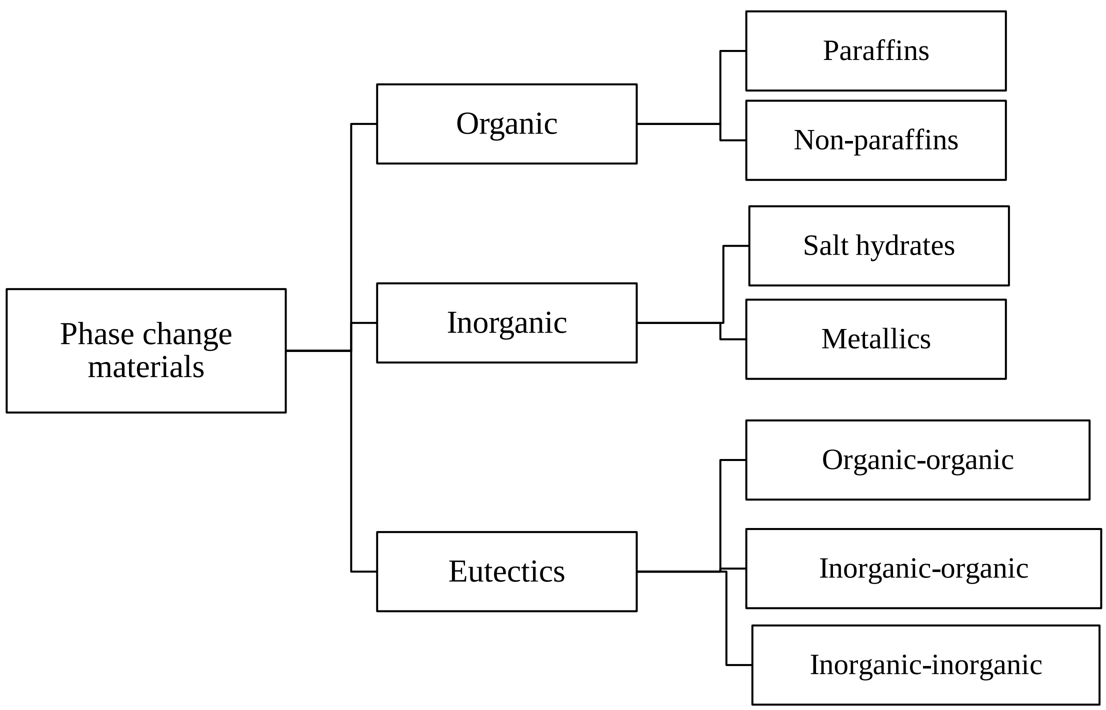

Figure 2.2: Classification of phase change materials.

Paraffins are mixtures of straight chain alkanes CH3-(CH2)-CH3 and are safe, reliable, non-corrosive and less expensive where as non-paraffins are mostly esters, fatty acids and alcohols and are flammable and 2-5 times costly than paraffins.

Table 2.1: Phase change materials advantages and disadvantages (Shalaby *et al.*, 2014).

	Advantages	Disadvantages
Organic	Low Cost, Chemically inert and stable, No phase segregation, Recyclable and self-nucleating, Available in large temperature range.	Flammable, Low thermal conductivity, Low volumetric storage density (90-200 MJ/m³)
Inorganic	Moderate cost, High volumetric storage density, (180-300 MJ/m³), Higher thermal conductivity, Nonflammable and low volume change.	Subcooling, Phase segregation, Corrosion of containment material.
Eutectics	Sharp melting point, Low volumetric storage density.	Limited available material property data.

2.3.2 Selection criteria of PCMs

In solar drying applications, the primary criteria to select a phase change material is its melting temperature range. The melting temperature of the selected PCM should be 5 to 10 ℃ higher than the desired drying temperature, i.e. the recommended temperature for drying the product. Other thermo physical, kinetic and chemical properties of a PCM are (Lingayat and Suple, 2013),

- ✓ High heat storage capacity.
- ✓ Isothermal operation and lesser storage space.
- ✓ Easy availability and cost effective.
- ✓ Large latent heat per unit volume.
- ✓ Low vapor pressure and small volume change on phase transformation.
- ✓ Safe, non-reactive and compatible with all metal containers.
- ✓ Favorable phase equilibrium.
- ✓ High density.

- ✓ Sufficient crystallization rate.
- ✓ Long-term chemical stability.

2.3.3 Previous works on latent heat storage

This section covers a review of literatures on latent heat storage systems. The reviewed literatures include advantages of using latent heat storages over sensible heat storages, how to select the appropriate phase change material as latent heat storage, advantages of using paraffin wax as phase change material, shape of the latent heat storage, cylinder orientation and effect of parameters like inlet temperature and flow rate on the performance of the storage. **Krishnan and Sivaraman (2017)** did an experimental investigation on the performance of thermal energy storage systems. It is concluded that PCMs can store 2-3 times more heat or cold per volume or mass, as can be stored as sensible heat in water in a temperature interval of 20 ℃. **Shalaby *et al.* (2014)** presented a review on the application of phase change material in the solar dryer. The advantages of phase change materials over the sensible heat storage material were investigated. It was concluded that the recent researches focused on PCMs as energy storage media because of their higher thermal energy storage density compared with sensible heat storage materials. Also, the importance of paraffin wax as it contains graphite which helps improve the thermal performance of dryer was explained.

Lane *et al*. (1983) performed an extensive study on solar latent heat storage materials background and scientific principles. The result shows that, there are about 20,000 substances with the melting point in the range 10-90 ℃ but the majority of them were abandoned due to the improper melting point, melting with decomposition or lack of essential reference data. Among these PCMs, paraffin has shown outstanding performance for application in low temperatures thermal energy storage systems like solar heating and cooling. Later, **Miro *et al*. (2016)** proposed a methodology to select a suitable PCM for a thermal storage application. It was concluded that, the selection of a PCM must be based on the phase change thermal range, enthalpy, specific heat, and thermal cycling stability.

Devahastin and Pitaksuriyarat (2006) studied the effect of paraffin wax based thermal energy storage systems on the drying kinetics of food products. The system consists of a compressor, temperature controller, heater and latent heat storage (LHS) vessel. The effects of inlet air velocities of 1 and 2 m/s on the charge and discharge period were determined. The result shows that, the discharge time was 180 and 165min and 1920 and 1386 kJ min/kg energy were extracted from the LHS and 40% and 34% energy were saved with an inlet air velocity of 1 and 2 m/s, respectively.

Bal *et al.* (2011) reported in their review that, **Sharma *et al.* (2005)** studied the changes in the melting point, latent heat of fusion and specific heat of stearic acid, acetamide and paraffin wax, both laboratory-grade and commercial-grade. It was reported that stearic acid melted over a range of temperatures but was thermally stable and acetamide and paraffin wax showed reasonably good stability throughout 300 melting/freezing cycles and could be considered as promising PCMs. It was also reported that, Abhat mentioned paraffin as qualified energy storage materials due to their availability in a large temperature range and high heat of fusion. Furthermore, paraffins are known to freeze without any supercooling. **Swami *et al*. (2018)** experimentally analyzed two different PCMs, Paraffin wax C23–24 (melting point 45-48 ℃) and Paraffin wax C31–33 (melting point 68-70 ℃) for drying fish. The result shows that, Heat compensation by PCM-1 maintains an average temperature higher than the dryer without PCM. PCM-2 was also tested for load condition and the average temperature maintained was 36.5 °C and it was stated that PCM-2 is not suitable for drying due to its temperature range.

Agrawal and Sarviya (2016) studied the heat transfer characteristics during the charging and discharging processes of a shell and tube latent heat storage system. The energy storage system comprises two concentric cylinders and the space between them was filled with paraffin wax with melting temperature ranging from 41 ℃ to 55 ℃. The effects of the airflow rate and temperature on the charging and discharging processes of the storage were investigated. The result shows that the charging time of the PCM decreased with an increase in the heat transfer fluid temperature. The discharging time decreased with an increase in the mass flow rate of air. High discharge temperature was observed at the low mass flow rate of air.

Wang *et al.* (2013) numerically studied the effect of inlet temperature and mass flow rate of a heat transfer fluid on the thermal performance of shell and tube latent heat storage system. The result shows that the inlet temperature of the heat transfer fluid had more effect on thermal energy storing capacity and melting rate than the mass flow rate. Similarly, **Kibria *et al.* (2014)** performed both experimental and numerical investigation of a shell and tube latent heat storage using paraffin wax as PCM. The result shows that the inlet temperature has a higher effect on the performance of the system than the mass flow rate of the heat transfer fluid. **Rathod and Banerjee (2014)** also experimentally investigated latent heat storage systems using paraffin wax as phase change material. The result shows that inlet temperature had a higher effect on the heat fraction during the PCM melting than the mass flow rate.

Karthikeyan and Velraj (2011) investigated the transient behavior of a packed bed latent heat storage. A cylindrical storage tank filled with PCM encapsulated spherical containers were used. An enthalpy based numerical model that also accounts for the thermal gradient inside the PCM capsules was developed, and the governing equations were discretized using the explicit finite difference method. The result shows that a mass flow rate of 0.015 kg/s was able to provide a near uniform heat flow during the charging and discharging processes. It was concluded that the study was good for designing PCM based thermal energy storage units with air as the heat transfer fluid like solar drying and space heating applications.

Seddegh *et al.* (2016) studied the effect of vertical and horizontal cylinder orientation on the thermal performance of shell and tube latent heat storage systems. The result shows that the horizontally oriented storage has better performance than vertically oriented. Similarly, **Gunjo *et al.* (2018)** studied the effect of cylinder orientation on the average temperature and melt fraction of paraffin wax filled latent heat storage during the charging process. The result shows that the average temperature and melt fraction variation is the same for both vertical and horizontal orientations at the beginning of the charging process. It is also reported that the horizontally oriented system reached a fully charged state much faster than the vertically oriented system. The rate of melting is higher in the horizontal orientation than the vertical because of the higher recirculation region along the axial direction than along the radial direction in the vertical orientation.

Vyshak and Jilani (2007) studied the effect of the shape of the latent heat storage system on the melting rate of the phase change material. The result shows that shell and tube arrangement have a faster melting rate compared to rectangular latent heat storage for the same heat transfer area and volume.

- From the above literatures, it can be concluded that latent heat storages are more preferable than sensible heat storages due to their high heat storing capacity. From the latent heat storages, paraffin can be used as a thermal storage material for the following reasons:
    - ✓ High heat storage capacity,
    - ✓ Low melting temperature,
    - ✓ Isothermal operation and lesser storage space,
    - ✓ Easy availability,
    - ✓ Large latent heat per unit volume,
    - ✓ Low vapor pressure and small volume changes on phase transformation,
    - ✓ It is safe, non-reactive and compatible with all metal containers.

The selection of these phase change materials must be based on the melting temperature range, enthalpy, specific heat, and thermal cycling stability. It was also observed that shell and tube arrangement have a faster melting rate compared to rectangular latent heat storage for the same heat transfer area and volume and horizontal orientation of the shell and tube storage has better thermal performance than the vertically oriented shell and tube storage. The charging time decreases with an increase of the air temperature and air velocity whereas air velocity did not affect much the discharging time since heat conduction is dominant during solidification.

2.4 Overall literature summary and research gaps

The literature reveals that solar energy has a significant role in the drying sector. By harnessing solar energy drying of food and other products has been effectively accomplished using solar dryers. The solar dryers reviewed are direct, indirect and mixed mode with and without thermal energy storage that works either by natural or forced circulation. From the literature survey, it is observed that indirect solar dryers have a high drying rate and protect the products from direct sunlight compared to direct solar dryers. The use of both sensible and latent heat storages is observed and, latent heat storages store more heat compared to sensible heat storages resulting in better enhancement on the performance of solar dryers. The most widely used latent heat storage is paraffin wax with melting temperatures in the range of 45 ℃ and 60 ℃. It was also observed that:

- Most of the previous works on solar dryers focus on the drying of agricultural products, fruits, vegetables and medical plants. There are also very few attempts on drying of fish but these dryers solely work in the time only when sunlight is available. Additional study should be done on fish drying using indirect solar dryers when the availability of sunlight is low or not available at all.

- In the existing methods, thermal energy storages are placed either at the bottom of the absorber plate or in the drying chamber. Placing the thermal energy storage at these two sections of the dryers has some disadvantages like the loss of heat from the storage to the sides and top of the absorber and the drying chamber. To minimize this heat loss a separate system can be used.

Therefore, this study focuses on a solar fish dryer integrated with thermal energy storage with a separate arrangement of the dryer and thermal energy storage system. Since temperature control is one of the advantages of thermal energy storage systems, the separate arrangement can provide better temperature control.

CHAPTER THREE

DATA COLLECTION AND METHODOLOGY

In this chapter the overall methodology followed to achieve the objectives of this thesis and collected data required for this study is presented. Both theoretical and experimental approaches are used. The theoretical approach is described by using governing equations for the analysis of each component of the dryer. Related literatures are studied to gain an insight to the area of interest background and other influencing factors. The literatures are obtained from academic literatures, articles, websites etc. The experimental approach is used to test the performance of the dryer. The prototype of the dryer has been developed after the sizing and selection of materials for each component was completed. The methodology followed to achieve the objective of this thesis is as shown in Figure 3.1.

Reviewing related literatures and data collection

↓

Determining parameters required for sizing the solar air dryer

↓

Determining the size of the solar air heater and the energy storage

↓

Energy and exergy analysis of each component of the dryer

↓

Collecting raw materials

↓

Manufacturing components of the dryer

↓

Assembling components of the dryer

↓

Experimental test and validation

↓

Conclusion and recommendation

Figure 3.1: Methodology of the study.

3.1 Data collection

Data is collected from both primary and secondary sources. The primary sources of data are data obtained from interviewing fishermen and meteorological data which is collected from the nearby metrological station. Secondary sources of data include reference books, journals, literatures and internet.

3.1.1 Estimation of fish post-harvest losses in Ethiopia

The average fish post-harvest losses in Ethiopian lakes is estimated by interviewing fishermen at lake Ziway and based on data obtained from previous researches. The most commercially important fish species found in different lakes of Ethiopia are Nile tilapia (*Oreochromis niloticus*), African sharp tooth catfish (*Clarias gariepinus*), Nile perch (*Lates niloticus*), Barbs (*Barbus species*), Redbelly tilapia (*Tilapia zilli*) and Common carp (*Cyprinus carpio*) (Masresha *et al.*, 2017).

The daily fish harvesting potential of a single fisherman is estimated from both primary and secondary data sources. Primary data is collected by interviewing fishermen at lake Ziway which is one of the freshwater rift valleys of Ethiopia located 161km south of Addis Ababa. The surface area of lake Ziway is 440 km^2 and its maximum depth is 8.9 m. There are seven indigenous fish species in the lake comprising *Barbus paludinosus, Garra dembecha, Garra makiensis, Labeobarbus ethiopicus, Labeobarbus intermedius, Labeobarbus microterolepis* and *Oreochromis niloticus* (Golubtsov *et al.*, 2002; Getahun, 2010; Jacobus *et al.*, 2012).
Fishermen use wooden boats and nets to capture the fish. The fishermen catch a maximum of 50 fishes and a minimum of 15 fishes per day. At times of maximum catch, 45 fishes were sold to customers during periods of high fish consumption and 30 fishes were sold during periods of low fish consumption. The remaining 5 and 20 fishes were discarded due to spoilage during high and low periods of fish consumption, respectively. The average weight of a single fish was 250 g and the maximum mass of fishes discarded per day were 5 kg.

Secondary data is collected from previous researches and the average estimated fish catch in Ethiopia was 73 fishes per person per day. From the average 73 fish catches, the maximum number of fishes discarded were 25 and the minimum were 10 fishes per day (Demeke, 2015; Getu, 2015; Solomon, 2017). The details of the estimation of both primary and secondary data is presented in Appendix A.

3.2 Solar data collection and radiation estimation

Metrological data of Adama is collected from Eastern and central Oromiya metrological service center. The collected data includes duration of sunshine hours, maximum temperature, minimum temperature, relative humidity and wind speed for six years (2013-2018 G.C) as indicated in Figures 3.2 and 3.3. Global, beam and diffuse solar radiation incident on a horizontal and tilted surface are estimated by taking the average sunshine hours of each month.

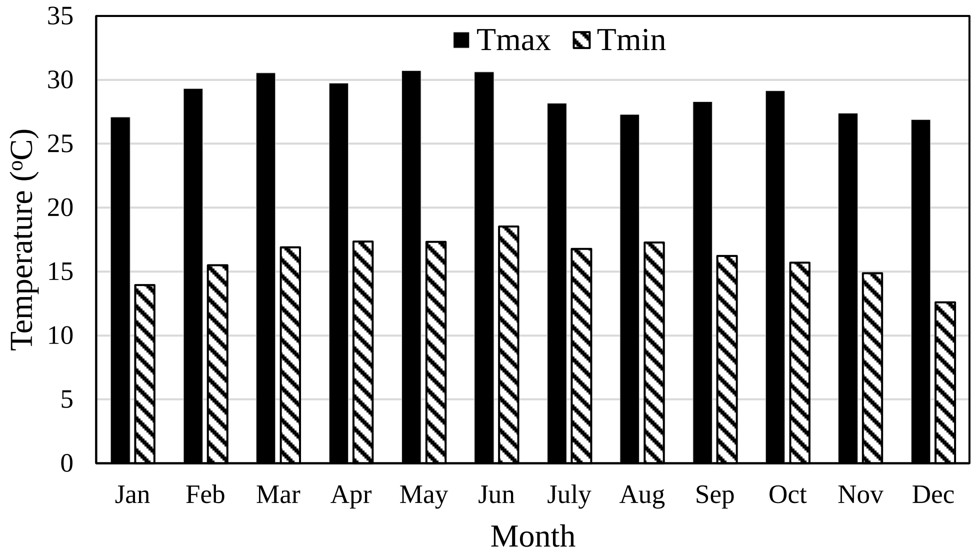

Figure 3.2: Maximum and minimum temperatures of Adama for average six years.

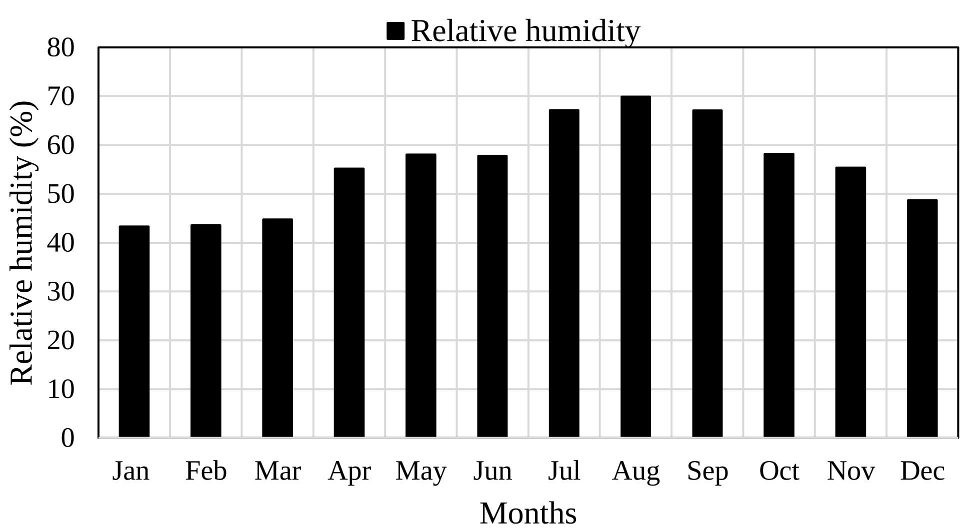

Figure 3.3: Relative humidity of Adama for an average six years.

3.2.1 Solar radiation estimation

The amount of solar radiation falling on a surface on earth is estimated using several correlations that relate the radiation outside of the earth's atmosphere (extraterrestrial radiation) with the radiation inside the earth's atmosphere (terrestrial radiation). In order to perform solar radiation analysis, the geometric relationship between a plane located on earth and the incoming solar radiation, that is the position of the sun relative to that plane, should be first determined. This relationship can be determined using several angles (Duffie and Beckman, 2013).

3.2.1.1 Fundamental sun-earth angles

The major angles that describe the geometric relationship between the earth and the incoming solar radiation from the sun are,

1. Latitude (ϕ): the angular location north or south of the equator, north positive; $-90° \leq \phi \leq 90°$. The latitude of Adama is 8.54° north of the equator.
2. Declination (δ): the angular position of the sun at solar noon with respect to the plane of the equator, north positive; $-23.45° \leq \delta \leq 23.45°$.

   $\delta = 23.45\sin(\frac{360(284+n)}{365})$……………………...……………………………..… (3.1)

   Where, n is the day of the year (counted from January 1).
3. Slope or tilt angle (β): the angle between the inclined plane surface under consideration and the horizontal; $-180° \leq \beta \leq 180°$.
4. Hour angle (ω): the angular displacement of the sun east or west of the local meridian due to the rotation of the earth on its axis at 15° per hour; positive in the afternoon and negative in the forenoon.

   ω = [solar time – 12:00] (in hours) x 15°……………………………………….… (3.2)
5. Zenith angle (θ_z): the angle between the vertical and the line to the sun, that is, the angle of incidence of beam radiation on a horizontal surface.

   $\cos\theta z = \cos\delta \cos\phi \cos\omega + \sin\phi \sin\delta$…….…...…………………….……. (3.3)
6. Surface azimuth angle (γ): the deviation of the projection on a horizontal plane of the normal to the surface from local meridian. $\gamma = 0$ for surfaces facing south.
7. Angle of incidence (θ): the angle between the sun's ray's incident on the plane surface and normal to that surface.

$$\cos\theta=(\cos\phi\cos\beta+\sin\phi\sin\beta\cos\gamma)\cos\delta\cos\omega+\cos\delta\sin\omega\sin\beta\sin\gamma+\sin\delta(\cos\beta\sin\phi+\cos\phi\sin\beta\cos\gamma) \quad (3.4)$$

3.2.1.2 Estimation of daily extraterrestrial radiation on a horizontal surface

The extraterrestrial radiation on a surface normal to the sun's rays kept at the actual sun-earth distance at a specific day and time which is modified to take into account the varying distance between the sun and the earth is determined by (Duffie and Beckman, 2013):

$$I_{ext} = I_{sc}\,[1.0 + 0.033\cos(\frac{360(n)}{365})] \quad (3.5)$$

Where, n is the day of the year (counted from January 1) and I_{sc} is solar constant =1367 W/m^2.

Extraterrestrial solar radiation that would fall on a horizontal surface at the location is given by:

$$I_o = I_{ext}\cos\theta z \quad (3.6)$$

$$I_o = I_{sc}\,[1.0 + 0.033\cos(\frac{360(n)}{365})][\cos\delta\cos\phi\cos\omega + \sin\phi\,\sin\delta] \quad (3.7)$$

The daily extraterrestrial solar radiation on a horizontal surface can be obtained by integrating equation (3.7) from sunrise to sunset and expressed as:

$$H_o = \frac{24\times3600}{\pi} I_{sc}\,[1.0 + 0.033\cos(\frac{360(n)}{365})][\cos\delta\cos\phi\sin\omega_{sr} + \frac{\pi\times\omega_{sr}}{180}\sin\phi\,\sin\delta] \quad (3.8)$$

Where, sunset hour angle $\omega_{sr}=\cos^{-1}(\tan\phi\tan\delta)$ …………………. (3.9)

3.2.1.3 Estimation of monthly average daily global radiations on a horizontal surface

The first empirical correlation for the estimation of global solar radiation is proposed by Angstrom. The correlation relates the radiation with the number of sunshine hours (Figure 3.4) in a day using empirical constants obtained by regression analysis. The well-known Angstrom relation for estimating the monthly average daily solar radiation on a horizontal surface is given as (Tiwari *et al*., 2016):

$$\frac{H_G}{H_o} = a_1 + b_1\,(\frac{\bar{n}}{\bar{N}}) \quad (3.10)$$

Where, H_G is monthly average daily global solar radiation in the terrestrial region,

$\bar{n}$ and $\bar{N}$ are the daily and maximum possible daily hours of bright sunshine,

a_1 and b_1 are regression coefficients given by,

$$a_1 = -0.11 + 0.235 \cos\phi + 0.32 \left(\frac{\bar{n}}{\bar{N}}\right) \quad (3.11)$$

$$b_1 = 1.449 - 0.533 \cos\phi - 0.694 \left(\frac{\bar{n}}{\bar{N}}\right) \quad (3.12)$$

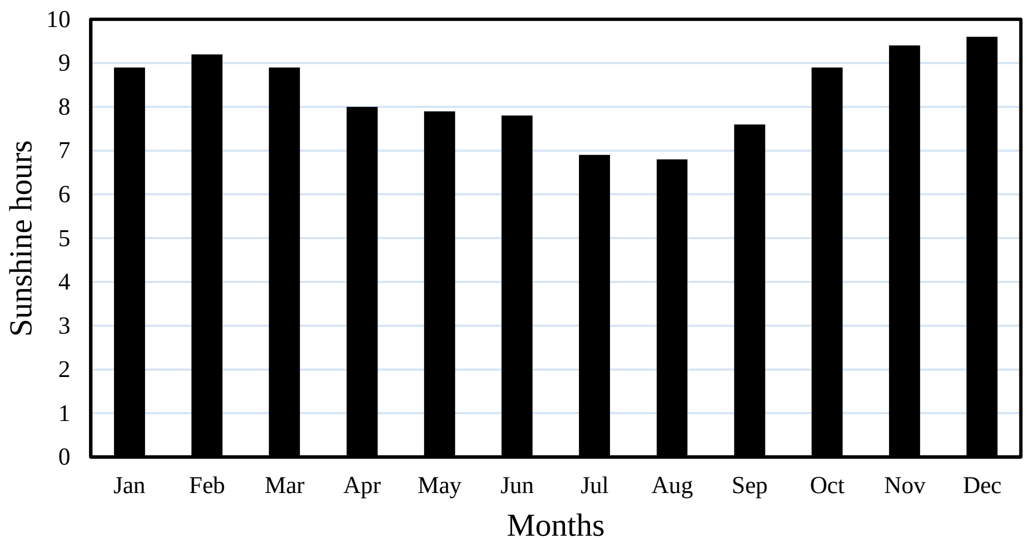

Figure 3.4: Sunshine hours of Adama for an average climatic condition of six years.

3.2.1.4 Estimation of monthly average daily diffuse and beam radiations on a horizontal surface

The monthly average daily diffuse radiation on a horizontal surface can be determined from the monthly average daily global radiation on a horizontal surface and the number of bright sunshine hours and is given by the correlation (Tiwari *et al.*, 2016):

$$\frac{H_d}{H_G} = 0.931 - 0.814\left(\frac{\bar{n}}{\bar{N}}\right) \quad (3.13)$$

The monthly average daily beam radiation on a horizontal surface is the difference between the monthly average daily global and diffuse radiations.

$$H_b = H_G - H_d \quad (3.14)$$

Figure 3.5 shows estimated variations of monthly average daily global, diffuse and beam radiations on a horizontal surface.

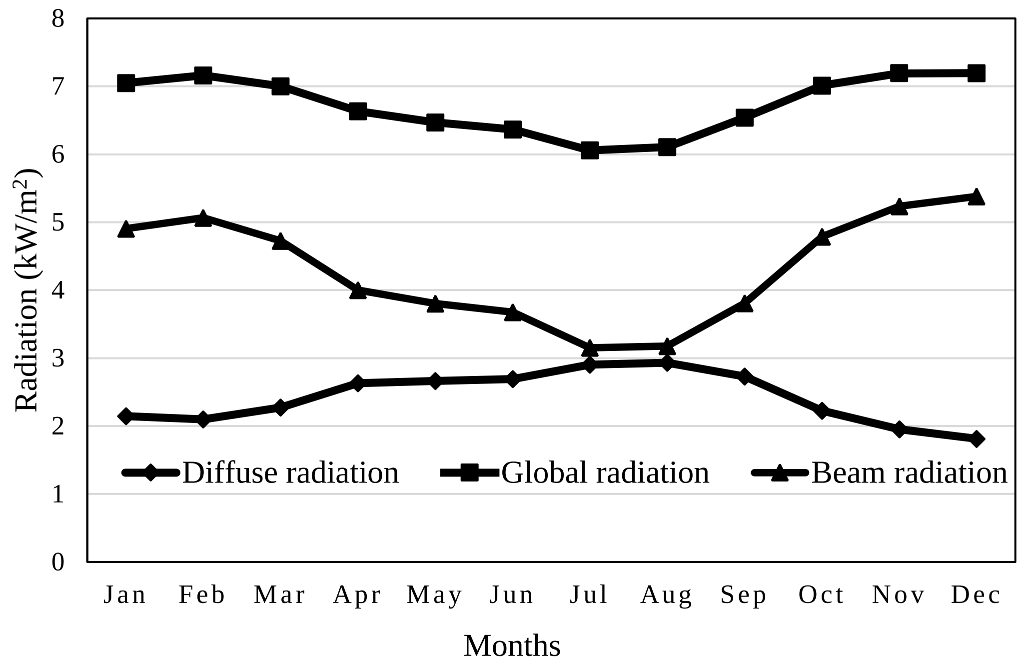

Figure 3.5: Monthly average daily global, diffuse and beam radiations on a horizontal surface.

3.2.1.5 Estimation of monthly average hourly global radiation on a horizontal surface

The monthly average hourly global radiation on a horizontal surface can be determined from the monthly average daily global radiation (Duffie and Beckman, 2013) as shown in Figure 3.6.

$$\frac{I_G}{H_G} = \frac{\pi}{24}(a_2 + b_2 \cos\omega)\left(\frac{\cos\omega - \cos\omega_{sr}}{\sin\omega_{sr} - \frac{\pi}{180}\,\omega_{sr}\cos\omega_{sr}}\right) \quad (3.15)$$

Where, $a_2 = 0.409 + 0.5016\sin(\omega_{sr} - 60)$ ………………………………………... (3.16)

$b_2 = 0.6609 - 0.4767\sin(\omega_{sr} - 60)$ ……………………………………… (3.17)

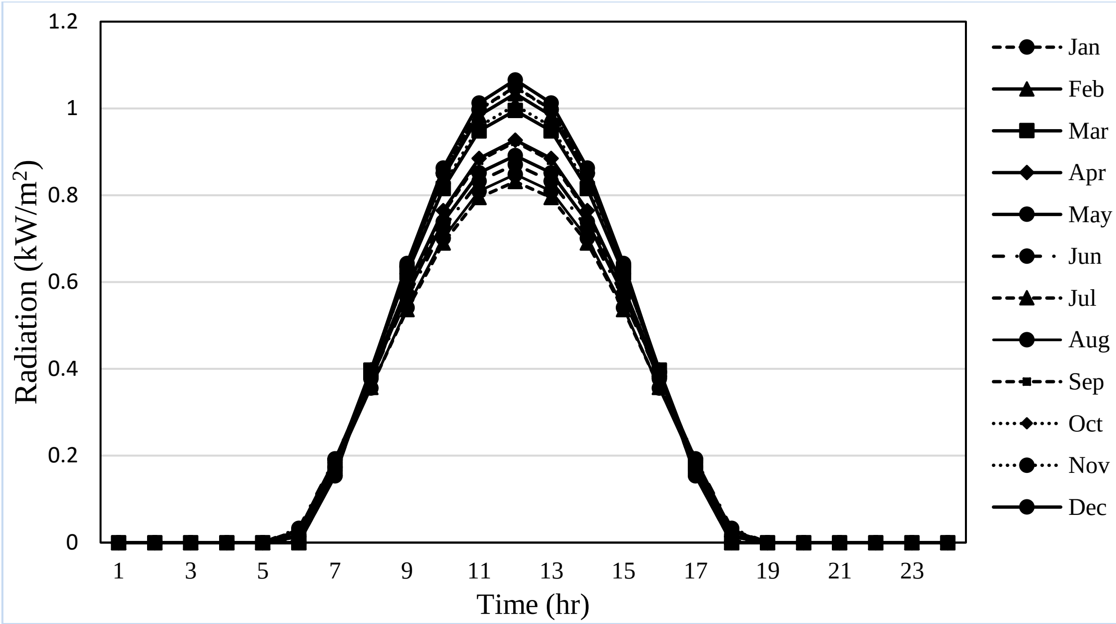

Figure 3.6: Monthly average hourly global radiation on a horizontal surface.

3.2.1.6 Estimation of monthly average hourly diffuse and beam radiations on a horizontal surface

The monthly average hourly diffuse radiation on a horizontal surface can be determined from the monthly average daily diffuse radiation on a horizontal surface (Duffie and Beckman, 2013) and presented in Figure 3.7.

$$\frac{I_d}{H_d} = \frac{\pi}{24}\left(\frac{\cos\omega - \cos\omega_{sr}}{\sin\omega_{sr} - \frac{\pi}{180}\,\omega_{sr}\cos\omega_{sr}}\right) \quad (3.18)$$

The monthly average hourly beam radiation on a horizontal surface is the difference between the monthly average hourly global and diffuse radiations as shown in Figure 3.8.

$$I_b = I_G - I_d \quad (3.19)$$

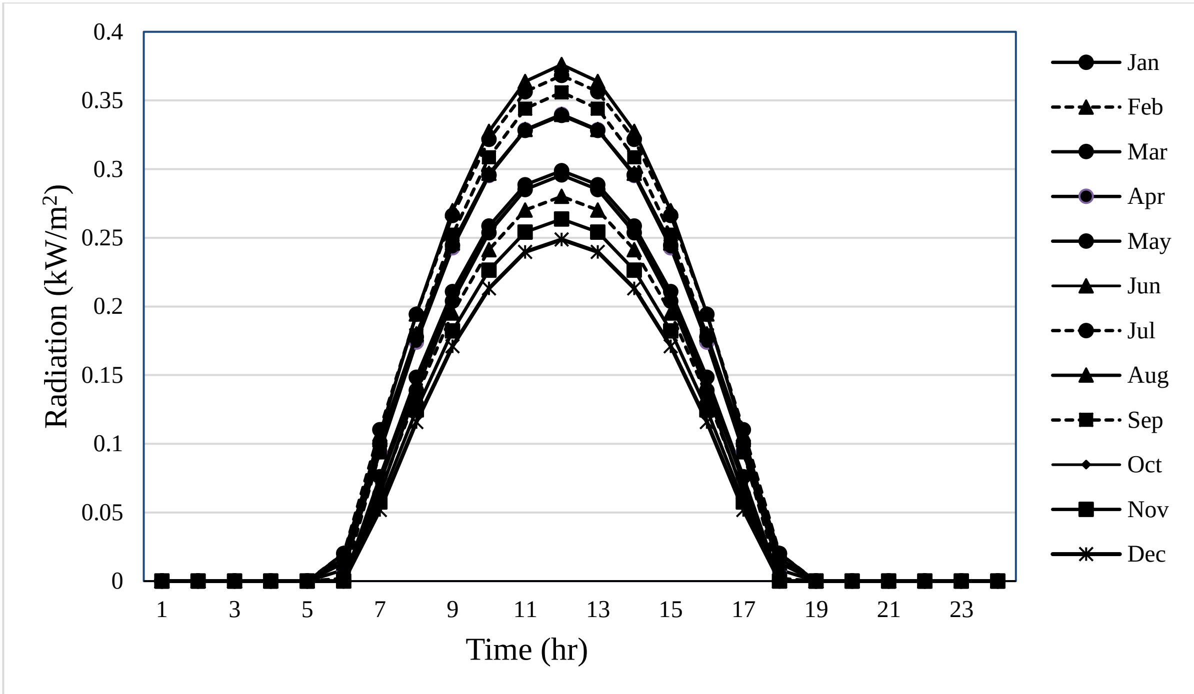

Figure 3.7: Monthly average hourly diffuse radiation on a horizontal surface.

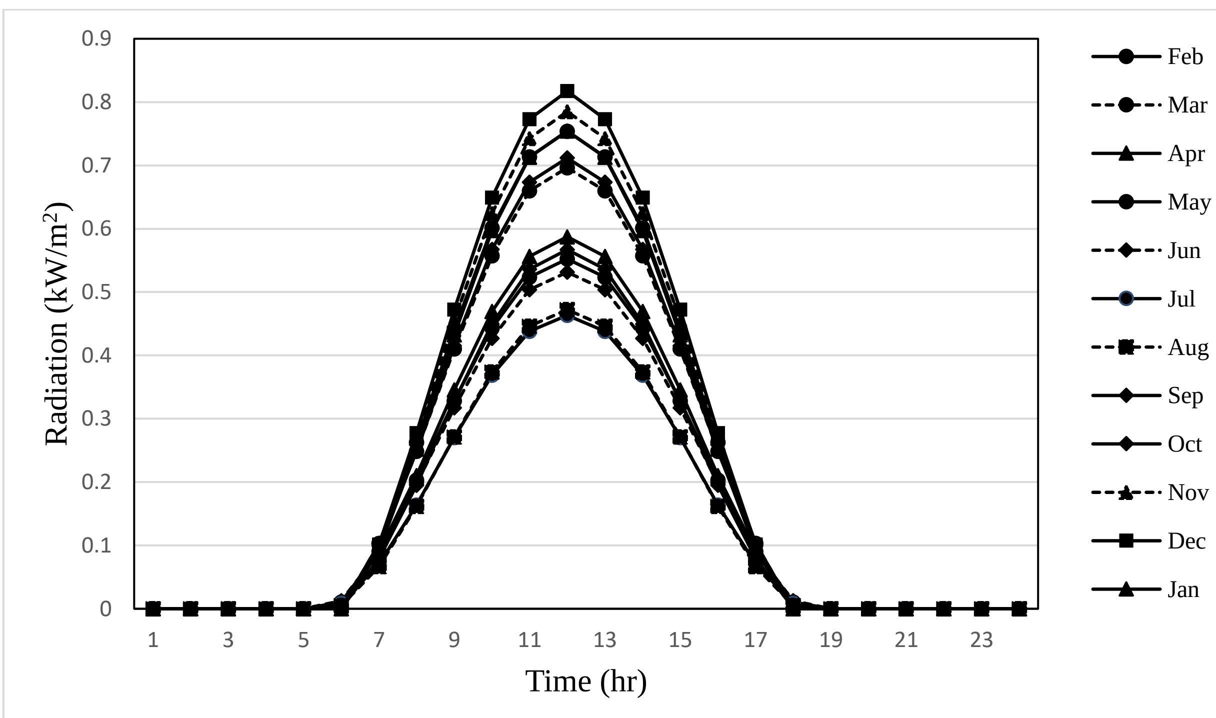

Figure 3.8: Monthly average hourly beam radiation on a horizontal surface.

3.2.1.7 Estimation of incident solar radiation on a tilted surface

The incident solar radiation on an inclined surface is the sum of the beam, diffuse and reflected solar radiation from various surfaces (from a horizontal surface and surfaces surrounding it). Therefore, the total incident solar radiation on a surface tilted at an angle **β** can be expressed in terms of the global, beam, diffuse and the total reflected radiation to the tilted surface (Duffie and Beckman, 2013) and shown in Figure 3.9.

$$I_T = I_b R_b + I_d \left(\frac{1+ \cos \beta}{2}\right) + I_G \rho_g \left(\frac{1- \cos \beta}{2}\right) \ldots\ldots\ldots\ldots\ldots\ldots\ldots\ldots \text{(3.20)}$$

Where, ρ_g is reflectivity of ground and its value is 0.2 for ordinary ground (Tiwari *et al.*, 2016).

R_b is the beam radiation factor which can be defined as the ratio of the incident beam radiation on a tilted surface to that on a horizontal surface.

$$R_b = \frac{\cos \theta}{\cos \theta_z} \ldots\ldots\ldots\ldots\ldots\ldots\ldots\ldots\ldots\ldots\ldots\ldots \text{(3.21)}$$

The collector tilt angle (β) for south facing collector can be expressed in terms of the latitude of the location where the collector is placed, usually β = latitude + 15° (Ahmad and Tiwari, 2009).

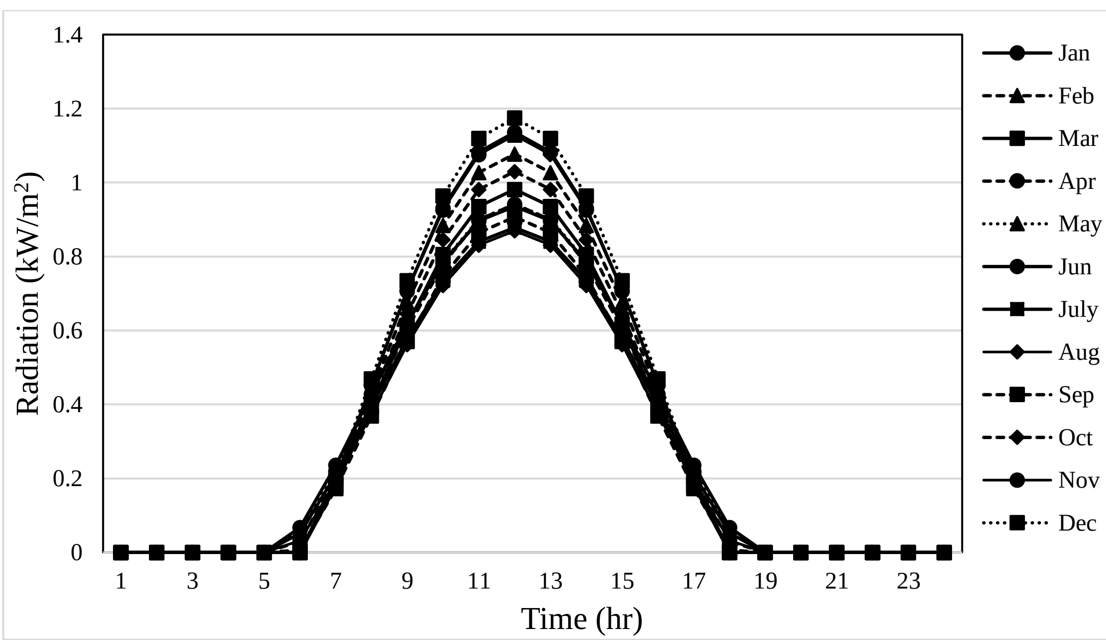

Figure 3.9: Monthly average hourly incident solar radiation on a tilted surface.

3.2.1.8 Estimation of hourly variation of atmospheric temperature

Hourly variation of atmospheric temperature is estimated from the daily maximum and minimum temperatures as shown in Figure 3.10. A sin-exponential model proposed by Parton and Logan (1981) is used and it describes the diurnal cycle by a sine function during daytime and a decreasing exponential function during nighttime. The major assumption of the model is the maximum temperature will occur sometime during the daylight hours before sunset and the minimum temperature will occur during the early morning hours. The mathematical description for day and nighttime, respectively are expressed as (Parton and Logan, 1981):

$$T_i = (T_{max} - T_{min}) \sin\left(\frac{\pi m}{Y+2a}\right) + T_{min} \quad (3.22)$$

$$T_i = (T_{sunset} - T_{min}) \exp\left(-\frac{bn}{Z}\right) + T_{min} \quad (3.23)$$

Where, T_i is temperature at the *i*th hour,

Y and Z are the length of the day and the night in h,

a is the lag coefficient for maximum temperature = 1.8 h and b is the nighttime temperature coefficient =2.2.

m is the number of hours after the minimum temperature occurs until sunset and n is the number of hours after sunset until the time of the minimum temperature.

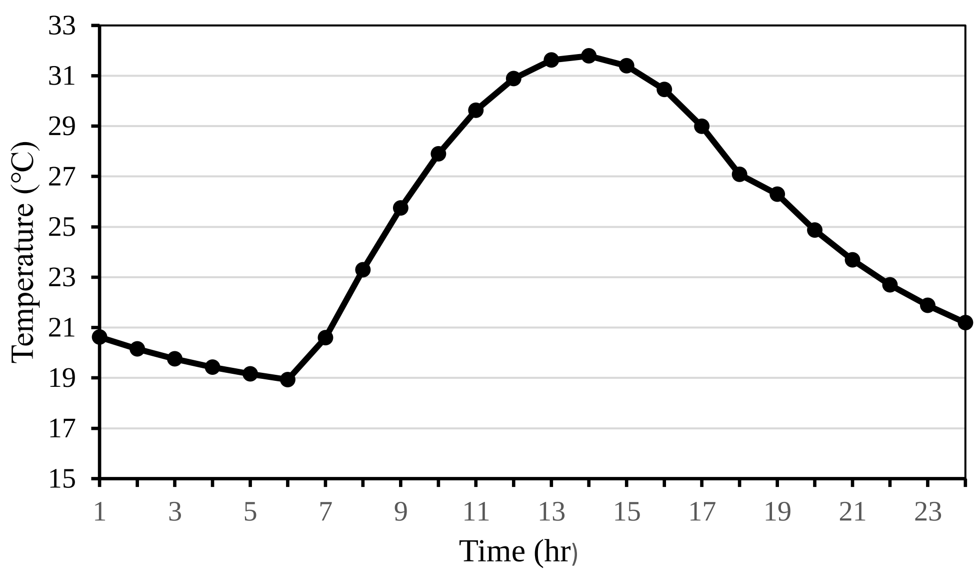

Figure 3.10: Average variation of ambient temperature of Adama.

CHAPTER FOUR

THEORETICAL ANALYSIS OF THE PCM INTEGRATED SOLAR DRYER

This chapter presents the theoretical analysis of the PCM integrated solar dryer. The analysis includes estimation of the quantity of energy and mass of air required for the drying process, sizing of the components of the dryer (flat plate solar air heater, latent heat storage and the drying chamber) and energy and exergy analysis of the flat plate solar air heater, latent heat storage and drying chamber. Numerical simulation of the solar air heater and latent heat storage is also presented in this chapter.

4.1 Description of the developed PCM integrated solar dryer

An indirect mode solar dryer integrated with a phase change material is developed in this study as shown in Figure 4.1. The main components of the dryer are a double pass flat plate solar air heater, a paraffin wax-based shell and tube latent heat storage system and a drying chamber. The main source of energy for the dryer is solar energy. Hot air required for the drying process is produced by the solar air heater by harvesting solar energy during the on-sunshine periods. This heated air is then passed through the latent heat thermal energy storage system. Part of the heat from the hot air is transferred to the storage and the remaining heat is used in the drying chamber. The heat stored in the thermal energy storage system is used to heat the air when the availability of solar energy is low or not available at all. This heated air is then supplied to the drying chamber where the products to be dried are placed. Finally, the hot air takes moisture from the product and leaves the drying chamber.

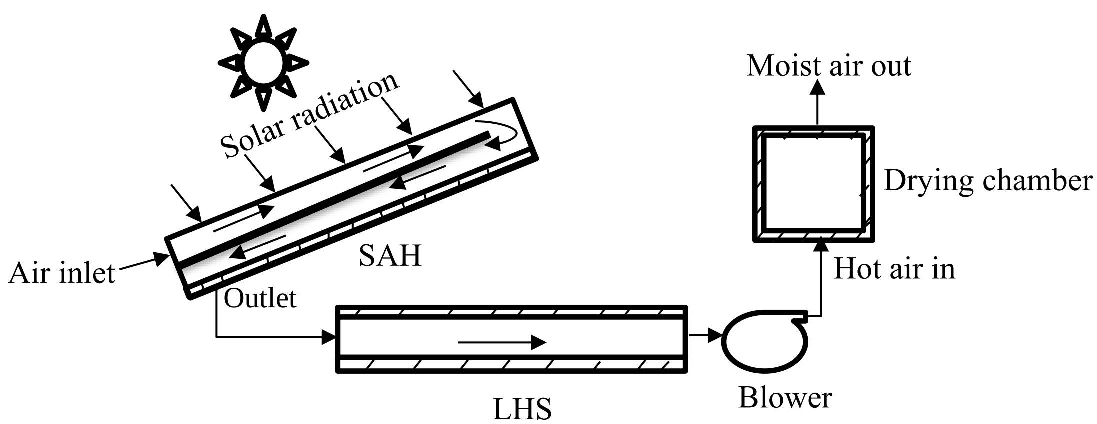

Figure 4.1: Schematic diagram of the developed dryer.

4.2 Design of the PCM integrated solar dryer

Drying is a process of removing moisture from products and energy is required to remove moisture. In solar dryers, the drying process is achieved by supplying hot air to the products from the solar air heater. The energy required to remove moisture from these products is supplied by this hot air. Therefore, energy and amount of air required should be first determined. Sizing of components of the dryer is then done based on the energy and air flow requirements.

Design of the PCM integrated flat plate solar dryer was done based on a capacity of 5 kg fish and the following points are considered while designing the dryer.

- ✓ Amount of moisture to be removed from the product.
- ✓ Amount of energy and air required for drying.
- ✓ Daily solar radiation to determine energy received by the dryer per day.
- ✓ Daily sunshine hours for the selection of total drying time.
- ✓ Wind speed to determine air vent dimensions.

4.2.1 Estimation of energy and air flow requirements

The quantity of energy and air flow required for the drying process mainly depends on the amount of moisture to be removed from the product. These parameters can be determined from the principle of psychometry and energy balance equation.

The following assumptions were made to estimate the amount of energy and air flow required for the drying process:

- ✓ Average initial moisture content of fish: 75% (wet basis) (Swami *et al.*, 2018)
- ✓ Desired final moisture content of fish: 10% (wet basis)
- ✓ Average ambient temperature of Adama: 28 ℃
- ✓ Average relative humidity of Adama: 55%
- ✓ Desired drying air temperature: 50 ℃

To preserve the color, texture, flavor and nutritional value of fish, the recommended temperature for drying fish is in the range of 45 and 55℃ (Reza *et al.*, 2009; Swami *et al.*, 2018; Sengar *et al.*, 2009; Hamdani *et al.*, 2018). Taking the average of these values, the desired drying temperature was taken as 50℃.

The amount of moisture to be removed from the product (m_v) during the drying process can be determined as (Forson *et al*., 2007):

$$m_v = \frac{m_p(M_i - M_f)}{(100 - M_f)} \qquad (4.1)$$

Where, m_p is mass of the product to be dried in kg and,

M_i and M_f are initial and final moisture contents of the product on a wet basis in %.

The amount of energy required to evaporate m_v kg of moisture was expressed as (Fudholi *et al*. 2014):

$$Q_v = m_v h_{fg} \qquad (4.2)$$

Where, h_{fg} is the latent heat of evaporation in kJ/kg H_2O, which can be determined using equation 4.3 and is to be increased by 20% to remove the bound moisture from the product (Youcef-Ali *et al*., 2001):

$$h_{fg} = 1.2 \times 4.186(597 - 0.56T_p) \qquad (4.3)$$

Where, T_p is the average temperature of the product in °C and can be determined as (Forson *et al*., 2007): $T_p = 0.25(3T_{id} + T_{amb})$ ………………………………………………… (4.4)

$T_p = 0.25(3 \times 50 + 28) = 44.5$ °C, $h_{fg} = 1.2 \times 4.186(597 - 0.56 \times 44.5) = 2873.67$ kJ/kg
Substituting the values of m_p =5 kg, M_i = 75%and M_f =10% into Eqn. (4.1) yields the amount of moisture to be removed from the product, m_v=3.6 kg and from Eqn. (4.2) the amount of energy required to evaporate 3.6 kg of moisture is Q_v =10.345 MJ.

The amount of air required for the drying process can be determined from the psychrometric chart if the equilibrium moisture content of the drying air is known (Sharma *et al*., 1986). If ambient air is heated from state A to state B, its relative humidity decreases and dry bulb temperature increases as shown in Figure 4.2. When drying air at a temperature of T_{id} and relative humidity of Rh_{id} passes through the drying product, its specific and relative humidity increases until an equilibrium state C is reached and the moisture content of the product at this state is known as equilibrium moisture content.

$$m_a = \frac{m_v}{w_f - w_i} \quad (4.5)$$

Where, w_f is the final or specific humidity of air corresponding to equilibrium condition and,

w_i is specific humidity of air at the beginning of drying process in kg vapour/kg dry air.

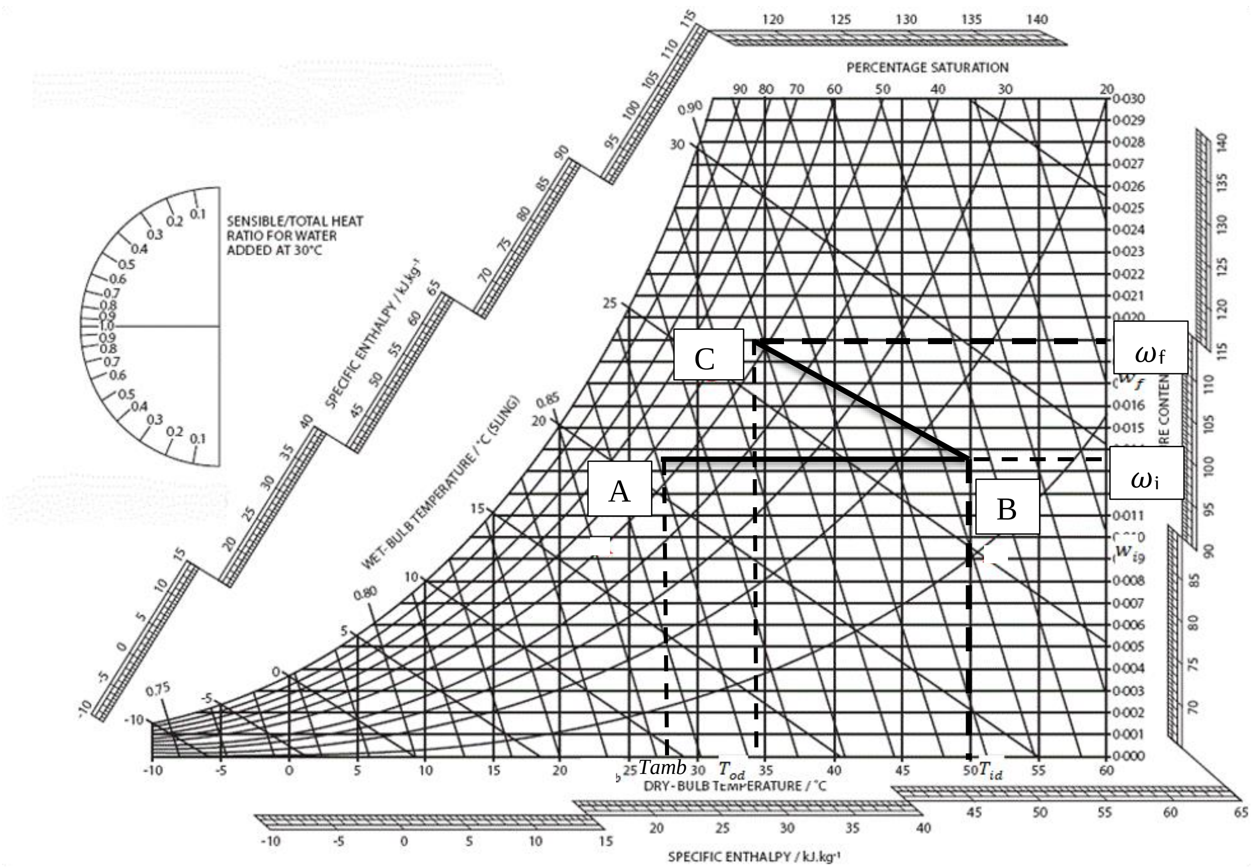

Figure 4.2: Sensible heating and theoretical drying on psychrometric chart.

The final or equilibrium specific humidity can be obtained from the final or equilibrium relative humidity using the psychrometric chart. The final or equilibrium relative humidity was calculated from the sorption isotherm equation (Dasin *et al*., 2019).

$$Rh_e = 100 a_w \quad (4.6)$$

Where, Rh_e is the final or equilibrium relative humidity in %,

a_w is the water activity determined using the sorption isotherm equation,

$$a_w = 1 - e^{\left[-e^{(0.914+0.5639 \ln M_e)}\right]} \quad (4.7)$$

Where, M_e is moisture content on a dry basis in percentage and can be expressed as:

$$M_e = \frac{M_f}{(100 - M_f)} \times 100 \quad \ldots\ldots\ldots\ldots\ldots\ldots\ldots\ldots\ldots\ldots \text{(4.8)}$$

Substituting the values of $M_f = 10\%$ into Eqn. (4.8) gives $M_e = 11.11\%$ and putting $M_e = 11.11\%$ into Eqn. (4.7) yields $a_w = 0.5144$, $Rh_e = 100 \times 0.5144 = 51.44\%$.

As shown in the psychrometric chart (Figure 4.2), when ambient air at a temperature of 28 ℃ and relative humidity 55% is heated to 50 ℃, its relative humidity decreases to 16% at a constant specific humidity of $w_i = 0.0135$ kg water/kg dry air. The dry bulb temperature and specific humidity corresponding to a relative humidity of 51.44% are T_{od} =34.5 ℃ and $w_f =$ 0.019 kg vapour/kg of dry air, respectively. Substituting the values of w_i and w_f into Eqn. (4.5), the quantity of air required to remove 3.6 kg of moisture is m_a =654.54 kg.

The amount of air required for the drying process can also be determined from the energy balance equation:

$$Q_v = m_a C_{pa}(T_{id} - T_{od}) \quad \ldots\ldots\ldots\ldots\ldots\ldots\ldots\ldots\ldots\ldots \text{(4.9)}$$

Where, m_a is mass of drying air in kg,

T_{id} and T_{od} are drying air temperature and dry bulb temperature of air corresponding to equilibrium state C in ℃.

C_{pa} is specific heat of humid air in kJ/kg. K, $C_{pa} = 1.005 + 1.88w$.

Substituting the values of $Q_v = 10.345$ MJ, T_{id} =50 ℃, T_{od} =34.5℃ and C_{pa}=1.033 kJ/kg. K into Eqn. (4.9) gives m_a = 646.098 kg which is almost the same as the value obtained in Eqn. (4.5).

The mass flow rate of air needed for drying was determined as (Forson *et al*., 2007):

$$\dot{m}_a = \frac{m_a}{t_d} \quad \ldots\ldots\ldots\ldots\ldots\ldots\ldots\ldots\ldots\ldots \text{(4.10)}$$

Where, t_d is the drying time in h.

The mass flow rate of the drying air affects the size of the components of the dryer and the energy requirement. The higher the mass flow rate, the larger the size of the components and the energy requirement. The average drying time of fish in different solar dryers varies from 8 h to 30 h (Yuwana *et al*., 2003; Hamdani *et al*., 2018; Sengar *et al*., 2009; Swami *et al*., 2018).

Assuming the average value of the drying time of 18 h, the total mass flow rate of air is found to be 0.01 kg/s.

The volumetric air flow rate was expressed as: $\dot{V}_a = \frac{\dot{m}_a}{\rho_a}$……...…………………...…… (4.11)

Where, ρ_a is density of drying air =1.18 kg/m^3.

Substituting the values of $\dot{m}_a = 0.01$ kg/s and $\rho_a = 1.18$ kg/m^3, $\dot{V}_a = 0.0085$ m^3/s.

4.2.2 Sizing of the energy storage

A phase change material (PCM) based shell and tube latent heat storage unit is selected as thermal energy storage for the developed solar drying system to reduce the fluctuations in the drying air temperature and also continuing the drying process for a few hours. The shell and tube type LHS have a faster melting rate compared to rectangular LHS for the same heat transfer area and volume (Vyshak and Jilani, 2007). To fix the size of the storage required for the drying process, the appropriate PCM should be selected first. The main criteria for selecting PCMs for drying operation is their melting temperature. The minimum melting temperature of the PCM should be 5 to 10 °C higher than the desired temperature of the drying air (Lane *et al.*, 1983). The desired average air temperature of the solar drying system is 50 °C. Therefore, paraffin wax of average melting temperature of 58-60 °C is selected as PCM since it is safe, non-toxic and easily available in the local market. List of some important paraffins and properties of the selected paraffin wax are presented in Table 4.1 and 4.2, respectively.

Table 4.1: List of some paraffins (Lingayat and Suple, 2013).

Paraffin	Melting temperature range (°C)	Heat of fusion (kJ/kg)
6106	44	189
P116	45-48	210
5853	48-50	189
6035	58-60	189
6403	62-64	189
6499	66-68	189

Table 4.2: Properties of the selected paraffin wax.

PCM	Melting point (°C)	Heat of fusion (kJ/kg)	Thermal conductivity (W/m. K)	Density (kg/m^3)	Specific heat (kJ/kg. K)
Paraffin wax	58-60	189	0.22	918	2.384

The latent heat storage is a shell and tube heat exchanger. The drying air passes through the tubes and the shell is filled with paraffin wax. Heat is transferred from the hot air to the paraffin wax through the tubes during the charging process and the process is reversed during the discharging time. The heat was stored during the day time when the solar radiation was available to heat the air in the solar air heater and this stored heat will then be supplied to the drying chamber when there is no more heat supply from the solar air heater.

The latent heat thermal energy storage system was designed for storing the heat needed in the drying chamber for the drying process. Assuming the storage will store the heat for 2 off-sunshine hours per day, the quantity of heat needed to be stored in the latent heat thermal energy storage system can be estimated by considering a safety factor of 1.5 for the change in temperature $\Delta T = T_{id} - T_{amb}$ (Niyas *et al*., 2017).

$$Q_s = \dot{m}_a C_{pa} t(1.5\Delta T) \quad (4.12)$$

The amount of PCM required to store Q_s amount of heat in the latent heat thermal energy storage system was determined as (Niyas *et al*., 2017):

$$Q_s = m_{pf} L_{pf} \quad (4.13)$$

Where, m_{pf} and L_{pf} are the mass and latent heat of fusion of paraffin wax in kg and kJ/kg.

The volume of the PCM can be calculated from, $V_{pf} = \frac{m_{pf}}{\rho_{pf}}$ ……………………… (4.14)

The volume of the tank is the sum of the volume of the PCM and the volume of the tubes.

$$V_T = V_{pf} + V_t \quad (4.15)$$

The volume of the tubes is: $V_t = \pi n_t {R_o}^2 L$ ……………………… (4.16)

To improve the heat transfer in the axial direction than in the radial direction, the length to diameter ratio of the storage can be taken as 5 (Niyas *et al*., 2017; Velraj *et al.*, 1997 and Sharma *et al*., 2005).

$$V_T = \frac{\pi}{4} D^2 L \quad \text{(4.17)}$$

Substituting the values of $\dot{m}_a$ =0.01 kg/s, C_{pa}= 1.033 kJ/kg. K, $T_{id} = 50$℃, $T_{amb} = 28$ °C and t = 2 h into Eqn. (4.12) gives $Q_s = 2975.04$ kJ and substituting the values of $Q_s = 2975.04$ kJ and L_{pf} =189 kJ/kg into Eqn. (4.13) gives m_{pf} =16 kg. From Eqns. (4.14), (4.15) and (4.16), $V_{pf} = 0.0174$ m^3, V_t=0.014 m^3 and V_T=0.0314 m^3 and from Eqn. (4.17), D = 0.2 m and L=1 m.

Other parameters and dimensions of the thermal energy storage system were fixed based on the design procedure proposed by Shamsundar *et al.* (1992) which is useful for the preliminary design of the shell and tube latent heat storage and are presented in Appendix B.

4.2.3 Sizing of flat plate solar air heater

A double pass (two pass) type SAH was selected for the drying system. In this type of SAH, the air first passes between the glass cover and the absorber and then passes under the absorber as shown in Figure 4.3. The efficiency of this SAH is 7 to 19% higher than the conventional SAH without incurring any additional cost (Omojaro and Aldabbagh, 2010).

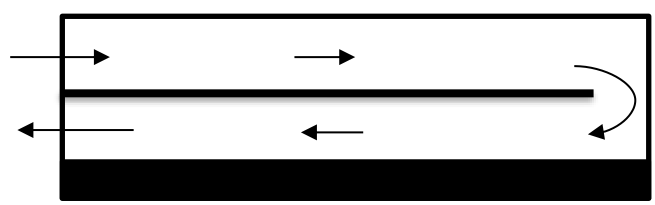

Figure 4.3: Schematic of double pass SAH.

The total area of the solar air heater required for producing the hot air can be determined if the total amount of heat required to be supplied, efficiency of the solar air heater for a given mass flow rate, duration of sunshine hours and average solar radiation intensity are known. The quantity of heat required for the drying process is the sum of the heat required for producing hot air at 50 ℃ and the heat required for melting the paraffin wax at the storage during the sunshine hours per day which can be estimated as:

$$Q_u = \dot{m}_a C_{pa} t(T_{id} - T_{amb}) + m_{pf} C_{pf}(T_m - T_{amb}) + m_{pf} L_{pf} \quad (4.18)$$

Where, $\dot{m}_a$ is the mass flow rate of drying air in kg/s,

C_{pa} and C_{pf} are specific heats of drying air and paraffin wax in kJ/kg.K, respectively,

T_{id} is drying air temperature or desired temperature to be supplied to the drying chamber in °C,

T_{amb} and T_m are ambient temperature and melting temperature in of paraffin wax in °C,

L_{pf} and m_{pf} are the latent heat of fusion in kJ/kg and mass of paraffin wax in kg.

The solar drying system collector area can be determined from the total amount of solar energy absorbed by the tilted collector during the drying period and the total amount of heat required for the drying process (Forson *et al.*, 2007).

$$A_c = \frac{Q_u}{(I\alpha_a \tau_c)t\eta} \quad (4.19)$$

Where, A_c is collector area in m^2,

I is average solar radiation intensity on an inclined surface in W/m^2 and t is total number of sunshine hours,

α_a and τ_c are absorptivity of the absorber plate and transmissivity of the cover plate,

η is collector efficiency and its value being 30 to 50% (Sodha *et al.*, 1987),

For optimum performance of solar air heaters, the recommended range of the aspect ratio (ratio of the length of the air-heater (solar collector) to the width) can be taken as 1.5. Therefore, the length, L_c, and width, W_c, of the solar air heater are determined as (Forson *et al.*, 2007):

$$L_c = \frac{A_c}{W_c} \quad (4.20)$$

Substituting the values of $\dot{m}_a$ =0.01 kg/s, T_{id} = 50 °C, T_{amb} = 28 °C, C_{pa} = 1.033 kJ/kg.K, C_{pf}= 2.384 kJ/kg.K, m_{pf} = 16 kg, T_m =58 °C, L_{pf} = 189kJ/kg and t = 7 h into Eqn. (4.18) gives Q_u = 9895.27 kJ and substituting the values of Q_u = 9895.27 kJ, I = 0.7 kW/m^2, α_a = 0.85, τ_c = 0.92, η = 0.35 and t=7 h into Eqn. (4.19), the area of the solar collector becomes, A_c = 2.05 m^2 and from Eqn. (4.20), W_c = 1.17 m and L_c = 1.76 m.

The specifications of the solar air heater are presented in Table 4.3.

Table 4.3: Specifications of the solar air heater.

Description	Specifications
Collector type	Flat plate collector
Number of passes	Two (double pass)
Collector area	2.05 m^2
Glazing	5 mm thick window glass
Absorber	Steel sheet metal
Insulation	25 mm thick foam
Space between glazing and absorber	60 mm
Space between absorber and base plate	40 mm
Emissivity of cover plate	0.8 (Dimitrios, 2015)
Absorptivity of absorber plate	0.85 (*https://www.engineersedge.com/properties_of_metals)*
Absorptivity of cover plate	0.05 (Dimitrios, 2015)
Transmissivity of cover plate	0.92 (Dimitrios, 2015)
Thermal conductivity of absorber plate	64.8 W/m. K (*https://www.engineersedge.com/properties_of_metals)*
Thermal conductivity of insulation	0.0256W/m. K *(https://thermtest.com/materials-database)*

4.2.4 Sizing of the drying chamber

The design of the drying chamber is based on the volume required for 5kg of fish. The bulk density of fish is 490 kg/m^3 (Khater *et al*., 2014).

The volume of the product can be determined as:

$$V_p = \frac{m_p}{\rho_p} \qquad (4.21)$$

The area of the drying bed is determined as:

$$A_{db} = \frac{V_p}{x_p \rho_p \zeta} \qquad (4.22)$$

Where, ρ_p is bulk density of the product in kg/m^3,

x_{dp} is thickness of the product in m and ζ is drying bed porosity.

The thickness of the fish after removing the organs is 25 mm and a porosity of 50% is used for the design.

The breadth of the drying chamber, B, is made equal to the Width (W_c) of the air heater. Thus, the length of the drying chamber (L_{dc}) was determined from the relation:

$$L_{dc} = \frac{A_{dc}}{W_c} \quad (4.23)$$

Substituting the values of m_p= 5 kg, ρ_p= 490 kg/m^3, ζ= 50% and x_p= 25 mm into Eqn. (4.21) and (4.22), V_p= 0.0102 m^3, A_{db} =0.82 m^2 and L_{dc}= 0.7 m considering the number of trays as 2. Taking the distance between the trays as 0.25 m and height of each tray as 0.05 m, the total height of the tray loading section becomes 0.35 m. The total height of the drying chamber is the sum of the height above the top tray, height below the bottom tray and the total height of the trays. The height above the top tray and below the bottom tray are taken as 0.3 m and the height of the drying chamber becomes 0.95m.

4.3 Energy and exergy analysis

Energy and exergy analysis of the PCM integrated solar dryer is performed based on the general mass and energy conservation equations employing first and second laws of thermodynamics. Energy and exergy analysis help to evaluate the performance of a system in terms of energy and exergy efficiencies. Energy and exergy analysis of the components of the dryer and also the efficiency of the overall drying system is presented in this section.

4.3.1 Energy analysis

Energy analysis is performed based on the first law of thermodynamics to evaluate energy efficiencies by using energy balance equations. This balance is employed to determine and reduce heat losses. The general mass and energy conservation equations for the steady flow open system can be expressed as (Cengel and Boles, 2010):

Mass balance: $\sum \dot{m}_i = \sum \dot{m}_o$ ……………………………………………………….… (4.24)

Energy balance: $\dot{Q} - \dot{W} = \sum \dot{m}_o \left(h_o + \frac{{v_o}^2}{2} + Z_o g\right) - \sum \dot{m}_i \left(h_i + \frac{{v_i}^2}{2} + Z_i g\right)$………….. (4.25)

Where, $\dot{Q}$ and $\dot{W}$ are heat and work transfer rates, respectively in W,

$\dot{m}_o$ and $\dot{m}_i$ are outlet and inlet mass flow rates of air in kg/s, respectively,

h_o and h_i are outlet and inlet enthalpies of air in kJ//kg, respectively,

v_o and v_i are inlet and outlet velocities of air in m/s, respectively,

Z_o and Z_i are inlet and outlet heights from the reference plane in m, respectively,

g is acceleration due to gravity in m/s^2.

4.3.1.1 Energy analysis of the solar air heater

The thermal performance of the solar air heater can be determined from the rate of heat input to the SAH, the rate of heat loss from the SAH and the rate of useful heat gained by the SAH (Ramani *et al*., 2010). Since the change in velocity between the inlet and the exit is negligible and also the inlet and outlet of the solar air heater were located at the same height, the effects of kinetic and potential energies can be neglected and the mass and energy conservation equation for the solar air heater can be expressed as:

$$\dot{Q}_{inSAH} - \dot{Q}_{lSAH} = \dot{m}_o(h_o - h_i) \quad (4.26)$$

$$\dot{m}_o = \dot{m}_i = \dot{m}_a \quad (4.27)$$

Where, $\dot{Q}_{inSAH}$ is the rate of heat input to the solar air heater in W,

$\dot{Q}_{lSAH}$ is the rate of heat loss in the solar air heater in W,

h_o and h_i are the specific enthalpy of air at the inlet and outlet of the solar air heater kJ/kg,

The right-hand term of Eqn. (4.26) is the rate of useful heat gained by the solar air heater and it can be written as (Struckmann, 2008):

$$\dot{Q}_{uSAH} = \dot{m}_a C_{pa}(T_{oSAH} - T_{iSAH}) \quad (4.28)$$

Where, T_{oSAH} and T_{iSAH} are the outlet and inlet temperatures of the solar air heater, respectively.

The rate of heat input to the solar air heater can be expressed as (Struckmann, 2008):

$$\dot{Q}_{inSAH} = \alpha_a \tau_c I A_{SAH} \quad (4.29)$$

Where, I is average solar radiation intensity in W/m^2,

α_a andτ_c are absorptivity of the absorber plate transmissivity of the cover plate,

A_{SAH} is the area of the solar air heater in m^2.

The rate of heat loss from the solar air heater can be determined as:

$$\dot{Q}_{lSAH} = \alpha_a \tau_c I A_{SAH} - \dot{Q}_{uSAH} \quad \text{(4.30)}$$

The rate of heat loss in the form of overall heat loss coefficient, plate temperature and ambient temperature can be written as (Duffie and Beckman, 2013):

$$\dot{Q}_{lSAH} = U A_{SAH}\left(T_p - T_{amb}\right) \quad \text{(4.31)}$$

Where, U is overall heat loss coefficient in W/m^2. K and T_p is absorber plate temperature in °C.

The rate of heat gain by the solar air heater is expressed as (Ramani *et al*., 2010):

$$\dot{Q}_{uSAH} = A_{SAH} F_R\left(I\alpha_a \tau_c - U(T_p - T_{amb}\right) \quad \text{(4.32)}$$

Where, $F_R$is the collector heat removal factor which relates the actual useful energy gain of the collector to the useful gain if the whole collector surface were at the fluid inlet temperature and is expressed as (Duffie and Beckman, 2013):

$$F_R = \frac{\dot{m}_a C_{pa}}{U A_{SAH}}\left[1 - exp\left(\frac{-F\prime U A_{SAH}}{\dot{m}_a C_{pa}}\right)\right] \quad \text{(4.33)}$$

The overall heat loss coefficient comprises the top, bottom and side losses. But the value of side loss is very small compared to the top and bottom and the overall heat loss coefficient is expressed as (Duffie and Beckman, 2013):

$$U = U_t + U_b \quad \text{(4.34)}$$

The top heat loss coefficient for single glazing is determined as:

$$U_t = \left[\frac{1}{h_w} + \frac{1}{\frac{C}{T_p}\left[\frac{T_p - T_{amb}}{1+f}\right]^e}\right]^{-1} + \frac{\sigma\left(T_p + T_{amb}\right)\left(T_p{}^2 + T_{amb}{}^2\right)}{\left(\varepsilon_p + 0.00591 h_w\right)^{-1} + \frac{1+f+0.133\varepsilon_p}{\varepsilon_g} - 1} \quad \text{(4.35)}$$

$$f = 1.07866\left(1 + 0.089 h_w - 0.1166 h_w \varepsilon_g\right) \quad \text{(4.36)}$$

$$C = 520(1 - 0.00005\beta^2) \quad \text{(4.37)}$$

$$e = 0.430\left(1 - \frac{100}{T_p}\right) \quad \text{(4.38)}$$

Where, β is collector tilt in degrees and ε_g and ε_p are the glass cover and absorber plate emissivity, respectively.

The top heat loss coefficient can also be expressed as a function of the glass cover temperature and sky temperature.

$$U_t = \frac{h_w(T_g - T_{amb}) + \sigma\varepsilon_g({T_g}^4 - {T_{sky}}^4)}{T_p - T_{amb}} \quad \text{(4.39)}$$

Where, T_g is the glass cover temperature in °C,

T_{sky} is sky temperature: $T_{sky} = T_{amb} - 6$ ..... (4.40)

V_w is wind speed and h_w is heat transfer coefficient due to wind: $h_w = 5.7 + 3.8V_w$ ... (4.41)

The bottom heat loss coefficient is given as:

$$U_b = \frac{k_b}{\delta_b} \quad \text{(4.42)}$$

Where, k_b and δ_b are the insulation thermal conductivity in W/m.K and thickness, respectively.

Energy efficiency: the thermal efficiency of the solar air heater is defined as the ratio of the useful heat gained to the absorbed solar energy and expressed as (Ramani *et al.*, 2010):

$$\eta_{SAH} = \frac{\dot{m}_a C_{pa}(T_{oSAH} - T_{iSAH})}{\alpha_a \tau_c I A_{SAH}} \quad \text{(4.43)}$$

4.3.1.2 Energy analysis of the thermal energy storage

The major performance parameters to evaluate the characteristics of a latent heat thermal energy storage system are (Niyas *et al.*, 2017),

a) Charging time: defined with respect to the temperature rise of the PCM. When the entire PCM is completely melted, the latent heat storage unit is called fully charged.

b) Discharging time: defined with respect to the temperature decrease of the PCM. When the entire PCM solidifies, the latent heat storage unit is called fully discharged.
c) Energy stored and discharged: energy gets stored in the PCM during the charging time and discharged from the PCM to the air during the discharging time in the form of sensible and latent heat.

The total energy stored and discharged as sensible and latent heat was expressed as:

$$E_{Tch} = m_{pf}C_{pf,s}\left(T_m - T_{ini,s}\right) + m_{pf}L_f\theta + m_{pf}C_{pf,l}\left(T_{fin,l} - T_m\right) \quad (4.44)$$

$$E_{Tdich} = m_{pf}C_{pf,l}\left(T_{ini,l} - T_m\right) + m_{pf}L_f(1-\theta) + m_{pf}C_{pf,s}\left(T_m - T_{fin,s}\right) \quad (4.45)$$

Where, T_{ini} is initial temperature in °C and θ is melt fraction.

The first and third terms of Eqns. (4.44) and (4.45) represent sensible heat stored and discharged, respectively and the second term represents latent heat stored and discharged.

d) Melt fraction: a non-dimensional parameter that quantifies the percentage of the liquid phase of the PCM when it exists in a two-phase form. The highest temperature at which the PCM is completely in the solid state is known as solidus temperature and the lowest temperature at which the PCM is completely in liquid state is called liquidus temperature.

$$\theta = \frac{T - T_s}{T_l - T_s} = \begin{cases} 0 \; for \; T < T_s \\ 0 - 1 \; for \; T_s \le T \le T_l \\ 1 \; for \; T > T_l \end{cases} \quad (4.46)$$

Where, T_s and T_l are the solidus and liquidus temperatures in °C, respectively

The performance of a latent heat storage system can also be determined in terms of the heat input and heat recovered by the heat transfer fluid (Dincer and Rosen, 2007). The instantaneous heat input and net heat input or transferred to the storage during the charging process is determined as:

$$\dot{Q}_{ich} = \dot{m}_a C_{pa}\left(T_{iES} - T_{oES}\right) \quad (4.47)$$

$$Q_{ich} = \int_0^t \dot{Q}_{ch}\,dt \quad (4.48)$$

Where, T_{iES} and T_{oES} are the inlet and outlet temperature of the energy storage, respectively.

The instantaneous and net heat recovered from the storage during the discharging process is expressed as:

$$\dot{Q}_{odich} = \dot{m}_a C_{pa}(T_{oES} - T_{iES}) \quad (4.49)$$

$$Q_{odich} = \int_0^t \dot{Q}_{dich} dt \quad (4.50)$$

The overall efficiency of the energy storage also called the percentage of the energy recovered, is defined as the ratio of the net heat recovered during the discharging period to the net heat input during the charging period.

$$\eta_{ES} = \frac{Q_{dich}}{Q_{ch}} \quad (4.51)$$

4.3.1.3 Energy analysis of the drying chamber

During the dehumidification process at the drying chamber, the heat used is estimated as (Akbulut and Durmus, 2010):

$$\dot{Q}_{dc} = \dot{m}_a C_{pa}(T_{idc} - T_{odc}) \quad (4.52)$$

Where, T_{idc} and T_{odc} are inlet and outlet temperatures of the drying chamber in °C, respectively.

The energy utilization ratio of the drying chamber is calculated as (Fudholi *et al*., 2014):

$$EUR = \frac{\dot{m}_a C_{pa}(T_{idc} - T_{odc})}{\dot{m}_a C_{pa}(T_{oSAH} - T_{iSAH})} \quad (4.53)$$

The total mass of moisture evaporated from the product during the drying process is expressed as:

$$m_v = \frac{m_p(M_i - M_f)}{(100 - M_f)} \quad (4.54)$$

Where, m_p, M_i and M_f are mass of product in kg and initial and final moisture contents of the product in %, respectively.

The thermal efficiency of the drying chamber is the ratio of the actual temperature drop to the maximum possible temperature drop of the drying air (Fudholi *et al*., 2014).

$$\eta_{dc} = \frac{(T_{idc} - T_{odc})}{(T_{idc} - T_{amb})} \quad (4.55)$$

4.3.2 Exergy analysis

Exergy is the maximum amount of work which can be produced by the system when it is in equilibrium with the surrounding. Exergy analysis is a thermodynamic analysis technique based on the second law of thermodynamics. It provides an alternative means of assessing and comparing processes and systems and yields efficiencies which provide a true measure of how nearly the performance of an actual system approaches the ideal. It clearly identifies the causes and locations of thermodynamic losses than energy analysis (Dincer and Rosen, 2007).

Exergy analysis for each component of the drying system is performed based on the exergy flow diagram shown in Figure 4.4 and the following assumptions were used during the analysis.

- The flow is assumed to be steady,
- Effects of kinetic and potential energies were neglected,
- Change in pressure between the inlet and outlet was neglected,
- Exergy loss in the product was negligible,

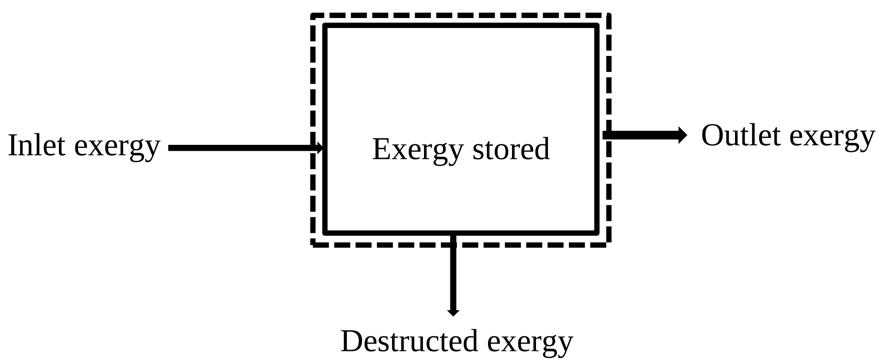

Figure 4.4: Exergy flow diagram

The steady flow exergy balance equation is written as:

$$\sum \dot{E}x_{in} - \sum \dot{E}x_{out} = \sum \dot{E}x_{dest} \quad \ldots\ldots (4.56)$$

Where, $\dot{E}x_{in}$, $\dot{E}x_{out}$, and $\dot{E}x_{dest}$ are the total inlet, outlet and destructed exergy rates, respectively.

The general form of a steady flow exergy equation is expressed as (Fudholi *et al.*, 2014):

$$\dot{E}x = \dot{m}_a C_{pa}\left(T - T_{amb} - T_{amb}\ln\frac{T}{T_{amb}}\right) \quad \ldots\ldots (4.57)$$

4.3.2.1 Exergy analysis of the solar air heater

The inlet exergy to the solar air heater consists of the exergy of inlet fluid and the exergy absorbed from the sun.

Exergy input to the solar air heater is given as (Jafarkazemi and Ahmadifard, 2013):

$$\dot{Ex}_{inSAH} = \left[1 - \frac{T_{amb}}{T_s}\right] \dot{Q}_{inSAH} \quad (4.58)$$

Where, T_s is the apparent sun temperature which is 75% of the black body temperature of the sun assumed to be 4500K.

The exergy of the inlet and outlet fluid is determined as:

$$\dot{Ex}_{if} = \dot{m}_a C_{pa} \left(T_{iSAH} - T_{amb} - T_{amb} \ln \frac{T_{iSAH}}{T_{amb}}\right) \quad (4.59)$$

$$\dot{Ex}_{of} = \dot{m}_a C_{pa} \left(T_{oSAH} - T_{amb} - T_{amb} \ln \frac{T_{oSAH}}{T_{amb}}\right) \quad (4.60)$$

From Eqns. (4.59) and (4.60), the exergy received by the working fluid of the solar air heater is computed as:

$$\dot{Ex}_{rSAH} = \dot{m}_a C_{pa} \left[(T_{oSAH} - T_{iSAH}) - T_{amb} \ln \left(\frac{T_{oSAH}}{T_{iSAH}}\right)\right] \quad (4.61)$$

Exergy destruction: the exergy destruction in the solar air heater is determined as (Jafarkazemi and Ahmadifard, 2013):

$$\dot{Ex}_{destSAH} = \left[1 - \frac{T_{amb}}{T_s}\right] \dot{Q}_{inSAH} - \dot{m}_a C_{pa} \left[(T_{oSAH} - T_{iSAH}) - T_{amb} \ln \left(\frac{T_{oSAH}}{T_{iSAH}}\right)\right] \quad (4.62)$$

Exergy efficiency: the exergy efficiency of the solar air heater was expressed as:

$$\eta_{ExSAH} = 1 - \frac{\dot{Ex}_{destSAH}}{\dot{Ex}_{inSAH}} = \frac{\dot{Ex}_{rSAH}}{\dot{Ex}_{inSAH}} \quad (4.63)$$

$$\eta_{ExSAH} = \frac{\dot{m}_a C_{pa}\left[(T_{oSAH} - T_{iSAH}) - T_{amb} \ln\left(\frac{T_{oSAH}}{T_{iSAH}}\right)\right]}{\left[1 - \frac{T_{amb}}{T_s}\right]\dot{Q}_{inSAH}} \quad (4.64)$$

4.3.2.2 Exergy analysis of the energy storage

The instantaneous exergy input to the energy storage and instantaneous exergy recovered from the energy storage during the charging and discharging process is expressed as (Dincer and Rosen, 2011):

$$\dot{E}x_{ich} = \dot{m}_a C_{pa}\left[(T_{iES} - T_{oES}) - T_{amb}\ln\left(\frac{T_{iES}}{T_{oES}}\right)\right] \quad (4.65)$$

$$\dot{E}x_{odich} = \dot{m}_a C_{pa}\left[(T_{oES} - T_{iES}) - T_{amb}\ln\left(\frac{T_{oES}}{T_{iES}}\right)\right] \quad (4.66)$$

The net exergy input and exergy recovered during the charging and discharging periods, respectively, are evaluated as:

$$Ex_{ich} = \int_0^t \dot{E}x_{ch}dt \quad (4.67)$$

$$Ex_{odich} = \int_0^t \dot{E}x_{dich}dt \quad (4.68)$$

The exergy efficiency of the energy storage is defined as the ratio of the net exergy recovered during the discharging period to the net exergy input during the charging period.

$$\eta_{ExES} = \frac{Ex_{dich}}{Ex_{ch}} \quad (4.69)$$

4.3.2.3 Exergy analysis of the drying chamber

The exergy inflow to the drying chamber is determined as (Fudholi *et al*., 2014):

$$\dot{E}x_{idc} = \dot{m}_a C_{pa}\left[(T_{idc} - T_{amb}) - T_{amb}\ln\left(\frac{T_{idc}}{T_{amb}}\right)\right] \quad (4.70)$$

The exergy outflow from the drying chamber is expressed as:

$$\dot{E}x_{odc} = \dot{m}_a C_{pa}\left[(T_{odc} - T_{amb}) - T_{amb}\ln\left(\frac{T_{odc}}{T_{amb}}\right)\right] \quad (4.71)$$

The exergy loss during the drying process is given as:

$$\dot{E}x_{loss} = \dot{E}x_{idc} - \dot{E}x_{odc} \quad (4.72)$$

$$\dot{E}x_{loss} = \dot{m}_a C_{pa}\left[(T_{idc} - T_{odc}) - T_{amb}\ln\left(\frac{T_{idc}}{T_{odc}}\right)\right] \quad (4.73)$$

The exergy efficiency of the drying chamber which is the ratio of the exergy outflow from the drying chamber to the exergy inflow to the drying chamber is expressed as (Fudholi *et al*., 2014):

$$\eta_{Exdc} = \frac{\dot{Ex}_{odc}}{\dot{Ex}_{idc}} \quad (4.74)$$

4.4 Performance of the drying system

The performance of the PCM integrated solar drying system can be evaluated in terms of specific energy consumption and overall drying efficiency of the system (Fudholi *et al*., 2014).

Specific energy consumption which is the ratio of the total energy input to the drying system to the total moisture removal from the product is expressed as.

$$SEC = \frac{P_t}{m_v} \quad (4.75)$$

Where, P_t is the total energy input which is the sum of the solar energy incident on the surface of the solar air heater and the electrical energy consumed by the blower.

$$P_t = (A_{SAH}I + P_b)t_d \quad (4.76)$$

The overall thermal efficiency of the drying system is the ratio of the energy required to evaporate the moisture from the product to the total energy input into the drying system.

$$\eta_{ds} = \frac{m_v h_{fg}}{P_t} \quad (4.77)$$

4.5 Numerical formulation of the solar air heater

The dimensions used for fabricating the solar air heater for the experimental analysis are used for numerical modelling. The area of the solar air heater used for the computation is 2.06 m^2 with a 1.2 mm thick absorber plate and 5 mm thick glass cover. ANSYS R16.2 CFD software is used for the simulation of the solar air heater.

4.5.1 Basic steps of the computation on ANSYS

1. Model description and meshing

The 3D geometry of the solar air heater is created on SOLIDWOKS using the dimensions obtained from the design as shown in Figure 4.5 and imported to ANSYS R16.2. The model consists of a glass cover, absorber plate, wooden box and inlet and outlet sections for the fluid.

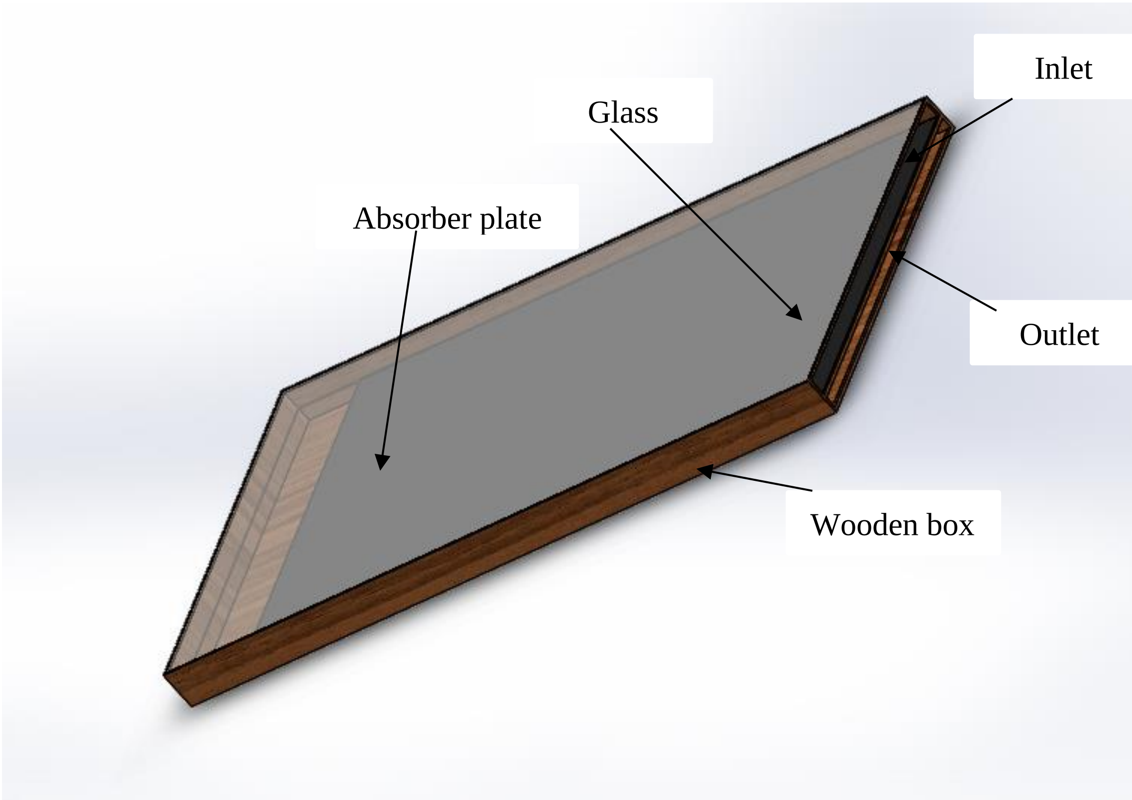

Figure 4.5: Geometry of the solar air heater.

Meshing of the solar air heater is done on ANSYS meshing as shown in Figure 4.6.

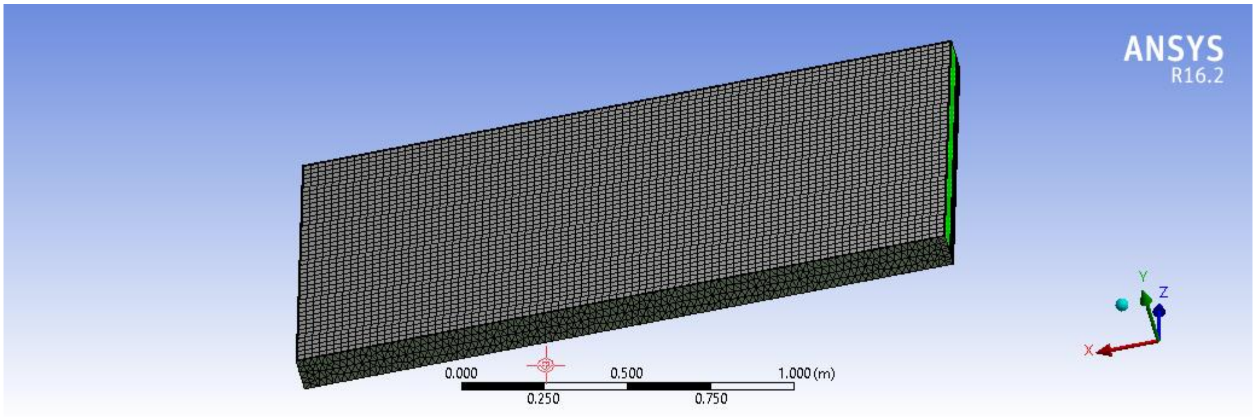

Figure 4.6: Meshed view of the solar air heater.

2. Setup

A steady state implicit pressure-based simulation has been carried out using ANSYS FLUENT and a SIMPLE algorithm was used for the pressure velocity coupling. Discretization is made using second order upwind scheme and a standard k-epsilon model was used for the simulation. A residual convergency criterion of 10^{-6} is given for the solution to converge and a standard solution initialization technique is used to initialize the solution.

3. Boundary conditions

The momentum and energy equations are solved using finite volume method and appropriate boundary conditions are imposed on the computational domain. The inlet is specified as a "mass-flow inlet" with a mass flow rate of 0.01 kg/s and the outlet as pressure outlet with gauge pressure of 0 pa. A heat flux equivalent to the solar radiation falling on the surface on June is given on the top and the sides are insulated.

4.5.2 Grid independency test

To check the dependency of the numerical results on the number of mesh elements, simulation with mesh elements of 12168, 16605 and 20250 is carried out. The variation of outlet air temperature between 16605 and 20250 elements is very small as indicated in Figure 4.7.

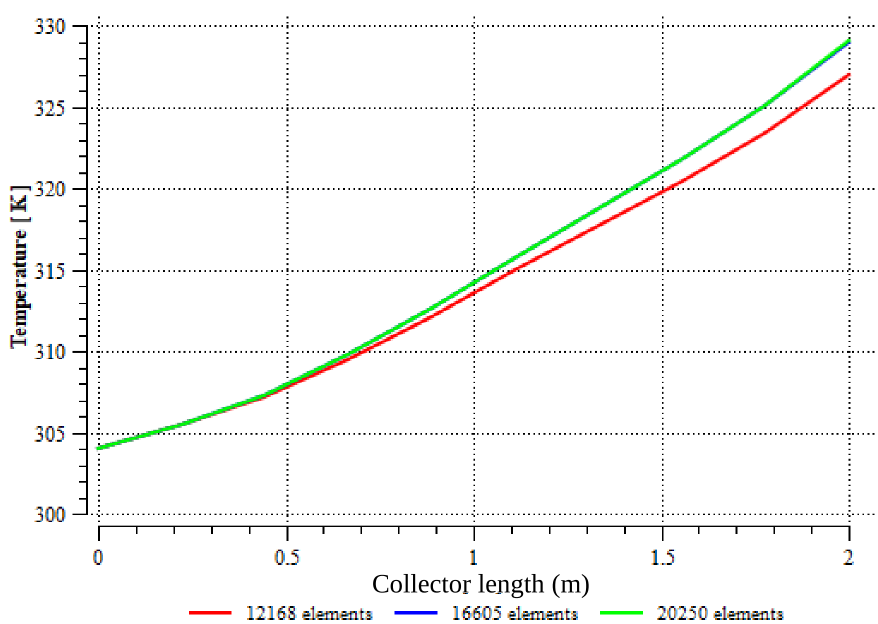

Figure 4.7: Grid independency test.

4.5.3 Governing equations for flat plate solar air heater

CFD methods consist of numerical solutions of mass, momentum, and energy conservation. The governing equation for the simulation is written based on the following assumptions.

1. The thermo-physical properties of air and absorber plate for the operating range of temperatures remain constant during the flow.
2. The flow is incompressible and continuous.
3. The material of duct wall and absorber plate are homogeneous and isotropic.
4. All the walls in contact with the fluid are assigned no-slip boundary condition.
5. Heat loss in the form of radiation is negligible.

Continuity equation:

$$\nabla.\rho\vec{V} + \frac{\partial\rho}{\partial t} = 0 \quad \text{(4.78)}$$

Momentum equation:

$$\frac{\partial\vec{v}}{\partial t} + (\vec{v}.\nabla)\vec{v} = \frac{1}{\rho}(-\nabla P + \mu\nabla^2\vec{v}) \quad \text{(4.79)}$$

Energy equation:

$$\left(\rho C_p u\frac{\partial T}{\partial x} + \rho C_p v\frac{\partial T}{\partial y} + \rho C_p w\frac{\partial T}{\partial z}\right) = K\nabla^2 T \quad \text{(4.80)}$$

4.6 Numerical modelling of the latent heat storage

For the simulation of the latent heat storage a finite element-based software COMSOL Multiphysics 4.3a is used.

4.6.1 Steps of the computation on COMSOL

1. Model description and meshing

A sectional view of a 3D shell and tube latent heat storage model filled with paraffin wax in the shell and air in the tubes is shown in Figure 4.8. The geometry of the storage has been created on COMSOL Multiphysics 4.3a using the dimension obtained from the design. The length and the diameter of the shell is 1 m and 0.2 m and the tubes are 1 m in length, 16 mm outer diameter and 14 mm inner diameter with a total of five tubes.

Meshing is carried out using free tetrahedral and triangular meshes for the domains and boundaries as shown in Figure 4.9. A special meshing feature of COMSOL Multiphysics called boundary layer is used to have finner meshes near the critical zones of the model.

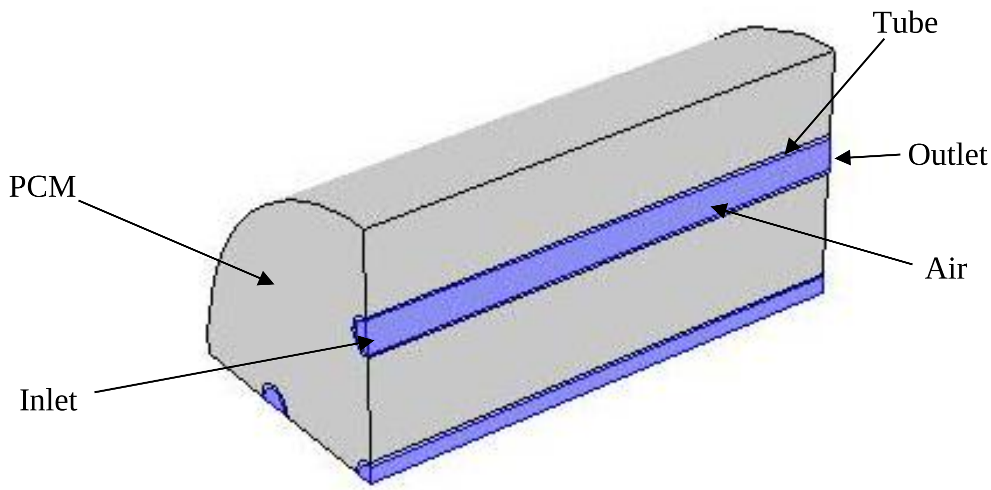

Figure 4.8: Sectional view of the latent heat storage.

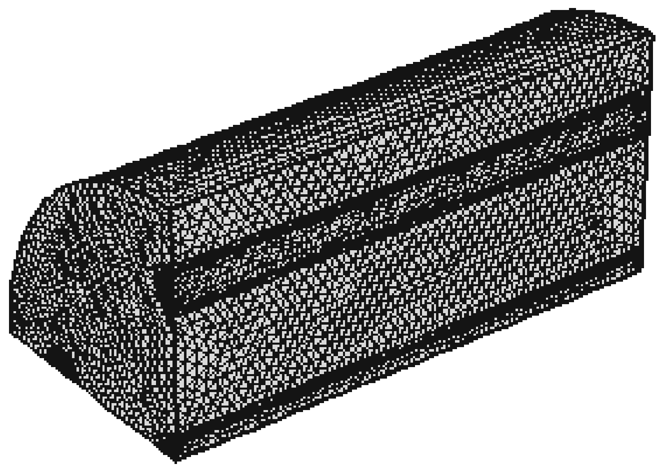

Figure 4.9: Meshed view of the latent heat storage.

2. Numerical treatment

A finite element-based software, COMSOL Multiphysics 4.3a which uses Galerkin method as a discretization technique is used to solve the governing equations of the LHS. PARDISO, a time dependent solver, is used to solve the equations and time stepping is done based on the backward differential formula (BDF) which has an initial minimum time step and a maximum time step. The minimum time step is set to 0.01 s and to solve the problem in the least possible run, the maximum time step is not set to automatically maximize the time step.

3. Boundary conditions

A constant 25 ℃ and 70 ℃ initial temperature for all the domains (air, PCM and tubes) and a zero velocity for the air is given initially (t = 0) during the charging and discharging process, respectively. At any time, t > 0, an inlet temperature of 70 ℃ and 25 ℃ is given for the inlet of the tubes during the charging and discharging process, respectively and outflow condition is given for the outlets. Adiabatic condition is given for the outer surfaces to avoid heat loss to the ambient.

4.6.2 Grid independency test

To check the dependency of the numerical results on the number of mesh elements, simulation is done with mesh sizes of 34287, 60488 and 107078. Avarage temperature of the PCM based on the charging process is compared and there is no a significant difference in temperature between the three mesh sizes as shown in Figure 4.10. But there is a difficulty in the convergence with 34287 mesh elements so to save computational time, 60488 mesh elements is selected for the simulation.

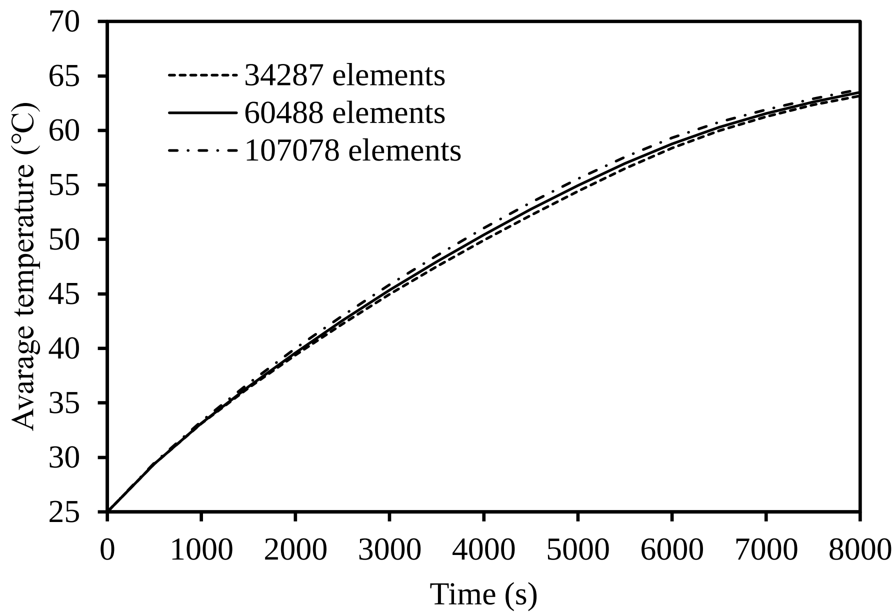

Figure 4.10: Grid independency test.

4.6.3 Governing equations for the latent heat storage

The thermal energy storage behavior of a latent heat storage can be studied by simulating four physical processes, HTF flow, phase change, convection and conduction. The thermal model is developed based on following assumptions:

- HTF is incompressible and Newtonian.
- HTF flow is laminar and exhibits negligible viscous dissipation.
- The initial temperature of PCM is uniform.
- Phase change during melting/solidification occurs in a temperature interval.
- Thermal losses through the outer wall of the PCM are negligible.
- PCM is homogeneous and isotropic.

A coupled conjugate heat transfer problem which simultaneously solves both the phase change behavior of the PCM and the flow behavior of the air is used to solve the developed LHS model. The effective heat capacity (EHC) method, first developed by Bonacina *et al.* (1973), which includes both the specific heat and latent heat of the PCM in a single term called EHC is used to solve the problem. The heat capacity of the PCM and the EHC were expressed as (Niyas *et al.*, 2017):

$$C_p = \begin{cases} C_{p,s} \; for \; T < T_s \\ C_{p,EFF} \; for \; T_s \leq T \leq T_l \\ C_{p,l} \; for \; T > T_l \end{cases} \quad \text{.....} \quad (4.81)$$

$$C_{p,EFF} = \frac{C_{p,s}+C_{p,l}}{2} + \frac{L_f}{T_l - T_s} \quad \text{.....} \quad (4.82)$$

The energy and continuity equations given in Eqns. (4.78) and (4.80) are used to simulate the model. To include the effect of buoyancy ($\vec{F}$) and Darcy law's source term and reduce the complexity in solving the Navier-Stokes equations, Boussinesq approximation is added to the momentum equation, which is given by (Niyas *et al.*, 2017):

$$\frac{\partial \vec{v}}{\partial t} + (\vec{v}.\nabla)\vec{v} = \frac{1}{\rho}(-\nabla P + \mu \nabla^2 \vec{v} + \vec{F} + \vec{S}) \quad \text{.....} \quad (4.83)$$

$$\vec{F} = \rho \vec{g} \beta (T - T_m) \quad \text{.....} \quad (4.84)$$

$$\vec{S} = \frac{(1-\theta)^2}{(\theta^3 + \varepsilon)} A_{mush} \vec{v} \quad \text{.....} \quad (4.85)$$

Where, β is thermal expansion of the PCM, θ is melt fraction, A_{mush} is mushy zone constant and ε is a constant value of 0.001.

Phase change problems occur during a temperature interval and they are often called mushy region problems. The mushy zone constant defines the transition of velocity in the mushy region and values between 10^3 and 10^7 are recommended for most computations (Niyas *et al.*, 2017).

CHAPTER FIVE

MANUFACTURING PROCESS AND EXPERIMENTAL SETUP

This chapter presents the fabrication process of the components of the dryer, the setup used for the experiment and the test procedure. Detailed fabrication process of each component of the dryer and the final assembly supported with photographs is presented.

5.1 Fabrication of components of the dryer

The components of the dryer are the solar air heater, latent heat storage and the drying chamber. The materials used for fabricating the components of the dryer are purchased from the local market. Availability and cost of the materials in the local market have been considered while selecting the materials for each component.

5.1.1 Fabrication of the solar air heater

The solar air heater contains a casing, base plate, cover plate, insulation and absorber plate. The casing is constructed from a 2.05 m × 1.05 m wooden box and a plywood of 2.05 m × 1.05 m and 6 mm thick is used as a base plate. A 25 mm thick foam insulation is placed above the plywood and covered with a 2 m × 1 m aluminum sheet as shown in Figure 5.1 (a). A black painted steel sheet of 1.8 m × 1 m and 1.2 mm thick is used as absorber plate and placed at a gap of 40 mm from the bottom. The glazing is a 2.05 m × 1.05 m and 5 mm thick window glass placed at a gap of 60 mm from the absorber plate. The collector is mounted facing south on a 2.09 m × 1.09 m frame constructed from steel bar and angle iron and tilted at angle of 25° as shown in Figure 5.1 (b).

a.

b.

Figure 5.1: Manufacturing process (a) and pictorial view (b) of the solar air heater.

5.1.2 Fabrication of the LHS

The shell of the energy storage is made from a 1 m × 0.63 m mild steel sheet. The diameter of the shell is 0.2 m and its length is 1m as shown in Figure 5.2 (a). Two headers with the same size and 5 holes of 17 mm in diameter are welded to both ends of the shell and five steel tubes with 16 mm outer diameter, 14 mm inner diameter and 1 m long are inserted through the holes and welded to the headers. Another two short shells are welded to the both ends of the main shell to distribute the air and polyester is rubbed around the weldments to eliminate leakages as shown in Figure 5.2 (b). The shell is filled with 16 kg paraffin wax to store the heat and covered with a 25 mm thick foam insulation. The paraffin wax modules are first crushed into smaller pieces and melted using fire and finally poured into the shell through the PCM filling cup as represented in Figure 5.3.

a.

b.

Figure 5.2: Manufacturing process of the LHS.

a.

b. c.

Figure 5.3: PCM filling process. (a) paraffin wax modules, (b) melting and (c) filling.

5.1.3 Fabrication of the drying chamber

The drying chamber is a rectangular wooden box of 1 m × 0.9 m × 1 m with inlet and outlet holes at the bottom and top of the chamber, respectively. A chimney shaped cover is placed at the top of the chamber to eliminate water accumulation at the top surface of the chamber. The drying chamber contains two trays made of wire mesh of 0.9 m×0.8 m. One side of the chamber is used as a door for loading and unloading. The drying chamber is placed on a 1.04m× 0.804m×1.04m frame constructed from steel bar and angle iron as shown in Figure 5.4.

Figure 5.4: Pictorial view of the drying chamber.

Table 5.1: Materials and specification of components of the dryer.

Main components	Components	Materials	Specification
Solar air heater	Absorber plate	Steel sheet metal	Size (1 m × 2 m), 1.2 mm thick
	Glazing	Glass	Size (1.04 m × 2.04 m), 5mm thick
	Base plate	Aluminum	Size (1 m × 2 m), 0.2 mm thick
	Insulation	Thermo foam	25 mm thick
	Casing	Wood and plywood	Thickness (25 mm) and (6 mm)
Energy storage	Shell	Mild steel	1.2 mm thick, diameter (0.2 m), length (1 m)
	Pipe	Steel tube	Diameter (16 mm), length (1 m)
	Insulation	Thermo foam	Thickness (25 mm)
	PCM	Paraffin wax	16 kg, melting temperature (58 °C)
Drying chamber	Wall	Wood and mild steel sheet	thickness (1.2 mm)
	Tray	Wire mesh	Size (0.9 m × 0.7 m)
	Insulation	Thermo foam	Thickness (25 mm)
Frame		Steel bar and angle iron	
Blower			100 W, 0.8 m^3/min and 1300 rpm

5.2 Working principle of the dryer

The developed solar dryer consists of a solar air heater, shell and tube LHS filled with paraffin wax, a drying chamber, and a blower as represented in Figure 5.5. Solar energy is the main source of energy for the drying system and harvested by the solar air heater. In this drying system, a double pass solar air heater is used to get the desired drying air temperature. Air at ambient temperature is passed through the solar air heater where it is heated up by trapping the solar energy incident on its surface. The air exiting from the solar air heater passes through the tubes of the shell and tube LHS located between the solar air heater and the drying chamber.

The energy storage has five tubes which are enclosed by a shell and the space between the tubes and the shell is filled with paraffin wax. During the charging period, when the temperature of the air coming out of the solar air heater is higher than the temperature of the PCM, the heat is transferred from the air to PCM. Whereas, during the discharging period, when the temperature of the air coming out of the solar air heater is lower than the temperature of the PCM, the accumulated thermal energy is released from the PCM resulting in an increase in the temperature of the air. The air leaving the LHS is then drawn into the drying chamber with the blower. The drying chamber consists of two trays and one side of the drying chamber is a door for loading and unloading. The hot air flows over the product on the drying trays and escapes to the atmosphere after removing the moisture from the surface of the products.

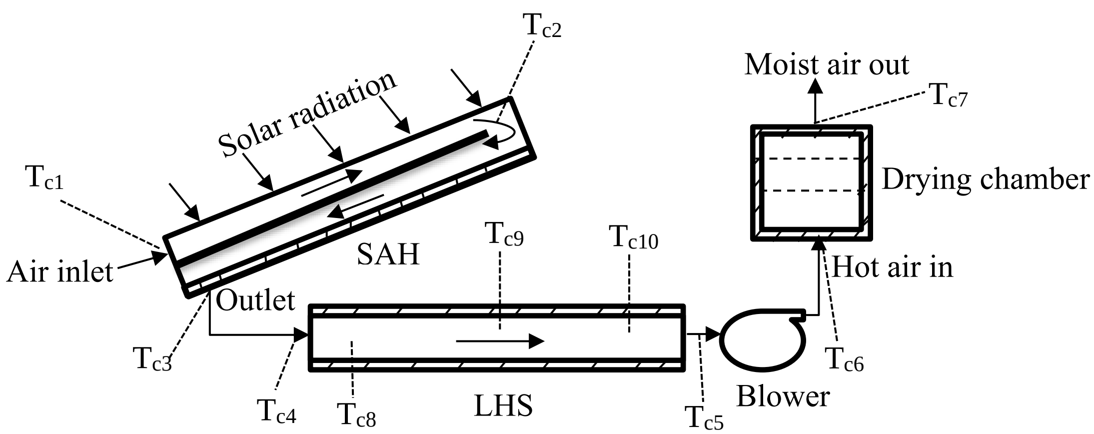

Figure 5.5: Schematic layout of the solar dryer. (Tc-thermocouple).

5.3 Experimental setup

The setup contains a double pass solar air heater, a shell and tube latent heat thermal energy storage, a drying chamber and a blower as shown in Figures 5.7 and 5.8. Pipe and fittings (Figure 5.6) are used to assemble the components and polyester is used to fill gaps between connections. The outlet of the solar air heater is connected to the inlet of the energy storage using a PVC pipe and a fitting and the outlet of the energy storage is connected to the inlet of the blower. The blower outlet is then connected to the inlet of the drying chamber.

Figure 5.6: Pipe and fittings used for assembling the dryer.

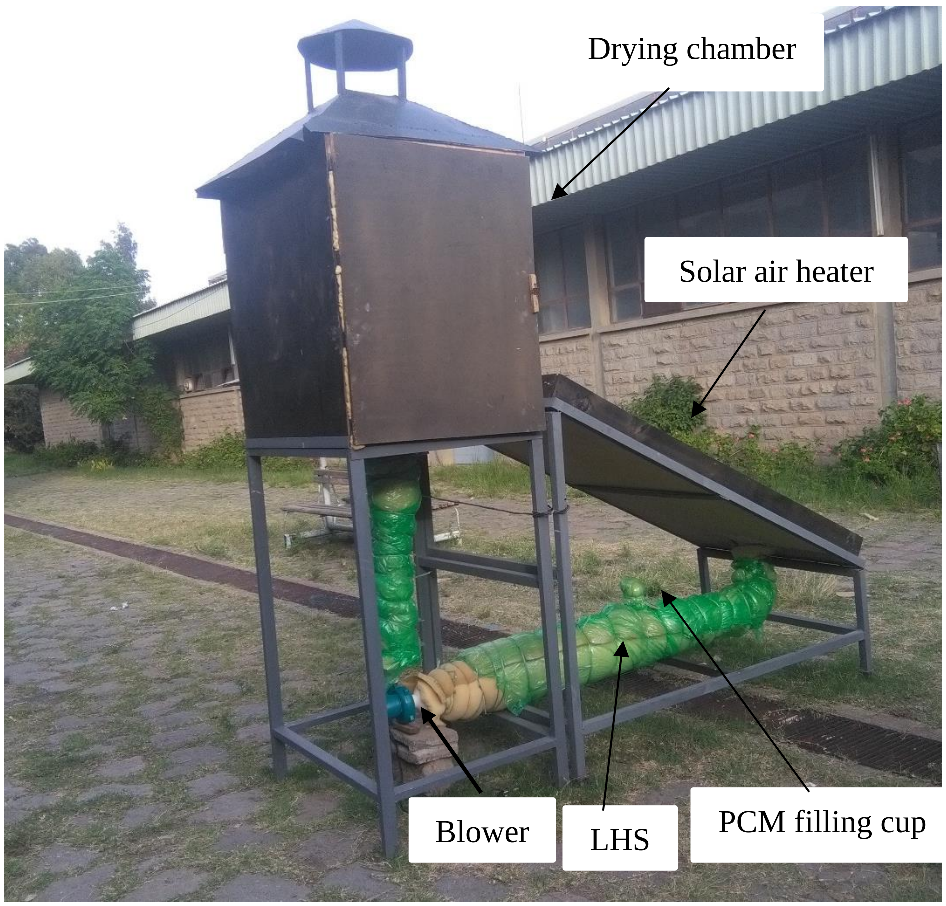

Figure 5.7: Pictorial view of the dryer.

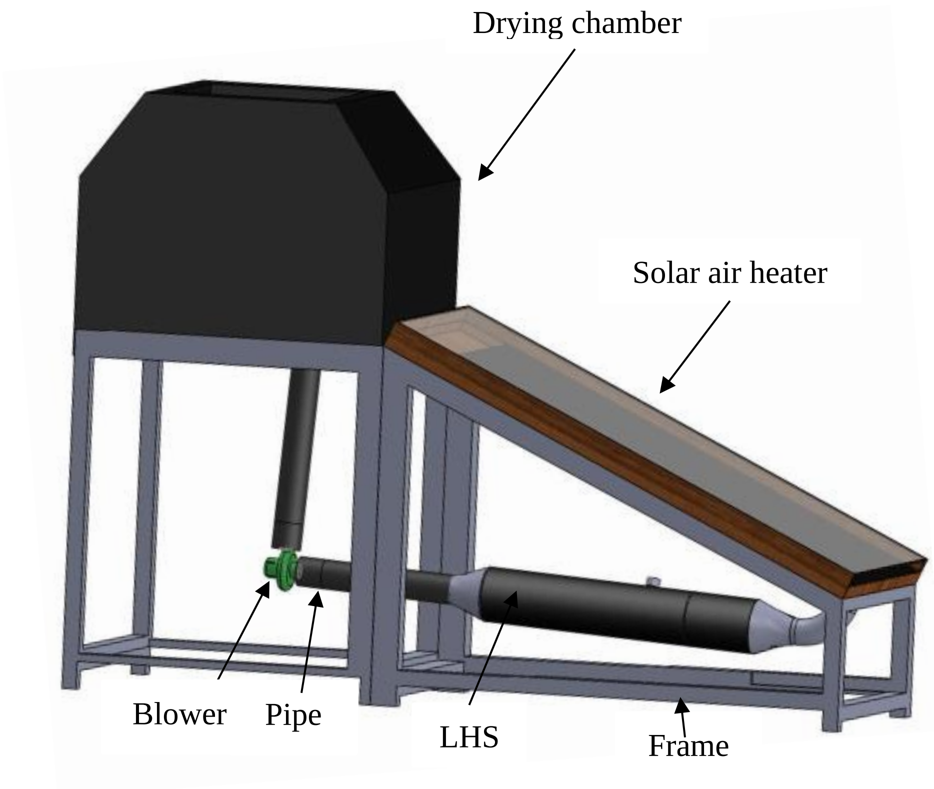

Figure 5.8: CAD view of the dryer.

Figure 5.9: Trays loaded with fish.

5.4 Experimental procedure

Two thermocouples are placed at the inlet and outlet of the solar air heater and another thermocouple is placed at the outlet of the first fluid pass to measure the temperature of the air. Three thermocouples are placed inside the thermal energy storage to measure the temperature of the PCM which determines whether the PCM is completely melted or not. Another two thermocouples are placed at the inlet and outlet of the latent heat storage to measure the temperature of the incoming and leaving air to and from the storage. Two thermocouples are placed at the inlet and outlet of the drying chamber to measure the temperature at each location as shown in Figure 5.5.

A no load test is done to check whether the outlet air temperature of the SAH and the energy storage are in the desired range for the drying application. During the load test, the trays of the drying chamber are loaded with 5 kg fresh fish (Figure 5.9) and the inlet and outlet temperatures of the drying chamber are recorded to evaluate its performance. Four samples are taken from four different locations and weighed in a three-hour interval to determine the moisture loss from the fish and evaluate the performance of the drying system. The performance of the solar air heater and thermal energy storage and the effect of the thermal energy storage on the inlet temperature of the drying chamber are evaluated during both tests.

5.5 Sample preparation

Prior to experimentation, the following procedure is used to prepare the fish for drying.

1. The raw fresh fish is cleaned with clean and fresh water.
2. The gills and internal organs are removed by splitting.
3. The splitted fish is washed thoroughly and drained.
4. A salt solution is prepared (60 g salt dissolved in one litter of water (Assefa *et al.*, 2008)).
5. The fish is soaked into the salt solution for one hour.
6. The salted fish is drained and arranged into the trays without placing the fish on top of the other.

5.6 Measuring instruments

A K-type thermocouple (Figure 5.10) is used to measure temperature at different locations of the dryer. The thermocouple is calibrated in a constant temperature bath before installing in the drying system. The detailed calibration process is presented in Appendix C.

A digital balance (Figure 5.11) with a ±0.5 g accuracy is used to measure the mass of the fresh fish and the mass of the samples.

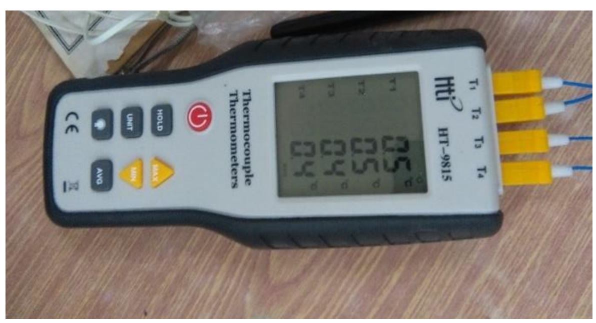

Figure 5.10: K-type thermocouple.

CHAPTER SIX

RESULTS AND DISCUSSIONS

This chapter presents the experimental and simulation results of the PCM integrated flat plate solar air dryer with a detailed discussion of each result. Performance of each component of the dryer and the overall performance of the drying system is discussed in detail.

6.1 Experimental results of the solar air heater

The experiment is conducted from 19th to 26th June 2020 and ambient air temperature and outlet temperature of the solar air heater is recorded from 9:30 h to 18:30 h in a 30 min interval. The estimated hourly variation of global, beam and diffuse radiation on a horizontal surface and radiation falling on the surface of the collector (tilted at an angle of 25°) during the month of June is shown in Figure 6.1.

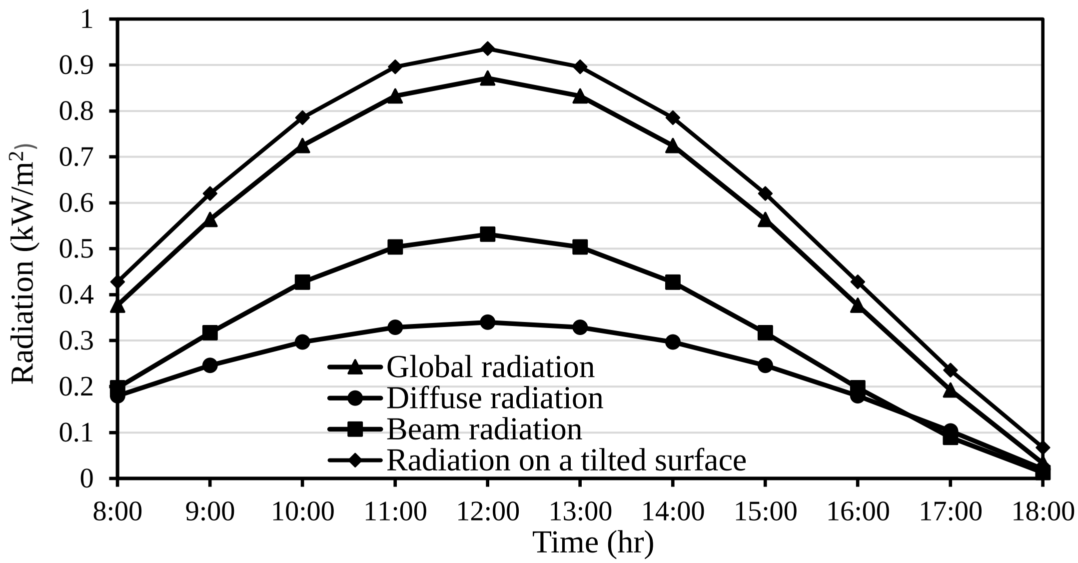

Figure 6.1: Estimated hourly variation of solar radiation of Adama on June.

6.1.1 Inlet and outlet temperature variation of the solar air heater

The variation of ambient air temperature and outlet air temperature of the solar air heater with time for the five days is presented in Figure 6.2. It is observed that the outlet temperature of the solar air heater increases with increase in solar radiation intensity. It starts increasing and becomes maximum between 12:00 h and 14:30 h, starts to decrease when the solar radiation decreases and becomes almost equal to the ambient at 18:30 h. The maximum outlet temperature recorded was 69.5 ℃ at 13:30 h and the minimum was 35 ℃ recorded at 9:00 h.

The ambient temperature varies between 25 ℃ and 32 ℃ each day. Fluctuations are observed during the first, third and fifth (19th, 24th and 26th) days of the experiment due to cloud covers.

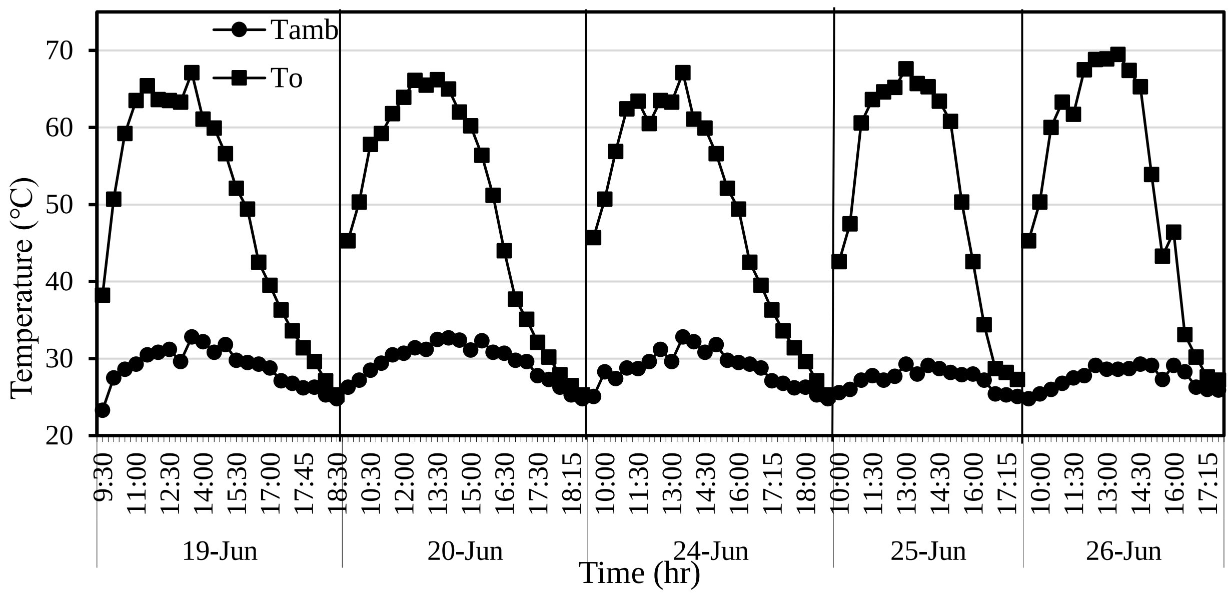

Figure 6.2: Variation of inlet and outlet temperatures of the SAH with time.

6.1.2 Effect of SAH configuration on outlet air temperature

Figure 6.3 shows the temperature variation of the air at the outlet of the first fluid pass and the outlet of the second fluid pass of the solar air heater for each day. It is observed that the air temperature at the outlet of the second fluid pass is 5 to 10 ℃ higher than the outlet of the first fluid pass from 10:00 to 16:00 h. The temperature rise is obtained by circulating the air between the absorber and the bottom plate after it passes through the absorber and the glass cover without incurring any additional cost on the solar air heater.

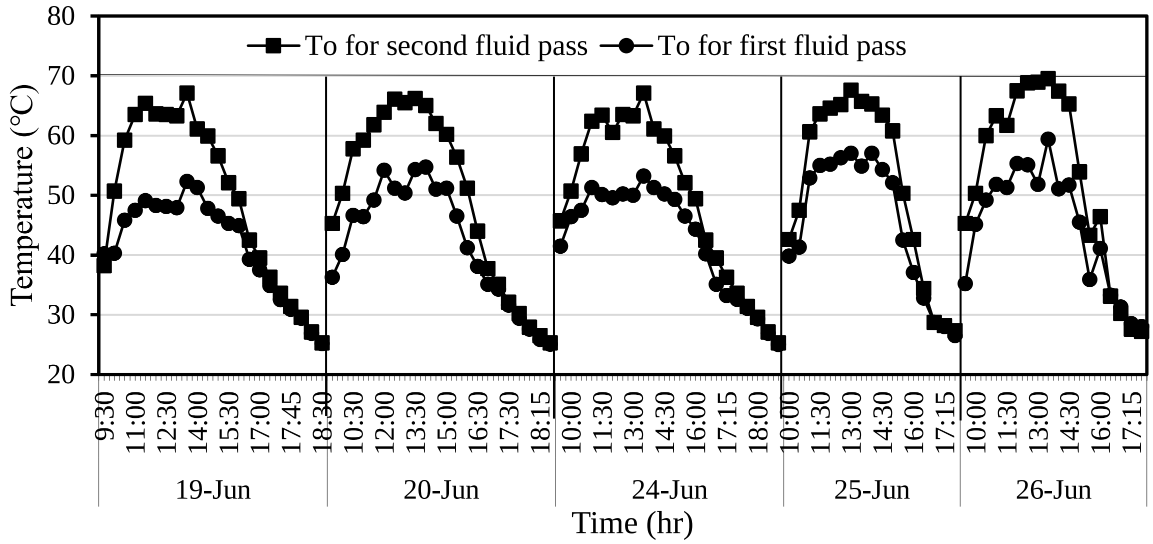

Figure 6.3: Temperature variation of the outlet air at the first and second fluid passes.

6.1.3 Variation of thermal efficiency of the solar air heater

The variation of the thermal efficiency of the solar air heater with time is illustrated in Figure 6.4. The thermal efficiency of the SAH increase with increase in the solar radiation intensity and decreases when the intensity becomes low. The maximum thermal efficiency of the SAH is 35% and the minimum is 10% from 9:30 to 16:30 h and the average thermal efficiencies of the SAH is 25%.

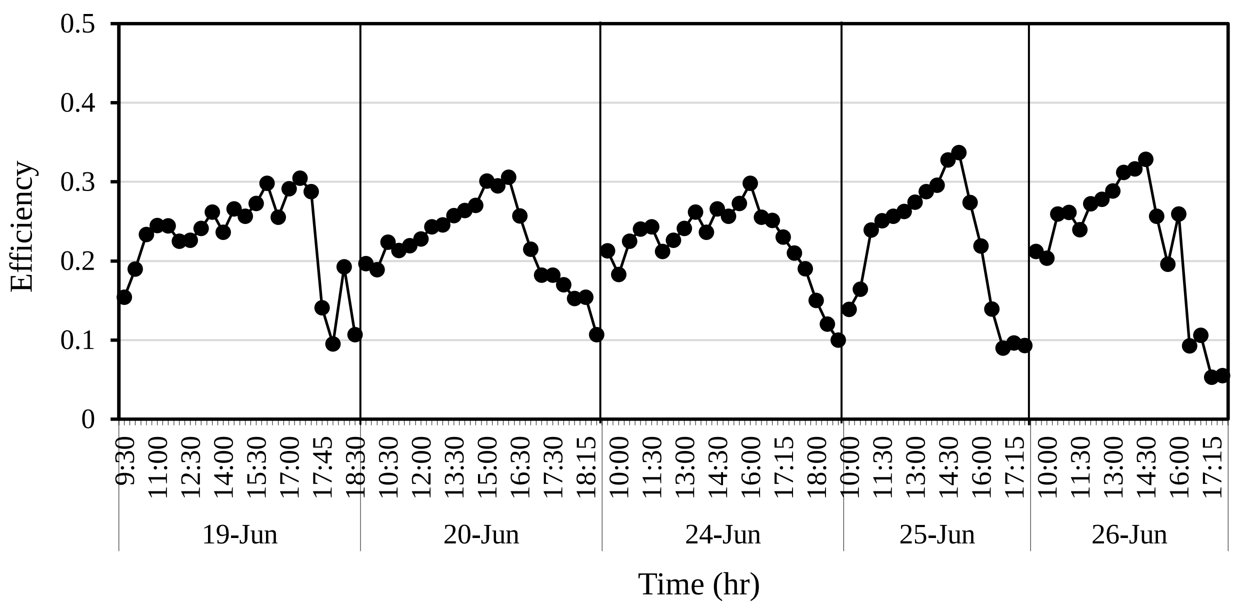

Figure 6.4: Variation of thermal efficiency with time.

6.1.4 Effect of SAH configuration on thermal efficiency

Figure 6.5 Shows the effect of the configuration of the solar air heater on thermal efficiency. It is clearly observed that the thermal efficiency of the double pass configuration is 8 to 15% higher than the single pass configuration. Omojaro and Aldabbagh (2010), Aldabbagh *et al*. (2011), Satcunanathan and Deonarine (1973) and Sukhatme and Nayak (2010) reported results with similar trends with a double pass SAH efficiency of 7 to 19.4%, 8 to 17%, 10 to 15% and 10 to 17% higher than the single pass, respectively.

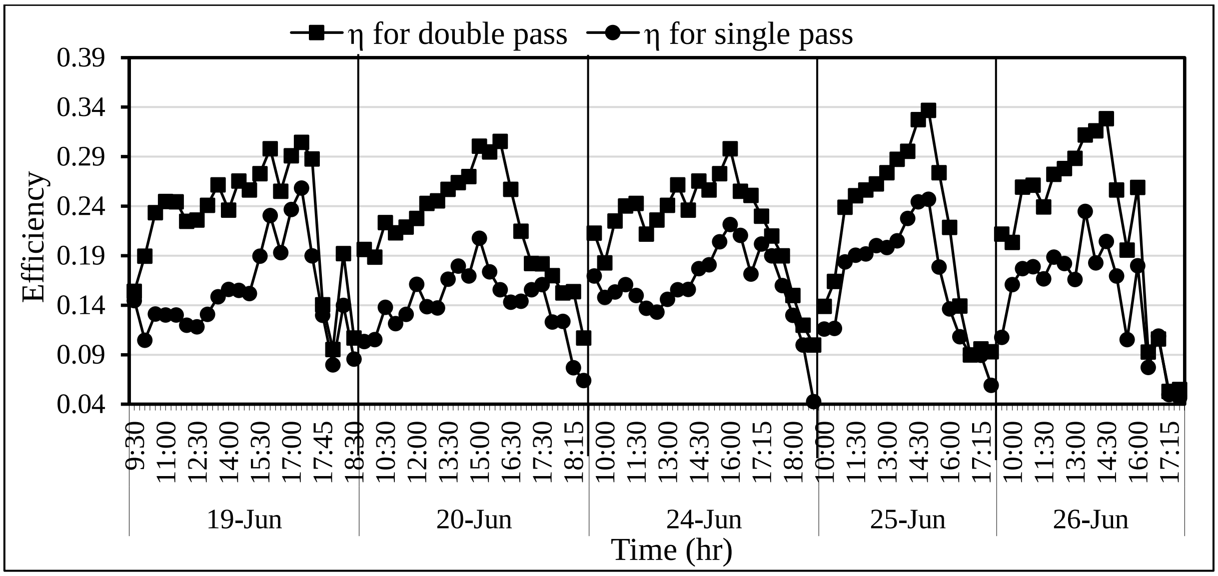

Figure 6.5: Effect of SAH configuration on thermal efficiency.

6.1.5 Exergetic efficiency variation of the SAH

The variation of the exergy efficiency of the SAH with time is depicted in Figure 6.6. The exergy efficiency increases as the outlet temperature increases with maximum values obtained around 13:00 h. Maximum exergy efficiencies are found at the last two days of the experiment due to the high outlet temperature and low inlet temperature of the SAH compared to the first two days. The maximum exergy efficiency of the SAH is 2% obtained at 13:00 h and the minimum is 0.4% obtained at 9:30 h and the average exergy efficiency of the SAH is 1.5%.

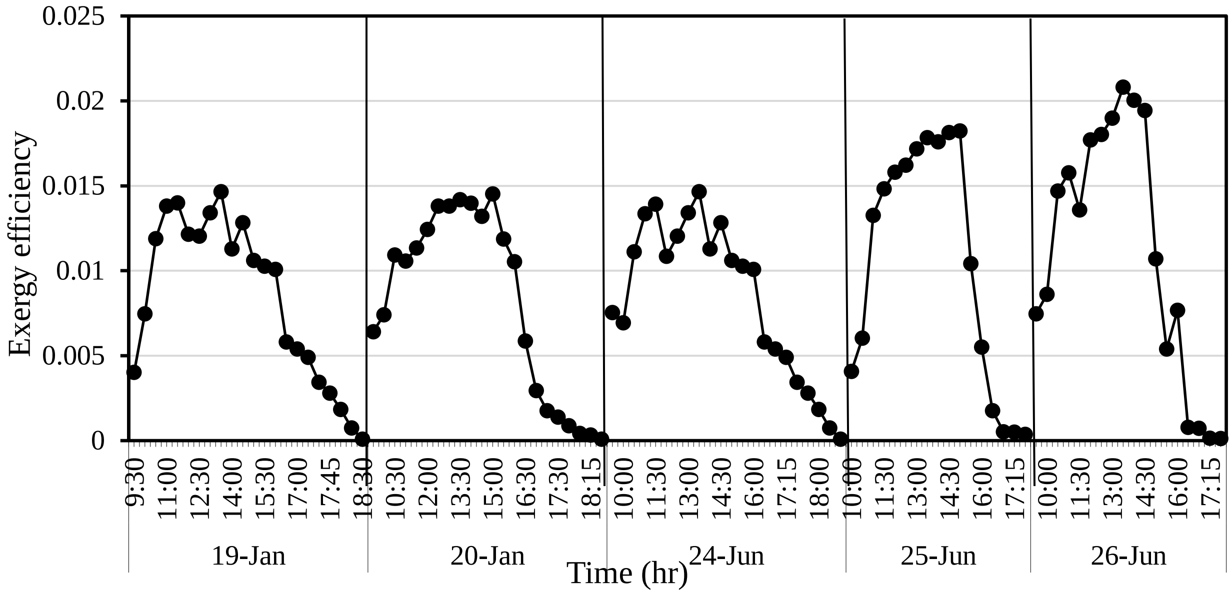

Figure 6.6: Variation of exergy efficiency of the SAH with time.

6.1.6 Effect of SAH configuration on exergetic efficiency of the SAH

Figure 6.7 represents the effect of SAH configuration on the exergy efficiency of the SAH. It is clearly observed that, the exergy efficiency of the double pass configuration is 0.6 to 1.2% higher than the single pass configuration.

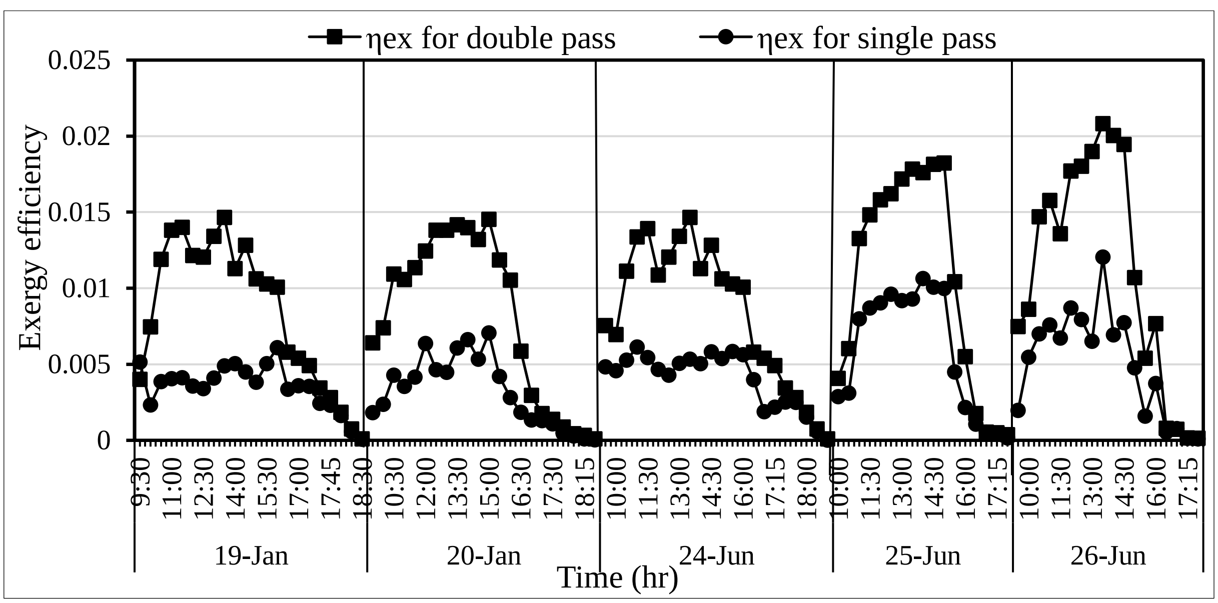

Figure 6.7: Effect of SAH configuration on exergy efficiency.

6.2 Simulation results of the solar air heater

Simulation of the solar air heater with inlet mass flow rates varying from 0.008 to 0.05 kg/s is carried out on ANSYS fluent 16.2 to check the effect of mass flow rate on the outlet air temperature, absorber plate temperature and air temperature variations across the flow length.

6.2.1 Temperature contours of the absorber plate

Temperature contours of the absorber plate at a heat flux corresponding to the radiation at 12:00 h and different air flow rates (a. 0.008 kg/s, b. 0.01 kg/s, c. 0.02 kg/s and d. 0.03 kg/s) are shown in Figure 6.8. It is observed that as the mass flow rate of the air increases, more heat is taken from the absorber and its temperature decreases.

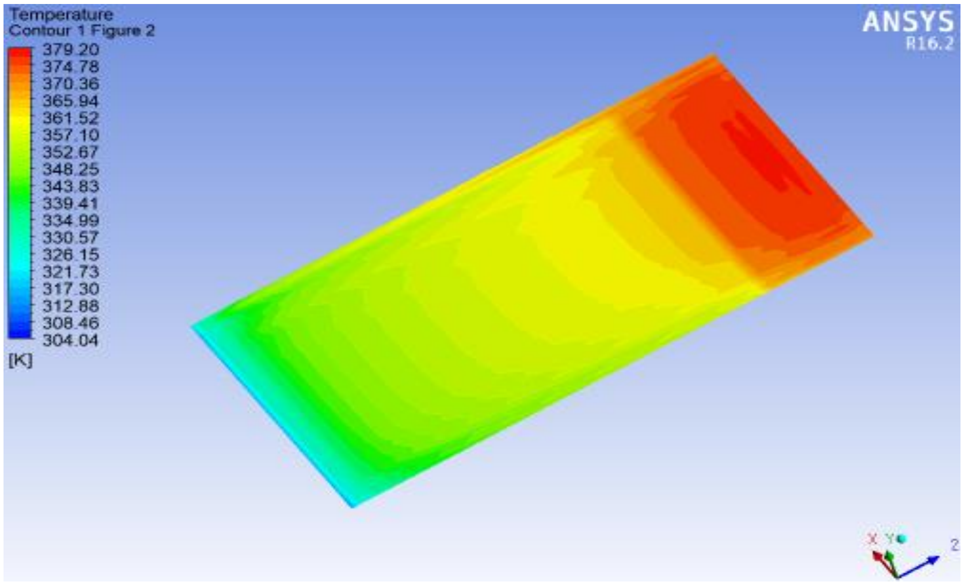

a.

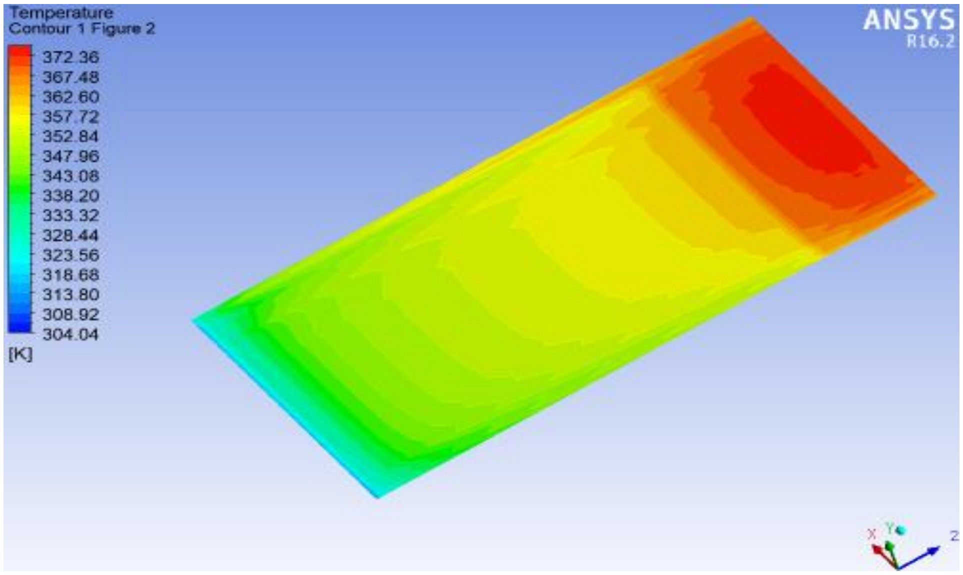

b.

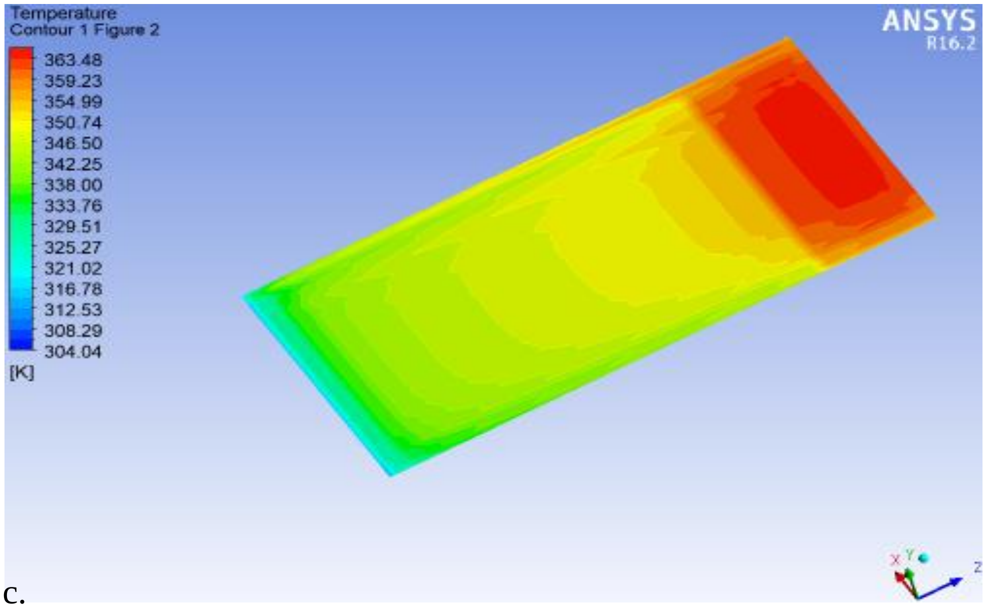

c.

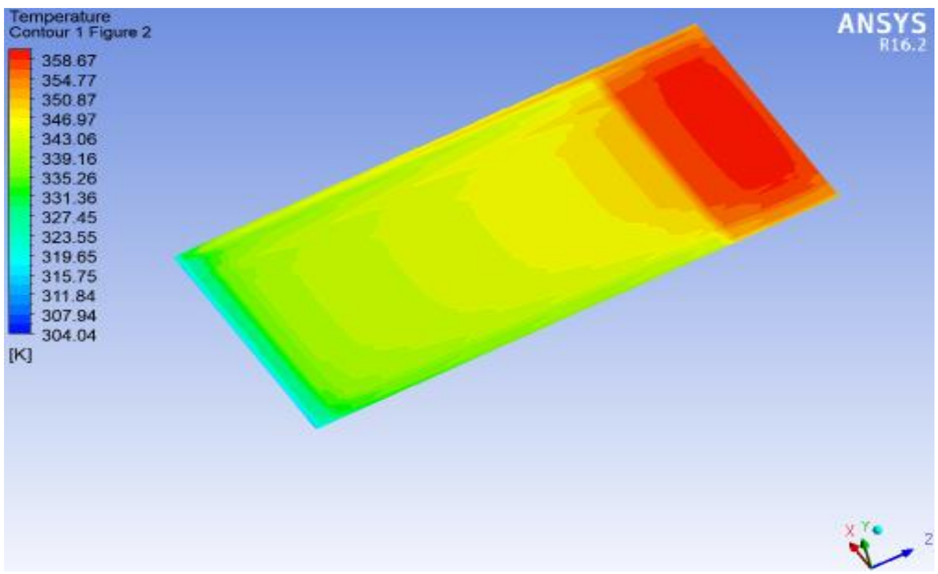

d.

Figure 6.8: Temperature contours of the absorber plate a) 0.008 kg/s, b) 0.01 kg/s, c) 0.02 kg/s and d) 0.03 kg/s.

6.2.2 Air temperature variation across the flow length at different inlet mass flow rates

Figure 6.9 (a) and (b) indicates the temperature variation of the air across the flow length at different inlet mass flow rates of air for the first and second fluid passes, respectively. The temperature of the air increases towards the outlet and it is maximum for mass flow rate of 0.008 kg/s and decreases as the mass flow rate increases. Since the air is heated as it passes inside the air channel, its temperature increases towards the outlet and the temperature increase is lower for high mass flow rates of air due to the large area required for heating the air.

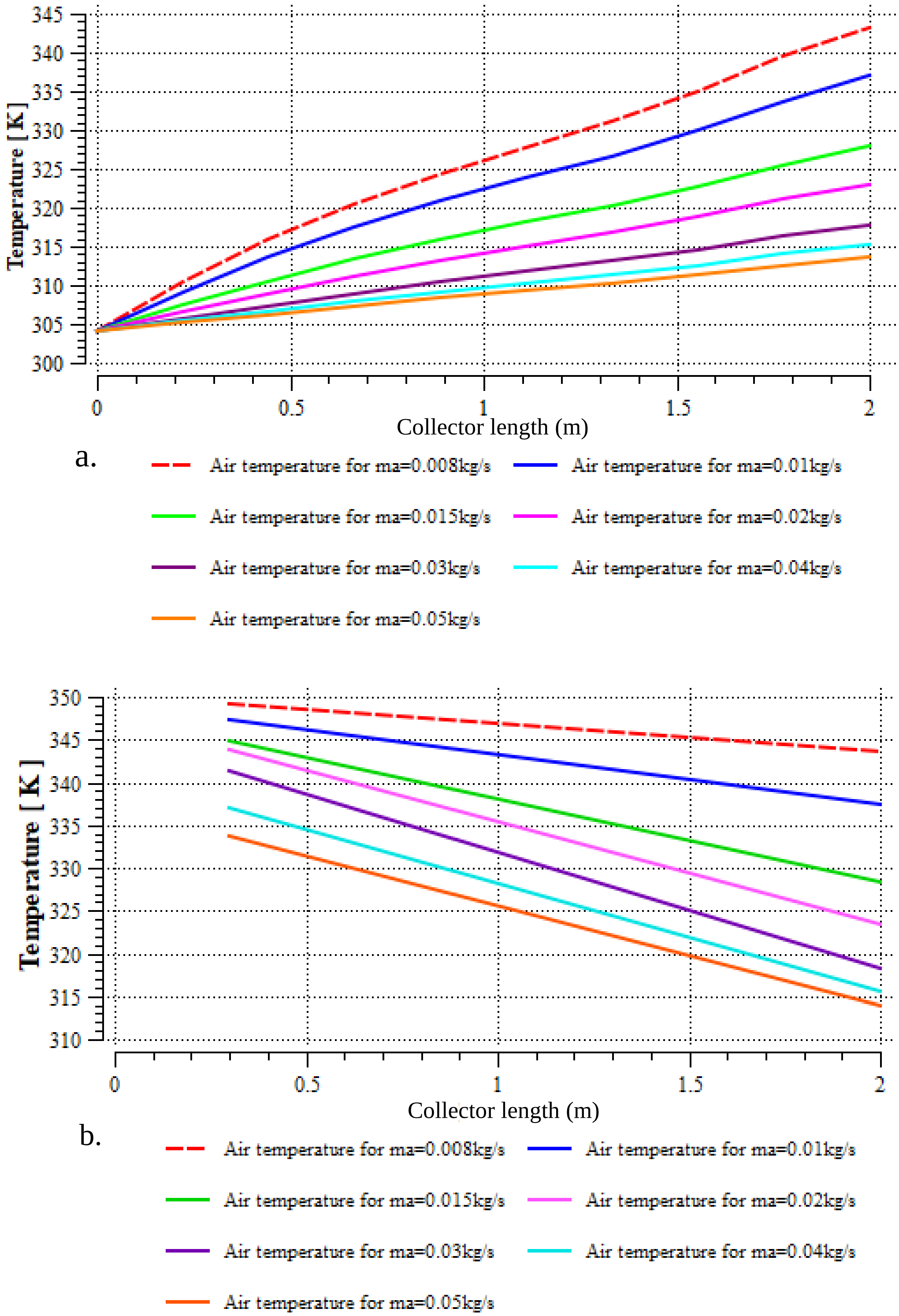

Figure 6.9: Air temperature variation across the flow length at different mass flow rates (a) first fluid pass and (b) second fluid pass.

6.2.3 Absorber plate temperature variation across the flow length

Figure 6.10 shows the temperature variation of the absorber plate across the flow length at different inlet mass flow rates. The temperature of the absorber plate increases towards the outlet and it is maximum for mass flow rate of 0.008 kg/s and decreases as the mass flow rate increases as more heat is taken from the absorber for higher mass flow rates.

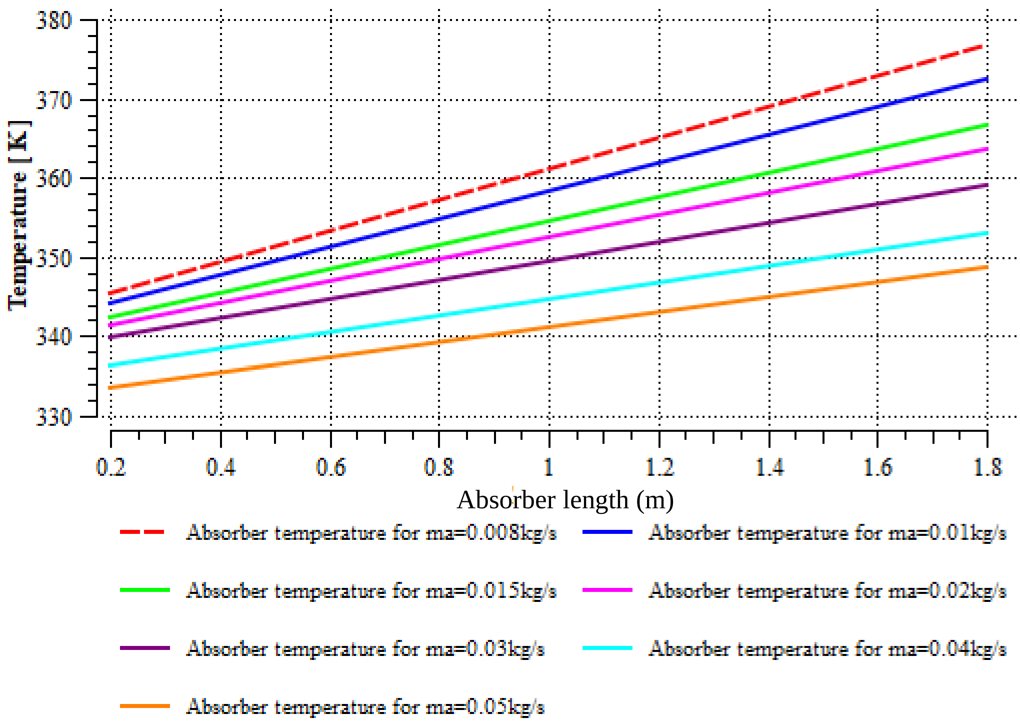

Figure 6.10: Absorber temperature variation across the flow length at different flow rates.

6.2.4 Effect of mass flow rate on outlet temperature and thermal efficiency

Figure 6.11 illustrates the variation of outlet temperature and thermal efficiency with mass flow rate of air at the outlet of the first and second fluid passes of the solar air heater. It is observed that the outlet temperature of the SAH decreases and thermal efficiency increases with increase in mass flow rate. This is because the temperature of the absorber decreases as more amount of air enters into the SAH resulting in lower outlet air temperature. Higher mass flow rates of air and low outlet air temperatures corresponding to the high air flow rate results higher thermal efficiency due to the higher thermal output power of the SAH. Since the air is heated again in the second air channel, the air temperature and thermal efficiency of the SAH at the outlet of the second fluid pass are higher than that of the outlet of the first fluid pass for each mass flow rates.

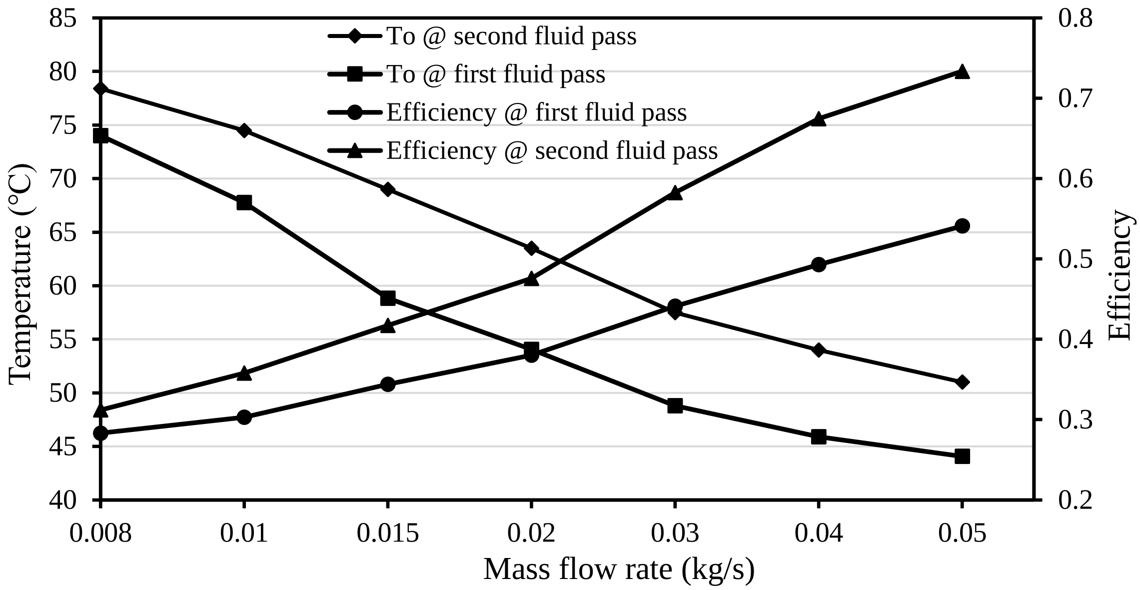

Figure 6.11: Variation of outlet temperature and thermal efficiency with mass flow rate.

6.2.5 Comparison between the experimental and simulation results of the SAH

Figure 6.12 shows comparison of experimental and simulated outlet air temperature of the double pass solar air heater at a mass flow rate of 0.01 kg/s. It is observed that the simulated outlet air temperature of the solar air heater is higher than the experimental. There is a maximum deviation of 5.5 % between the experimental and simulation outlet air temperature which is less than the maximum acceptable value, 10%.

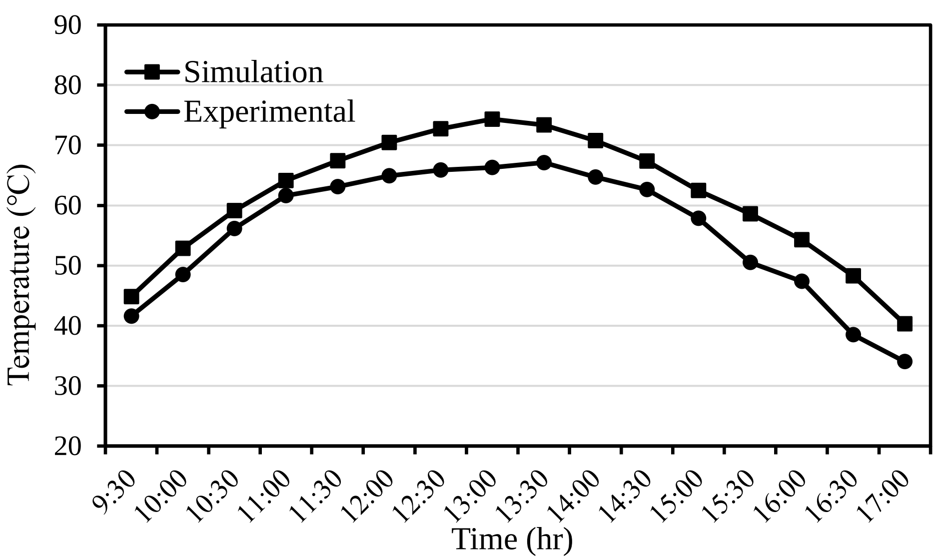

Figure 6.12: Comparison of simulated and experimental outlet air temperature.

The variation of experimental and simulated thermal efficiency of the solar air heater is indicated in Figure 6.13 and it can be noted that the thermal efficiency of the simulated SAH is higher than the experimental thermal efficiency due to the higher outlet air temperature of the simulation model. There is a maximum deviation of 6.8% between the experimental and simulation thermal efficiencies which is less than the maximum acceptable value, 10%.

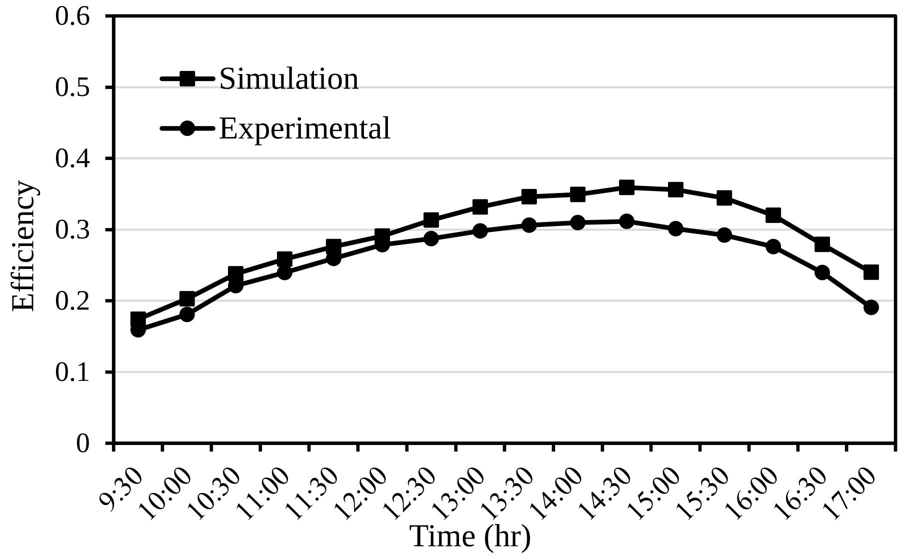

Figure 6.13: Variation of experimental and simulated thermal efficiency of the SAH.

6.3 Experimental results of the thermal energy storage

The temperature of the air at the inlet and outlet of the LHS and the temperature of the paraffin wax at three different locations (near the inlet, at the center and near the outlet) are measured and the results are presented as follows.

6.3.1 Variation of inlet and outlet temperatures of the energy storage

Figure 6.14 shows the variation of the inlet and outlet air temperatures of the thermal energy storage during the charging and discharging process. It is observed that, the inlet air temperature varied between 35 ℃ and 70 ℃ whereas the outlet temperature varies between 30 ℃ and 60 ℃. The inlet temperature of the storage varied with the change in solar intensity. It starts increasing and becomes maximum between 12:00 h and 14:30 h and starts decreasing and became almost equal to the ambient at 18:30 h. However, the outlet air temperature remains 5 to 10 ℃ higher than the inlet after 16:30h. Charging starts from 09:30 h and completed around

14:30 h and discharging starts around 15:30h when the inlet air temperature is lower than the storage temperature. During the charging process, a highest drop in air temperature of 12 ℃ between the inlet and outlet of the storage is observed and during the discharging process, a rise in air temperature of 10 ℃ is observed. When temperature of the air does not change while passing through the energy storage, the PCM is assumed as completely melted.

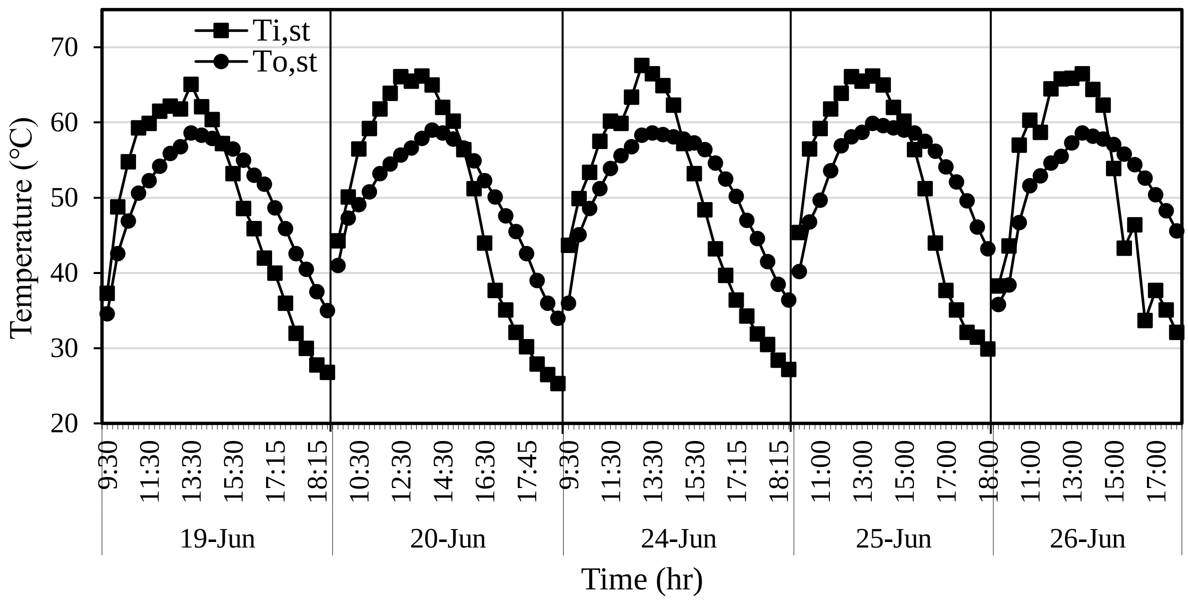

Figure 6.14: Inlet and outlet temperature variation of the energy storage.

6.3.2 Heat input/recovered during the charging and discharging process

The instantaneous heat input and heat recovered during the charging and discharging process is presented in Figure 6.15. The positive and negative values on the secondary Y-axis represents the heat input and heat recovered by the air respectively. The heat input starts increasing with increase in the inlet air temperature and becomes maximum around 13:00 h, starts to decrease as the inlet temperature decreases and becomes zero when the inlet and outlet air temperatures becomes equal. Heat recovery starts when the inlet air temperature becomes less than the temperature of the PCM. The average instantaneous heat input during the charging process of the energy storage varied between 106 W and 125 W and heat recovered by the air during the discharging process varied between 83 W and 110 W.

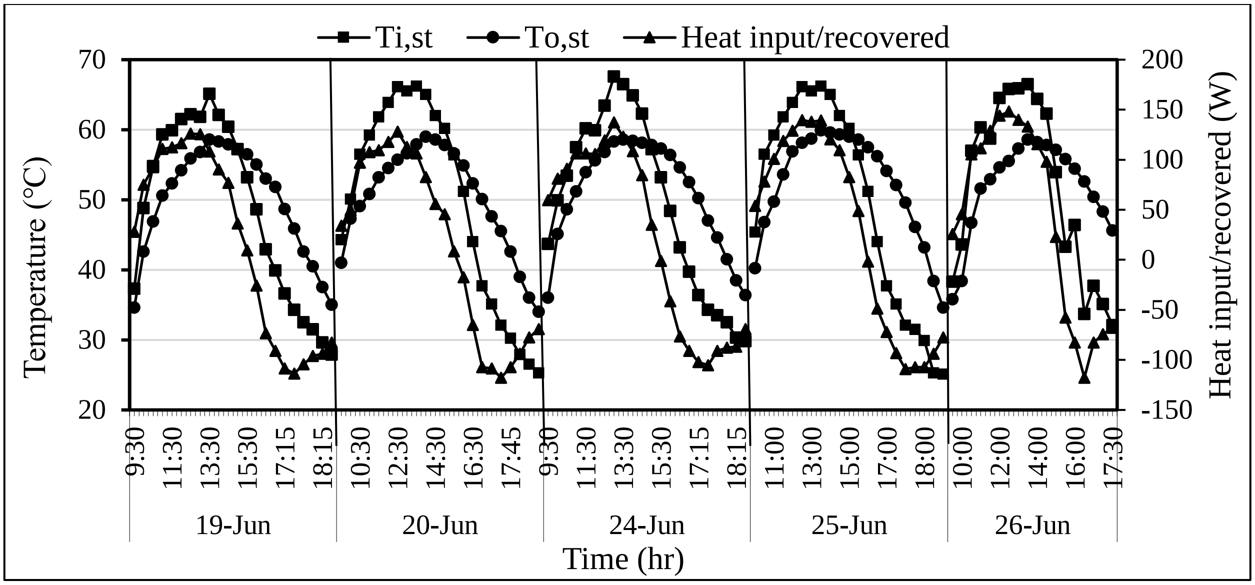

Figure 6.15: Heat input/recovered by the air during the charging and discharging process.

The net heat input and recovered from the energy storage during the charging and discharging processes is depicted in Figure 6.16. The net heat input to the storage varies between 3.1 MJ and 3.6 MJ whereas the net heat recovered from the storage varies between 1.2 MJ and 1.6 MJ with average energy efficiency of 38.7 to 46%.

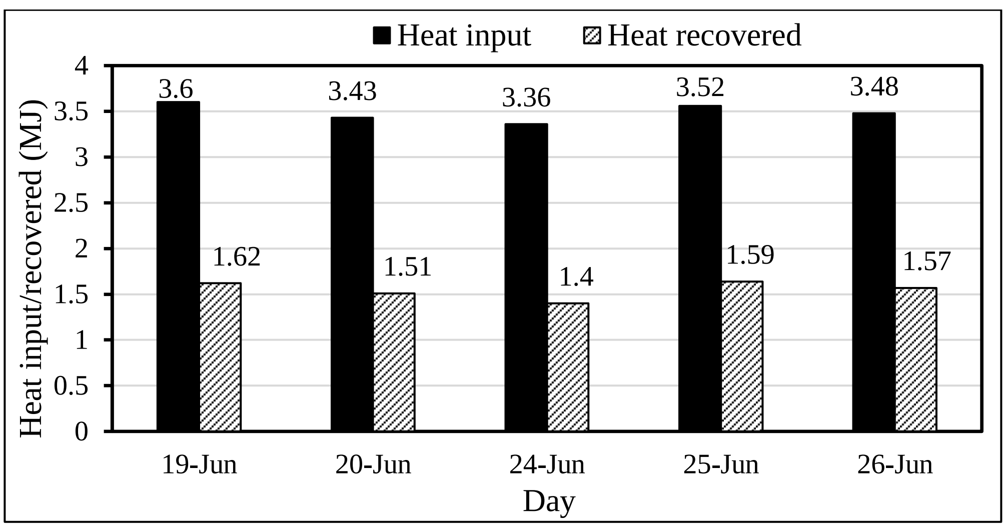

Figure 6.16: Net heat input/recovered during the charging and discharging process.

6.3.3 Exergy input/recovered during the charging and discharging process

Figure 6.17 represents the instantaneous exergy input and exergy recovered during the charging and discharging process of the energy storage. The exergy input and recovered are shown as positive and negative on the secondary Y-axis respectively. The average instantaneous exergy input during the charging process varied between 6.3 W and 8.9 W and the exergy recovered during the discharging process varied between 2.1 W and 3.4 W.

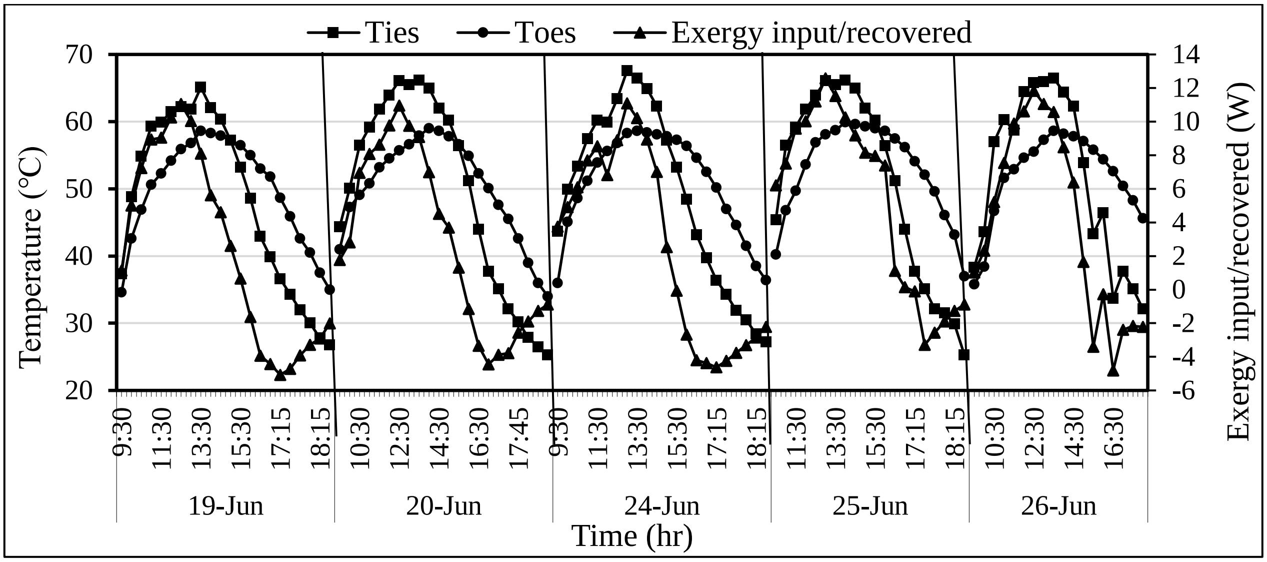

Figure 6.17: Exergy input/recovered by the air during the charging and discharging process.

The net exergy input and exergy recovered during the charging and discharging process is presented in Figure 6.18. The net exergy input to the storage varies between 0.27 MJ and 0.31 MJ and the net exergy recovered from the storage varies between 0.048 MJ and 0.053 MJ with overall exergy efficiency of 15.6 to 18.5%.

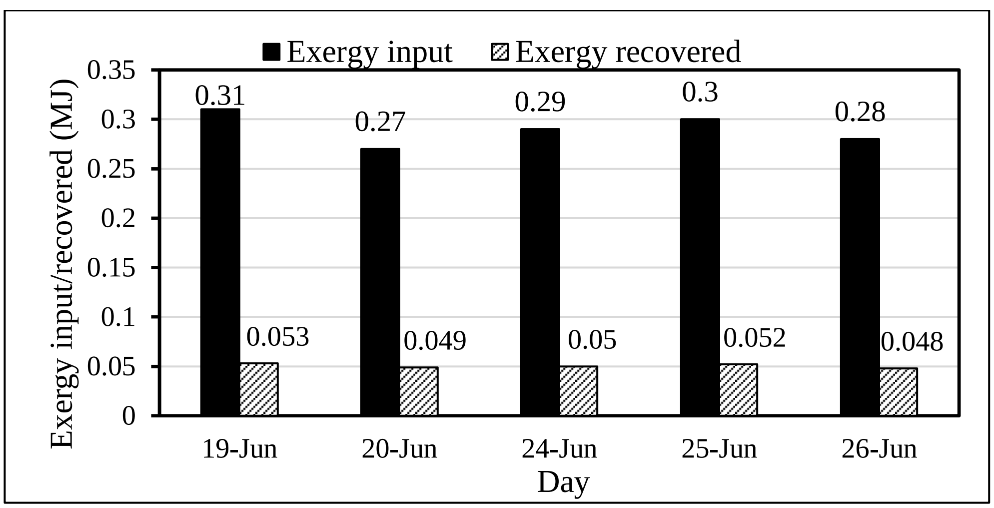

Figure 6.18: Net exergy input/recovered during the charging and discharging process.

6.3.4 Temperature variation of the paraffin wax at different locations

Figure 6.19 (a) shows the temperature variation of the paraffin wax at different locations of the energy storage during the charging and discharging process. Apart from measuring the inlet and outlet temperature of the heat transfer fluid, measuring the temperature of the wax at different locations gives the best information about melting and freezing behavior of the wax. Three thermocouples were fixed near the inlet (T_{c8}), at the center (T_{c9}) and near the outlet (T_{c10}) of the energy storage as represented in Figure 5.5. It is observed that, near the inlet of the energy storage, the temperature of the wax increases and decreases first. The temperature of the wax increases as the inlet air temperature of the storage increases and decrease when the inlet air temperature becomes lower than the PCM. The PCM is said completely melted when its temperature at the three locations reaches the melting temperature of the PCM and does not change. The average temperature variation of the wax is also shown in Figure 6.19 (b).

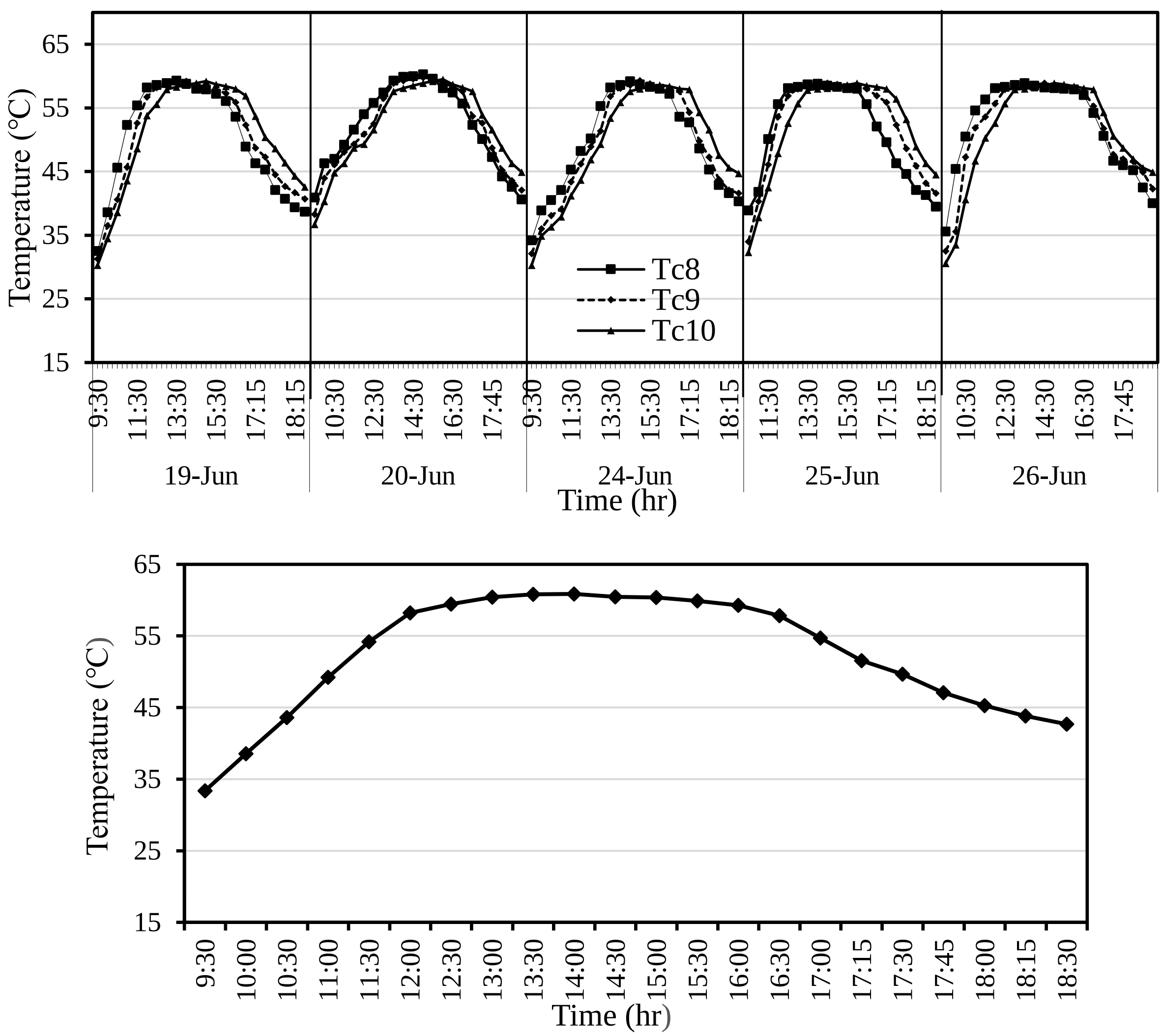

Figure 6.19: Variation of wax temperature, (a) at different locations and (b) average temperature variation of the wax.

6.4 Simulation results of the thermal energy storage

Average temperature variation of the PCM, the charging and discharging time and amount of energy stored and released during the charging and discharging process are predicted with simulation on COMSOL Multiphysics 4.3a and presented as follows.

6.4.1 Temperature variation of the PCM

Figure 6.20 (a) and (b) represents the volumetric average temperature variation of the latent heat storage during the charging and discharging process. Initially the storage is at 25/70 ℃ during the charging and discharging process. When the heat transfer fluid at 70/25 ℃ passes through the tubes, heat transfer takes place between the heat transfer fluid and the PCM. From Figure 6.20, it is observed that the initial part of the curve shows a steady increase/decrease of temperature due to the higher heat transfer potential available during the initial period of the charging/discharging process. After 3000 s, the storage stores/discharges a large amount of heat and the slope of the curve starts decreasing. PCM temperature variations with similar trends were also reported by Niyas *et al.* (2017) and Gunjo *et al*. (2018) with oil and water as a heat transfer fluid, respectively.

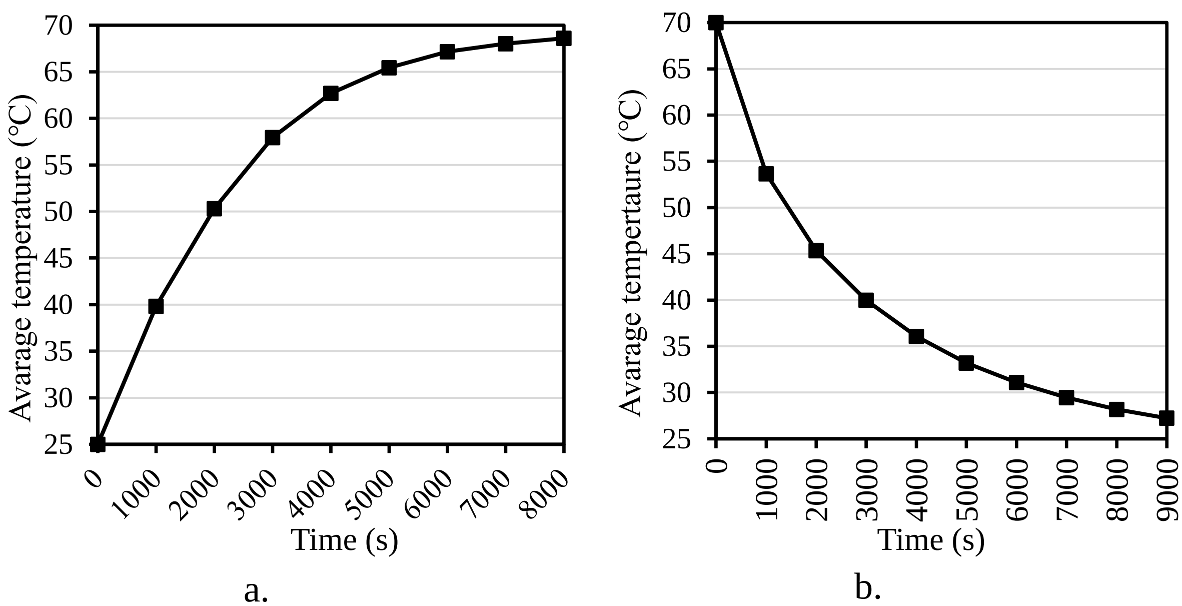

Figure 6.20: Average temperature of the PCM a) charging and b) discharging process.

6.4.2 Charging and discharging time

Figure 6.21 (a) and (b) shows the volumetric average melt fraction variation of the latent heat storage during the charging and discharging process. Melt fraction only shows the latent heat storing and discharging characteristics of a latent heat storage during the charging and discharging periods. The PCM took 8000 s (133 min) to completely melt and 9000 s (150 min) to completely solidify. It is observed that there is a faster rise/fall of melt fraction at the beginning of each process due to the higher heat transfer rate between the PCM and the air.

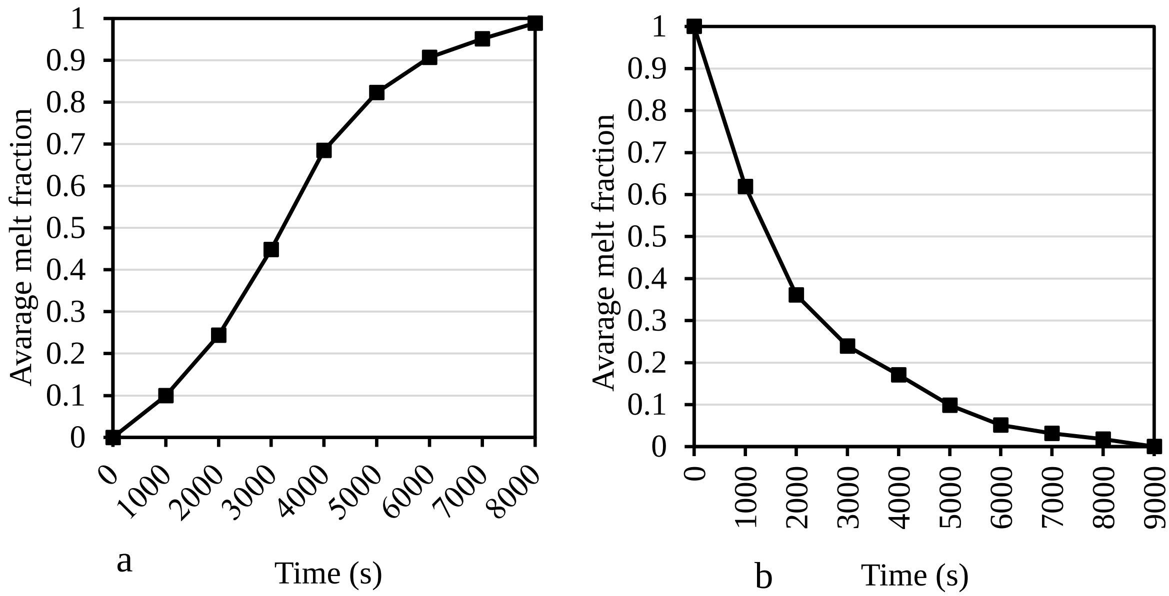

Figure 6.21: Average melt fraction of PCM a) charging and b) discharging process.

6.4.3 Contours of average melt fraction

Figure 6.22 (a) and (b) shows the contours of average melt fraction during the charging and discharging process. At the beginning of the charging/discharging process (t = 0 s), the average melt fraction of the PCM is 0/1 and at the end of the process it becomes 1/0, respectively.

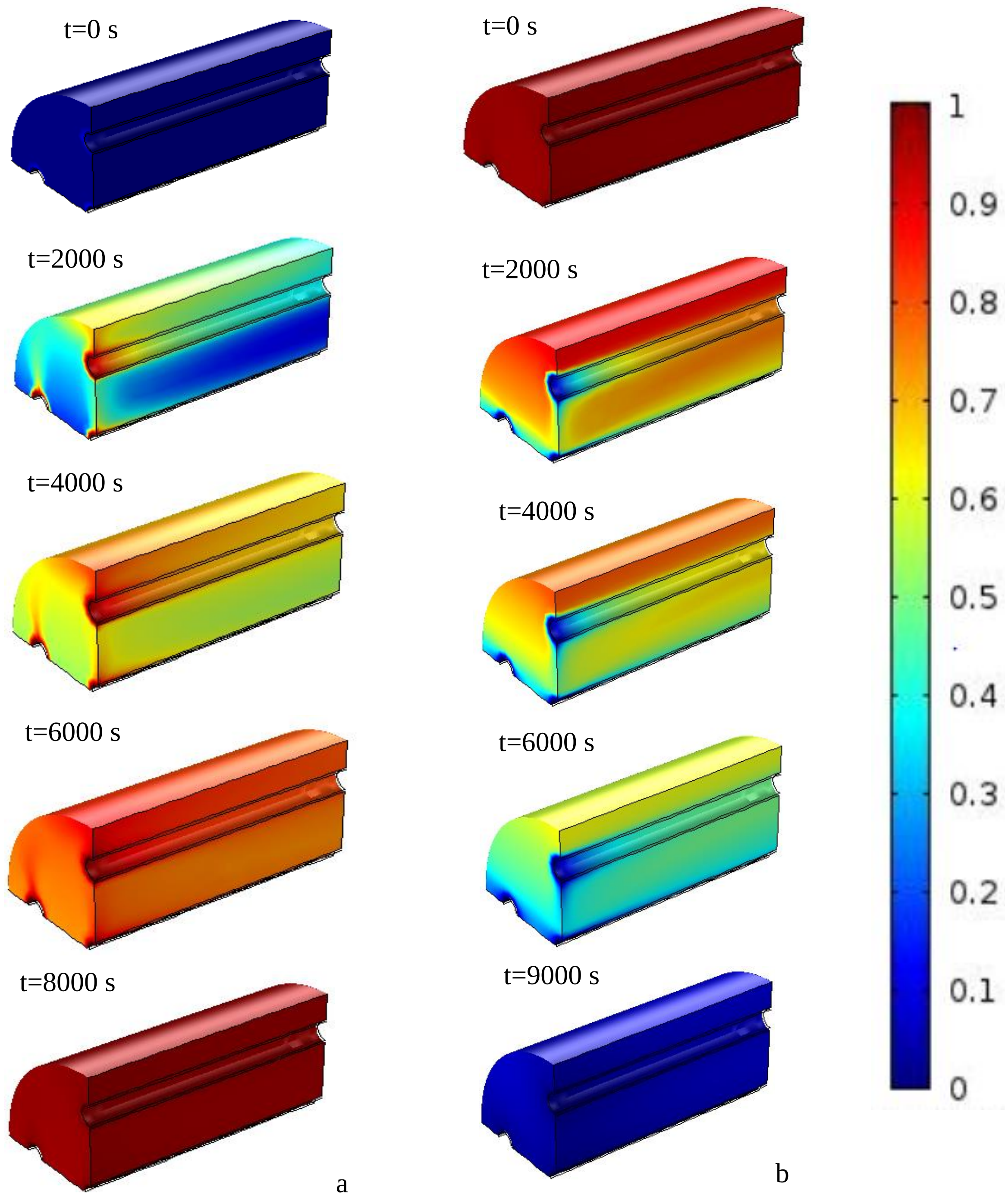

Figure 6.22: Contours of melt fraction a) charging and b) discharging process.

6.4.4 Total energy stored and discharged during the charging and discharging process

The total energy stored/discharged during the charging/discharging process is in the form of both sensible and latent heat is described by Figure 6.23 (a) and (b). At the beginning of the process, heat gets stored/discharges as sensible heat. When the PCM reaches its melting temperature (phase change temperature) (58 °C), heat gets stored/discharged as latent heat. After the melting temperature heat gets stored/discharged in the form of sensible heat. The amount of sensible and latent heat stored during the charging process is 1.67 MJ and 2.96 MJ and the total heat stored is 4.63 MJ. The amount of sensible and latent heat released during the discharging process is 1.63 MJ and 2.93 MJ and the total heat discharged is 4.56 MJ.

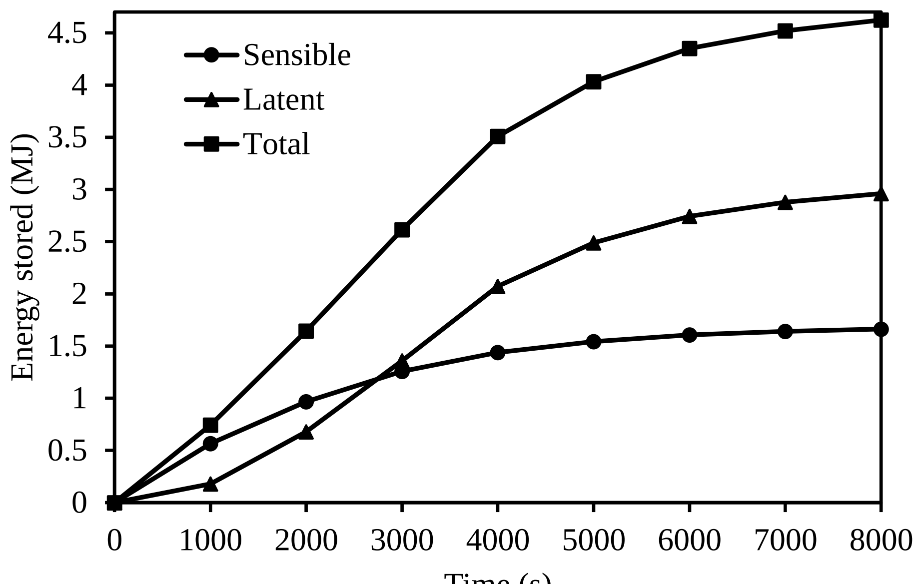

a.

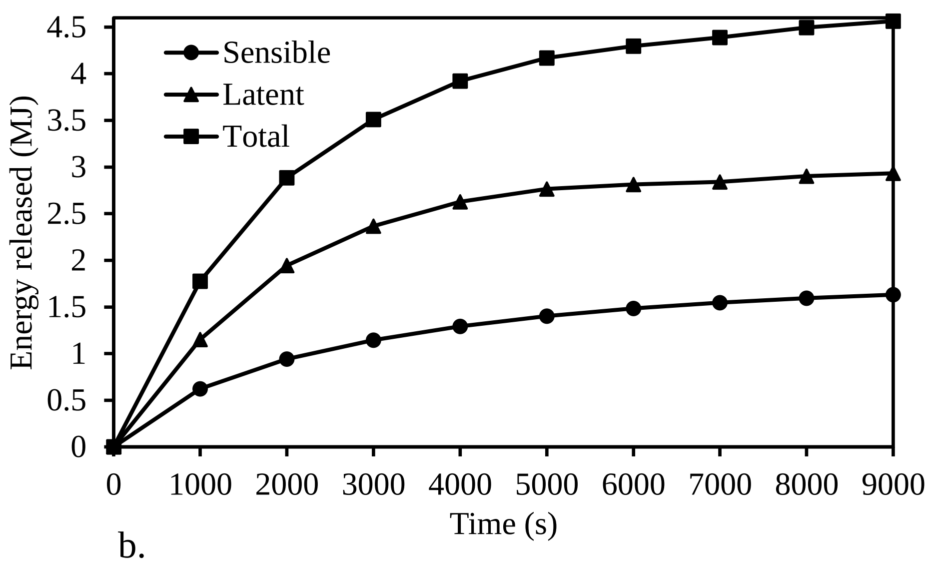

b.

Figure 6.23: Energy stored and released during a) charging and b) discharging process.

6.4.5 Model validation

The predicted charging time of the PCM with the simulated model is 2 h and 14 min with inlet air temperature of 70 ℃. This result is validated with the experimental result of the energy storage. During the experiment, charging starts from 9:30 h and completed at 14:30 h. Between 9:30 h and 11:30 h, only sensible heating takes place and the PCM starts melting after 11:30 h. The inlet temperature of the energy storage becomes 5 ℃ to 9 ℃ higher than the melting temperature of the PCM from 11:30 h to 14:30 h (3 h) and the average temperature of the PCM within this time interval is between 53 ℃ and 60 ℃. Therefore, complete melting of the PCM is insured within the 3hrs and agrees with the predicted results of the simulation.

6.5 Experimental results of the drying chamber

Drying experiments have been performed for three consecutive days (24th, 25th and 26th June, 2020). 5 kg fresh fish is loaded in the drying chamber and the inlet and outlet temperatures of the chamber are recorded in a 30-minute interval to determine performance of the drying chamber. The weight of four samples from four different locations are measured in a three-hour interval till the experiment is stopped to determine the moisture loss from the fish.

6.5.1 Effect of the thermal energy storage on inlet temperature of the drying chamber

Figure 6.24 shows the effect of the thermal energy storage on the inlet temperature of the drying chamber. If the thermal storage was not integrated with the drying system, the outlet of the solar air heater would have been directly connected to the inlet of the drying chamber. It is observed that, the inlet air temperature of the drying chamber varies between 40 ℃ and 70 ℃ without PCM and 35 ℃ and 57 ℃ with PCM. The fluctuations of the inlet temperature of the drying chamber due to the fluctuation of the outlet temperature of the solar air heater are corrected by integrating the latent heat storage between the solar air heater and the drying chamber. The inlet temperature of the drying chamber with PCM is also 5 ℃ to 10 ℃ higher than without PCM after 16:30 h due to the additional heat recovered from the energy storage.

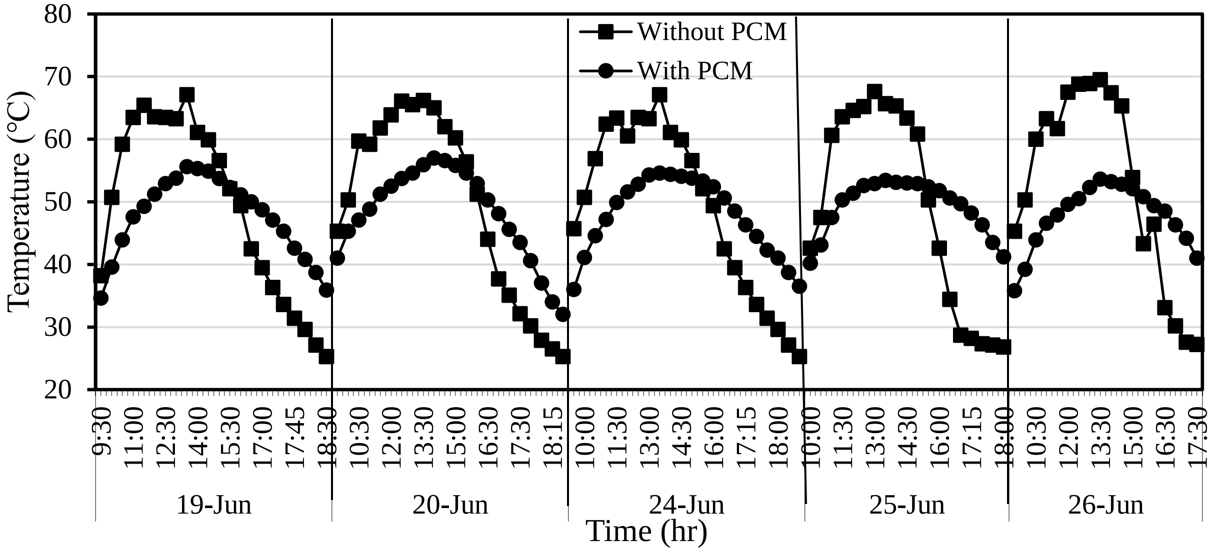

Figure 6.24: Effect of PCM on inlet temperature of the drying chamber.

6.5.2 Inlet and outlet temperature variation of the drying chamber

The temperature variation of the drying air at the inlet and outlet of the drying chamber for the three consecutive days of drying is depicted in Figure 6.25. The inlet temperature of the drying chamber varies between 40 ℃ and 57 ℃ whereas the outlet temperature varies between 35 ℃ and 47 ℃. The outlet air temperature of the drying chamber increases with the number of days of drying due to the less moisture content of the fish. During the first day of drying, the drying air takes higher moisture than the latter days resulting in lower outlet temperature during the first day.

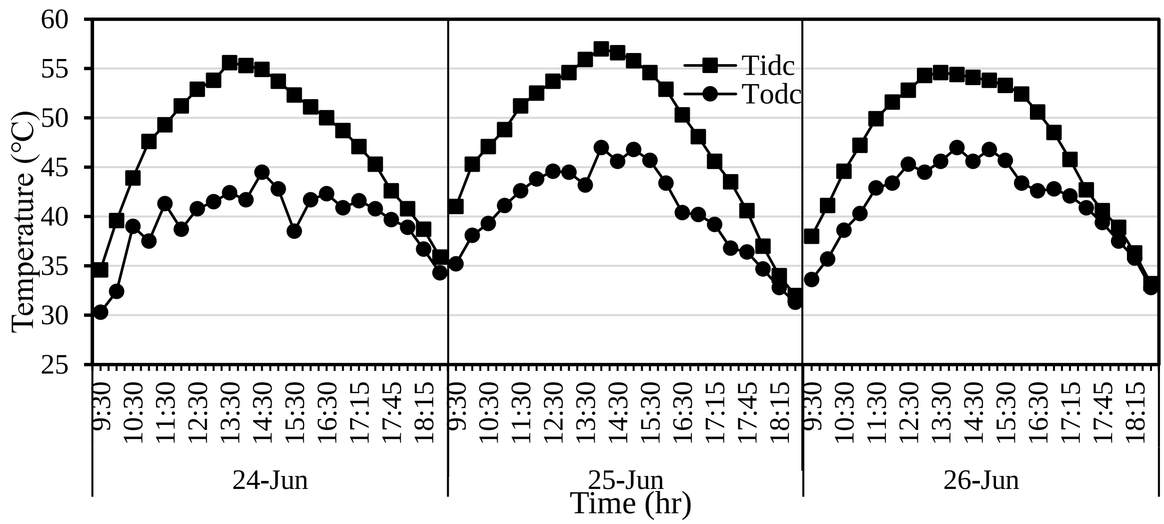

Figure 6.25: Inlet and outlet temperature variations of the drying chamber.

6.5.3 Variation of heat used by the drying chamber

The variation of heat used by the drying chamber for the three consecutive days of drying is represented in Figure 6.26. The maximum heat used in the drying chamber varies between 10 to 145 W. The heat used increases as the inlet temperature of the drying chamber increases and decreases as it decreases. It is also observed that the heat used during the first day is higher and it decreases as the drying time increases since the amount of moisture removed is lower toward the end of drying compared to the early days resulting in higher outlet air temperature of the drying chamber.

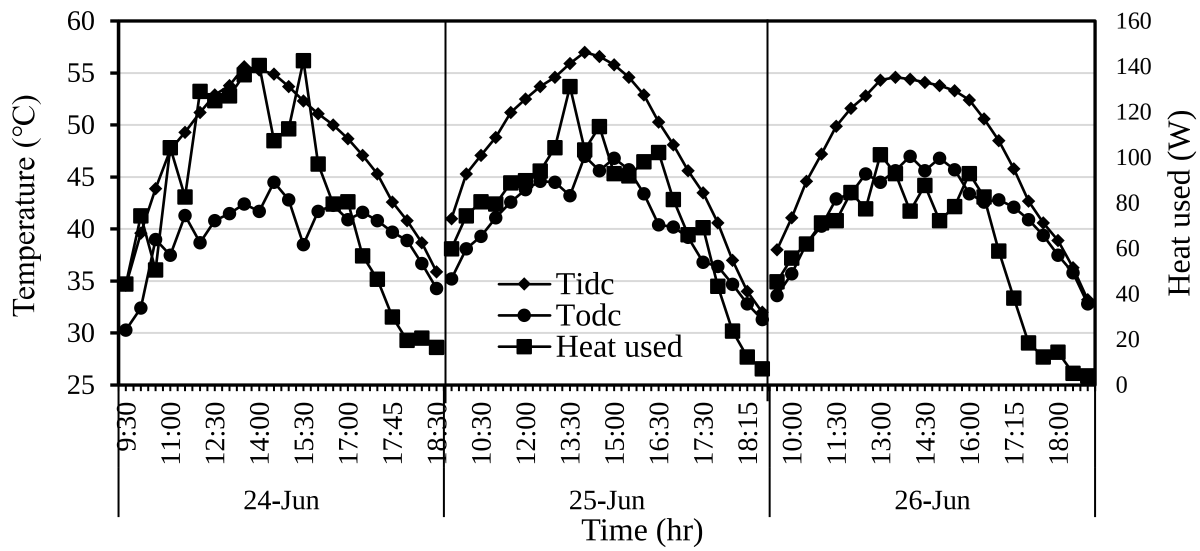

Figure 6.26: Variation of heat used by the drying chamber with inlet and outlet temperatures.

6.5.4 Efficiency of the drying chamber

Figure 6.27 shows the variation of thermal efficiency of the drying chamber with time. The thermal efficiency of the drying chamber varies between 13 to 62% during the three consecutive days of drying and the average thermal efficiency of the drying chamber is 35.4%. It is observed that the thermal efficiency of the drying chamber decreases as the drying time advances and it is higher for the first day and decreases with the next days. This is due to the high amount of moisture removed during the first day of drying resulting in a high temperature drop between the inlet and outlet of the drying chamber. The thermal efficiency of the drying chamber also decreases during the last hours of drying in each day as the inlet temperature of the drying chamber decreases during the last hours.

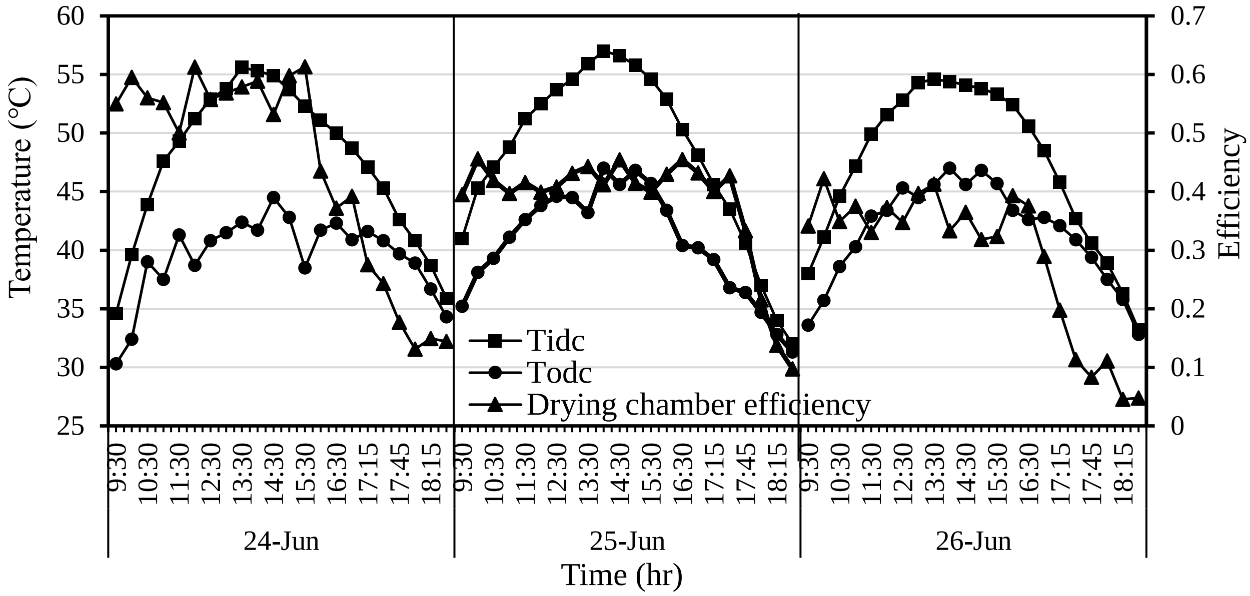

Figure 6.27: Variation of drying chamber efficiency.

6.5.5 Variation of exergy inflow, outflow and exergy efficiency of the drying chamber

Figure 6.28 shows the variation of exergy inflow, outflow and exergy efficiency of the drying chamber. The exergy inflow depends on the inlet temperature of the drying chamber whereas the exergy outflow is related to the outlet temperature variation of the drying chamber. The exergy efficiency of the drying chamber varies between 15.4% and 90.8% and the average exergetic efficiency is 52.2%. The exergy efficiency of the drying chamber is higher for the last day of drying than the first two days as the amount of moisture left in the fish is lower resulting a higher exergy outflow due to increase in outlet temperature of the chamber. During the last hours of drying, the inlet temperature of the drying chamber decreases resulting a lower exergy inflow. But the outlet temperature of the drying chamber does not decrease in the same manner as the inlet temperature due to the accumulated heat released from the chamber to the air resulting in an addition of exergy. Therefore, the exergy efficiency is higher during the last hours of drying each day. Similar trends of exergy efficiencies were reported by Fudholi *et al.* (2014) and Akpinar (2010).

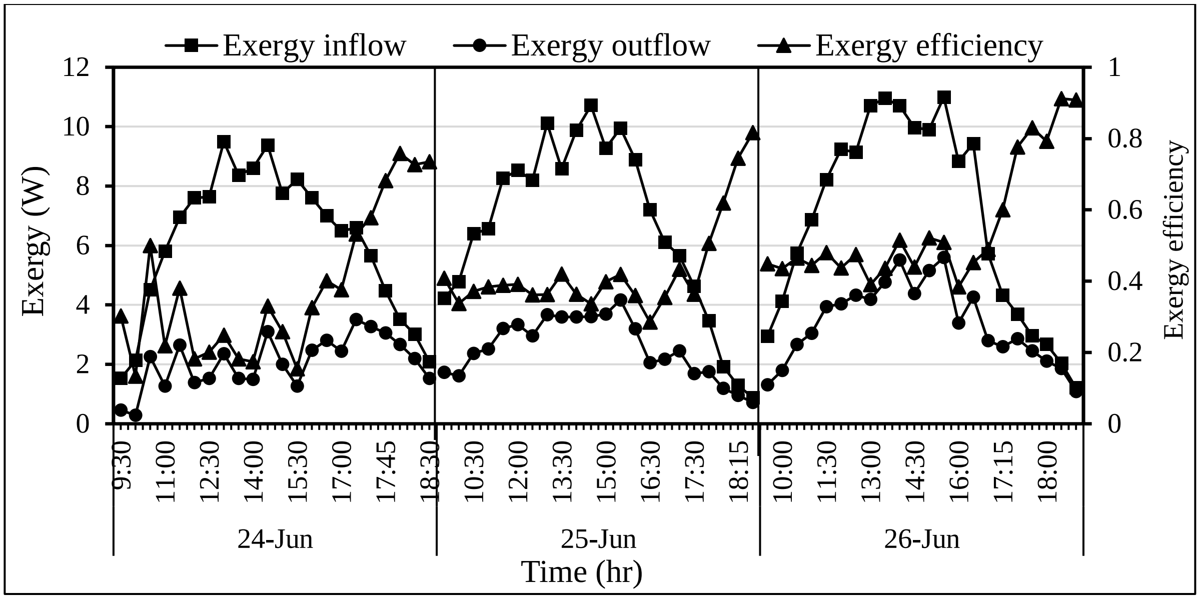

Figure 6.28: Variation of exergy inflow, outflow and exergy efficiency of the drying chamber.

6.6 Performance of the drying system

The variation of moisture content with drying time for the three consecutive days of drying is shown in Figure 6.29. The moisture content of the fish is determined by measuring the weight of the fish and calculating the weight loss in a three-hour interval. The moisture content of the fish is reduced from the initial value of 75% (w.b.) to a final moisture content of 12.5% (w.b.) in 21hrs. The moisture content of the fish is reduced from 75% (w.b.) to 45% (w.b.), 24% (w.b.) and 12.5% (w.b.) during the first, second and third days of drying respectively. Figure 6.30 (a) shows the photograph of fresh fish samples taken before they are loaded into the drying chamber and (b) shows the photograph taken after drying in the solar dryer. It is clearly observed from Figure 6.30 that the color and texture of the fish is preserved during the drying process.

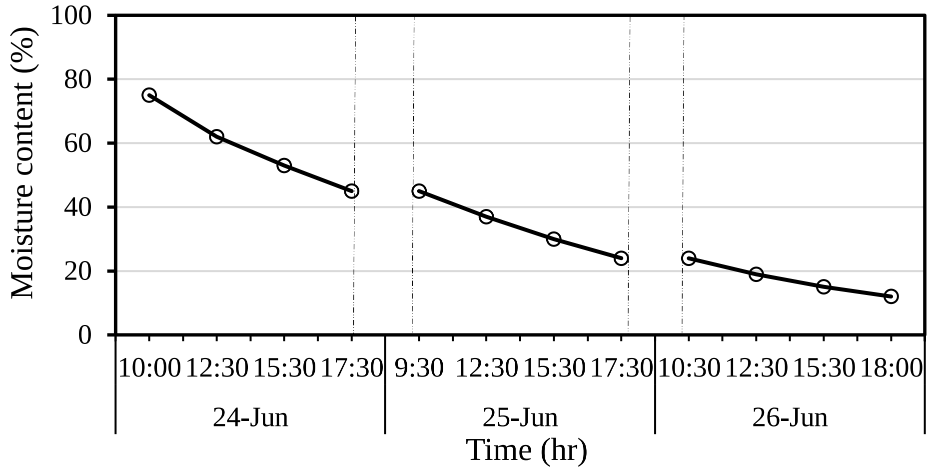

Figure 6.29: Variation of moisture content of the fish with drying time.

(a)

(b)

Figure 6.30: Fish samples (a) before drying and (b) after drying.

3.57 kg of moisture is evaporated from 5 kg of fresh fish while reducing the moisture content of the fish from an initial value of 75% (w.b.) to a final value of 12.5% (w.b.). The average solar radiation intensity falling on the surface of the solar air heater is estimated to be 539.6 W/m^2. The area of the solar air heater was 2.06 m^2 and the power consumed by the blower is 100 W. The dryer is operated for 7 h a day. The latent heat of evaporation of water at an average drying air temperature of 50 °C (Eqn.4.3) is 2396.5 kJ/kg and the heat required to evaporate 3.57 kg of moisture from the fish is 8.4 MJ. The total energy input to the drying system is determined from Eqn. (4.79) and found as 91.6MJ. The specific energy consumption of the dryer is determined from Eqn. (4.78) which is found as 7.3 kWh per kg of moisture. From the 7.3 kWh per kilogram of moisture consumption, the electrical energy consumption of the blower per kilogram of moisture removal is 0.6 kWh which is 8.3% of the total specific energy consumption of the dryer. The remaining 91.7% of energy consumed by the dryer is harvested from the free, easily available, eco-friendly renewable type of energy, solar energy. The overall efficiency of the drying system is determined using Eqn. (4.80) and found to be 9.4%. Sengar *et al.* (2009), Sain *et al.* (2013), Ayyapan *et al.* (2015) and Hubackova *et al.* (2014) reported almost similar results for drying fish, ginger and coconuts, respectively.

6.7 Economic analysis

The life cycle cost of the dryer is calculated considering 10% maintenance cost, 10% interest rate and 6% depreciation. The life cycle saving is then calculated using the life cycle cost and the payback period is determined.

The annual cost of the dryer is calculated by (Elkhadraoui *et al*., 2015):

$$C_d = C_{ac} + C_m - S_a + C_e \quad (6.1)$$

Where, C_{ac} is annual capital cost, C_m is maintenance cost, S_a is annual salvage value and C_e is annual electricity cost for running the blower.

The annual capital cost: $C_{ac} = C_{dc}F_c$ …………………………………………………. (6.2)

Where, C_{dc} is capital cost of the dryer and F_c is the capital recovery factor given by:

$$F_c = \frac{i(1+i)^n}{(1+i)^n - 1} \quad (6.3)$$

Where, i is the interest rate assumed to be 10% and n is the life period assumed to be 10 years.

Annual salvage value: $S_a = S \times F_s$ ……………………………………………… (6.4)

Where, S is the salvage value taken as 10% of the capital cost of the dryer and F_s is the salvage fund factor given by:

$$F_s = \frac{i}{(1+i)^n - 1} \quad (6.5)$$

The annual running cost of the dryer: $C_e = C_{ele} \times P_f \times t_{hr}$ ……………………………… (6.6)

Where, P_f is the power consumed by the blower, C_{ele} is unit cost of electricity and t_{hr} is annual running hour of the dryer.

The cost of drying per kilogram of dried product is calculated by (Elkhadraoui *et al*., 2015):

$$C_{dr} = \frac{C_d}{m_y} \quad (6.7)$$

Where, m_y is the mass of the product dried per year which is calculated as:

$$m_y = \frac{m_b N_y}{N_b} \quad (6.8)$$

Where, m_b is the mass of the product dried per batch, N_y is the number of days of operation of the dryer per year and N_b is the number of days of operation of the dryer per batch.

The cost of fresh product per kilogram of dried product is calculated as:

$$C_{dp} = C_{fp} \frac{m_f}{m_b} \quad (6.9)$$

Where, C_{fp} is the cost per kg of fresh product and m_f is mass of fresh product loaded in the solar dryer per batch in kg.

The cost of 1 kg of dried product (C_{ds}) for the solar dryer is the summation of the cost of fresh product (C_{dp}) and the cost of drying per kilogram of dried product (C_{dr}) which is determined as:

$$C_{ds} = C_{dp} + C_{dr} \quad (6.10)$$

The saving per kilogram of dried product (S_{kg}) in the base year due to use of the solar dryer is calculated as:

$$S_{kg} = C_b - C_{ds} \quad (6.11)$$

Where, C_b is selling price of dried product.

The saving per batch (S_b) and the saving per day (S_d) in the base year are then calculated using equations (6.12) and (6.13), respectively.

$$S_b = S_{kg} m_b \quad \text{(6.12)}$$

$$S_d = \frac{S_b}{N_b} \quad \text{(6.13)}$$

For the life of the system, the annual savings (S_j) for drying the typical product in the j[th] year is obtained as (Elkhadraoui *et al*., 2015):

$$S_j = S_d N_y (1 + d)^{j-1} \quad \text{(6.14)}$$

The payback period (N) is the calculated as (Elkhadraoui *et al*., 2015):

$$N = \frac{\ln\left[1 - \frac{C_{dc}}{S_j}(i - d)\right]}{\ln\left(\frac{1+d}{1+i}\right)} \quad \text{(6.15)}$$

The economic analysis is performed using Eqns. (6.1) to (6.15) and presented in Tables 6.1 and 6.2. The capital cost of the dryer is 10100 ET. birr and the unit cost of electricity in Ethiopia is 1.8 ET. birr/kWh. The annual saving due to the use of the dryer is 8025 ET. birr and the payback period is 1.39 years.

Table 6.1: Cost of components of the dryer.

Components	Cost (ET. birr)
Solar air heater	3750
LHS	3200
Drying chamber with trays	800
Pipe and fittings	200
Blower	900
Manufacturing cost	1250
Total	10100

Table 6.2: Annualized costs.

Category	Cost
Capital cost (ET. birr)	10100
Life of the dryer (years)	10
Annual capital cost (ET. birr)	1644
Maintenance cost (ET. birr)	164.4
Salvage value (ET. birr)	1010
Annual salvage value (ET. birr)	64
Electricity cost (ET. birr)	315
Annual cost of the dryer (ET. birr)	2059.4
Quantity of product dried per year (kg)	155
Quantity of product dried per batch (kg)	1.428
Number of operations of the dryer per year (days)	250
Number of operations of the dryer per batch (days)	3
Cost of drying per kilogram of dried product (ET. birr)	13.4
Cost of 1 kg of dried product (ET. birr)	230
Saving per kilogram of dried product (ET. birr)	30
Saving per batch (ET. birr)	56
Saving per day (ET. birr)	19
Annual savings (ET. birr)	8026
Payback period (years)	1.39

CHAPTER SEVEN

CONCLUSIONS AND RECOMMENDATIONS

7.1 Conclusions

A flat plate solar air dryer integrated with a shell and tube type latent heat storage filled with 16kg paraffin wax with melting temperature of 58 ℃ is developed and experimentally tested. The components of the dryer have been sized based on the energy and mass of air required for drying 5 kg fresh fish. The dryer is fabricated from locally available materials and the performance of the components of the dryer and the performance of the overall drying system is evaluated using energy and exergy analysis. No load testing is done on 19^{th} and 20^{th} June,2020 to evaluate the performance of the SAH and the energy storage and the effect of integrating the energy storage on the inlet temperature of the drying chamber. The drying chamber is then loaded with 5kg fresh fish and the drying experiment was conducted for three consecutive days (24^{th}, 25^{th} and 26^{th} June, 2020). Finally, economic analysis of the dryer is done based on annualized cost method to determine the life cycle saving and payback period. The following conclusions are drawn from this study:

- ❖ The energy and exergy efficiency of the SAH increases with increasing solar radiation intensity and the average energy and exergy efficiency of the double pass SAH was 25% and 1.5%, respectively.
- ❖ The outlet air temperature of the SAH with double pass configuration was 5 to 10℃ higher than the single pass configuration and the energy and exergy efficiency of the double pass SAH were 8 to 15% and 0.6 to 1.2% higher than the single pass.
- ❖ Integration of the energy storage reduces the fluctuations in the outlet air temperature of the SAH and extends the drying process beyond the sunny hours.
- ❖ The average energy and exergy efficiency of the energy storage varies between 38.7% to 45% and 13.6% to 17.5%, respectively.
- ❖ The average energy and exergy efficiency of the drying chamber were 35% and 52%, respectively.
- ❖ The specific energy consumption was 7.3kWh per kilogram of moisture and the electrical energy consumption of the blower was 0.6 kWh per kilogram of moisture which was

8.3% of the total energy consumption and the remaining 91.7% energy was harvested from solar energy.

- 3.57 kg moisture was removed from 5 kg fresh fish while drying the fish from an initial moisture content of 75% (w.b.) to a final moisture content of 12.5% (w.b.) within 21h of drying preserving the color and texture of the product and the overall efficiency of the drying system was 9.4%.

7.2 Recommendations for future work

The performance of a flat plate solar air dryer integrated with phase change material was experimentally investigated by drying fish and the drying was effectively accomplished. However, there is a scope for improvement in the drying system.

- The outlet temperature of the drying chamber becomes high during the last days of drying. Addition of a mechanism for recirculating this hot air can be studied further.
- The performance of the SAH was improved by passing the air between the absorber and the bottom plate after it passes through the glazing and the absorber plate. Further improvements like addition of wire mesh in the second fluid channel can enhance its performance and thereby enhancing the performance of the system.
- The performance of the drying system was evaluated using energy and exergy analysis by drying fish. Further study on the drying kinetics of fish may help improve the performance of the system.
- The dryer was designed based on the daily fish loss of a single fisherman. Large scale application of the dryer for collective use can be investigated further.

SPECIAL ACKNOWLEDGEMENT

This research project is funded by Adama Science and Technology University under the grant number ASTU/SM-R/143/19, Adama, Ethiopia.

REFERENCES

1. Addisu Bekele, Manish Mishra, Sushanta Dutta and Chandraprabu Venkatachalam (2019). Heat transfer and friction factor correlation for solar dryer fitted with delta shaped turbulators. *Journal of Information and Computational Science*, 9(12), 1442-1456.
2. Afriyie, J. K., Nazha, M. A., Rajakaruna, H., & Forson, F. K. (2009). Experimental investigations of a chimney-dependent solar crop dryer. *Renewable Energy*, *34*(1), 217-222.
3. Agarwal, A., & Sarviya, R. M. (2016). An experimental investigation of shell and tube latent heat storage for solar dryer using paraffin wax as heat storage material. *Engineering Science and Technology, an International Journal*, *19*(1), 619-631.
4. Aissa, W., El-Sallak, M., & Elhakem, A. (2012). An experimental investigation of forced convection flat plate solar air heater with storage material. *Thermal Science*, *16*(4).
5. Aklilu Tesfamichael. (2004). Experimental Analysis for Performance Evaluation of Solar Dryer. *Department of Mechanical Engineering, AAU*.
6. Al-Juamily, K. E., Khalifa, A. J. N., & Yassen, T. A. (2007). Testing of the performance of a fruit and vegetable solar drying system in Iraq. *Desalination*, *209*(1-3), 163-170.
7. Alkilani, M. M., Sopian, K., Alghoul, M. A., Sohif, M., & Ruslan, M. H. (2011). Review of solar air collectors with thermal storage units. *Renewable and Sustainable Energy Reviews*, *15*(3), 1476-1490.
8. Asmare, E., Tewabe, D., Mohamed, B., & Hailu, B. (2015). Pre-Scaling Up of Solar Tent Fish Drier in Northern and North Western Part of Lake Tana, Ethiopia. *International Journal of Aquaculture and Fishery Sciences*, *1*(2), 48-53.
9. Assefa, A., Abunna, F., Biset, W., & Leta, S. (2018). Assessment of post-harvest fish losses in two selected lakes of Amhara Region, Northern Ethiopia. *Heliyon*, *4*(11), e00949.
10. Ayyappan, S., & Mayilsamy, K. (2012). Solar tunnel drier with thermal storage for drying of copra. *International journal of energy technology and policy*, *8*(1), 3-13.
11. Ayyappan, S., Mayilsamy, K., & Sreenarayanan, V. V. (2016). Performance improvement studies in a solar greenhouse drier using sensible heat storage materials. *Heat and Mass Transfer*, *52*(3), 459-467.
12. Bakari, R., Minja, R. J., & Njau, K. N. (2014). Effect of glass thickness on performance of flat plate solar collectors for fruits drying. *Journal of Energy*, 1-8.

13. Bal, L. M., Satya, S., & Naik, S. N. (2010). Solar dryer with thermal energy storage systems for drying agricultural food products: A review. *Renewable and Sustainable Energy Reviews*, *14*(8), 2298-2314.
14. Bala, B. K., & Mondol, M. R. A. (2001). Experimental investigation on solar drying of fish using solar tunnel dryer. *Drying technology*, *19*(2), 427-436.
15. Basu, S., Shivhare, U. S., & Mujumdar, A. S. (2006). Models for sorption isotherms for foods: a review. *Drying technology*, *24*(8), 917-930.
16. Bhargava, A. K., Garg, H. P., & Sharma, V. K. (1983). A two-pass solar air heater. *Energy*, *8*(4), 267-276.
17. Bolaji, B. O. (2005). Development and Performance Evaluation of a Box-type Absorber Solar Air Collector for Crop Drying. *Journal of Food Technology*, *3*(4), 595-600.
18. Bolaji, B. O., & Olalusi, A. P. (2008). Performance evaluation of a mixed-mode solar dryer. *AU Journal of Technology*, 11(4), 225–231.
19. Bouadila, S., Kooli, S., Lazaar, M., Skouri, S., & Farhat, A. (2013). Performance of a new solar air heater with packed-bed latent storage energy for nocturnal use. *Applied Energy*, *110*, 267-275.
20. Curran, C. A., & Trim, D. S. (1983). Comparative study of solar and sun drying of fish. *FAO Fisheries Reports (FAO)*.
21. Das, S. K., & Kumar, Y. (1989). Design and performance of a solar dryer with vertical collector chimney suitable for rural application. *Energy Conversion and Management*, *29*(2), 129-135.
22. Devahastin, S., & Pitaksuriyarat, S. (2006). Use of latent heat storage to conserve energy during drying and its effect on drying kinetics of a food product. *Applied thermal engineering*, *26*(14-15), 1705-1713.
23. Dhatkar Samir A, Khandelwal Ankit C, and Patil A B Kanase. (2015). A Review of Solar Air Heaters using wire Mesh Absorber. *ISSN*, 4, 2319-3182.
24. Dhiman, P., Thakur, N. S., & Chauhan, S. R. (2012). Thermal and thermos-hydraulic performance of counter and parallel flow packed bed solar air heaters. *Renewable Energy*, *46*, 259-268.
25. Do Ango, A. M., Médale, M., & Abid, C. (2013). Optimization of the design of a polymer flat plate solar collector. *Solar Energy*, *87*, 64-75.

26. Duffie and Beckman. (1991). *Solar Engineering of Thermal Processes. 4th edition.* New York: J. Wiley and Sons.
27. El-Sebaii, A. A., Aboul-Enein, S., Ramadan, M. R. I., & El-Gohary, H. G. (2002). Experimental investigation of an indirect type natural convection solar dryer. *Energy Conversion and Management*, *43*(16), 2251-2266.
28. Enibe, S. O. (2003). Thermal analysis of a natural circulation solar air heater with phase change material energy storage. *Renewable Energy*, *28*(14), 2269-2299.
29. Fath, H. E. (1995). Thermal performance of a simple design solar air heater with built-in thermal energy storage system. *Renewable energy*, *6*(8), 1033-1039.
30. Fath, H. E. (1995). Transient analysis of thermosyphon solar air heater with built-in latent heat thermal energy storage system. *Renewable Energy*, *6*(2), 119-124.
31. Forson, F. K., Nazha, M. A. A., Akuffo, F. O., & Rajakaruna, H. (2007). Design of mixed-mode natural convection solar crop dryers: Application of principles and rules of thumb. *Renewable Energy*, *32*(14), 2306-2319.
32. Getu, A., Misganaw, K., & Bazezew, M. (2015). Post-harvesting and major related problems of fish production. *Fisheries and Aquaculture Journal*, *6*(4).
33. Gram, L., & Dalgaard, P. (2002). Fish spoilage bacteria–problems and solutions. *Current opinion in biotechnology*, *13*(3), 262-266.
34. Gunjo, D. G., Jena, S. R., Mahanta, P., & Robi, P. S. (2018). Melting enhancement of a latent heat storage with dispersed Cu, CuO and Al_2O_3 nanoparticles for solar thermal application. *Renewable energy*, *121*, 652-665.
35. Habtamu Tkubet. (2007). Simulation of Solar Cereal Dryer using TRNSYS. *Department of Mechanical Engineering, AAU*.
36. He, W., Hong, X., Luo, B., Chen, H., & Ji, J. (2016). CFD and comparative study on the dual-function solar collectors with and without tile-shaped covers in water heating mode. *Renewable energy*, *86*, 1205-1214.
37. Hubackova, A., Kucerova, I., Chrun, R., Chaloupkova, P., & Banout, J. (2014). Development of solar drying model for selected Cambodian fish species. *The Scientific World Journal*, *2014*.

38. Ihaddadene, N., Ihaddadene, R., & Mahdi, A. (2014, April). Effect of distance between double glazing on the performance of a solar thermal collector. In *International Conference on Renewable Energies and Power Quality*, 1(12), 302-306.

39. Jain, D., & Tewari, P. (2015). Performance of indirect through pass natural convective solar crop dryer with phase change thermal energy storage. *Renewable energy*, *80*, 244-250.

40. Karthikeyan, S., & Velraj, R. (2011). Numerical and experimental investigation of the charging and discharging processes in a packed bed PCM based storage unit for air heating applications. *European Journal of Scientific Research*, *66*(1), 105-119.

41. Khater, E. S. G., Bahnasawy, A. H., & Ali, S. A. (2014). Physical and mechanical properties of fish feed pellets. *Journal of Food Processing & Technology*, *5*(10), 1.

42. Kibria, M. A., Anisur, M. R., Mahfuz, M. H., Saidur, R., & Metselaar, I. H. S. C. (2014). Numerical and experimental investigation of heat transfer in a shell and tube thermal energy storage system. *International Communications in Heat and Mass Transfer*, *53*, 71-78.

43. Kituu, G. M., Shitanda, D., Kanali, C. L., Mailutha, J. T., Njoroge, C. K., Wainaina, J. K., & Silayo, V. K. (2010). Thin layer drying model for simulating the drying of Tilapia fish (Oreochromis niloticus) in a solar tunnel dryer. *Journal of Food Engineering*, *98*(3), 325-331.

44. Komolafe, C. A., Ogunleye, I. O., & Adejumo, A. O. D. (2011). Design and Fabrication of a Convective Fish Dryer. *The Pacific Journal of Science and Technology*, *12*(1), 89-97.

45. Krishnan, S., & Sivaraman, B. (2017). Experimental investigations on thermal storage in a solar dryer. *International Energy Journal*, *17*(1), 23-36.

46. Lane G.A. (1983). Solar Heat Storage: Latent Heat Materials, Background and Scientific Principles. *Florida: CRC Press Inc* 1.

47. Lingayat, A. B., & Suple, Y. R. (2013). Review on phase change material as thermal energy storage medium: materials, application. *International Journal of Engineering Research and Applications*, *3*(4), 916-921.

48. Madhlopa, A., & Ngwalo, G. (2007). Solar dryer with thermal storage and biomass-backup heater. *Solar Energy*, *81*(4), 449-462.

49. Madhusudan, M., Tiwari, G. N., Hrishikeshan, D. S., & Sehgal, H. K. (1981). Optimization of heat losses in normal and reverse flat-plate collector configurations: Analysis and performance. *Energy Conversion and Management*, *21*(3), 191-198.

50. Matuska, T., Zmrhal, V., & Metzger, J. (2009, July). Detailed modelling of solar flat-plate collectors with design tool kolektor 2.2. In *Eleventh International IBPSA Conference Glasgow, Scotland*, 2289-2296.
51. Miró, L., Barreneche, C., Ferrer, G., Solé, A., Martorell, I., & Cabeza, L. F. (2016). Health hazard, cycling and thermal stability as key parameters when selecting a suitable phase change material (PCM). *Thermochimica acta*, *627*, 39-47.
52. Mohanraj, M., & Chandrasekar, P. (2009). Performance of a forced convection solar drier integrated with gravel as heat storage material for chili drying. *Journal of Engineering Science and Technology*, *4*(3), 305-314.
53. N'Jai, A. E. (1987). Outlook for solar drying of fish in the Gambia. In *Solar drying in Africa: proceedings of a workshop held in Dakar, Senegal, 21-24 July 1986*. IDRC, Ottawa, ON, CA.
54. Njomo, D., & Daguenet, M. (2006). Sensitivity analysis of thermal performances of flat plate solar air heaters. *Heat and Mass Transfer*, *42*(12), 1065-1081.
55. Osei-Opare F. and A. Kukah. (1989). Improving the quality of dried fish through solar drying. *Proceedings of the FAO Expert Consultants of Fish Technology, In Africa Abidjan*, 400, 164-168.
56. Prakash, B. J., Vishnuprasad, B., & Ramana, V. V. (2013). Performance study on effect of nano coatings on liquid flat plate collector: An experimental approach. *Int. J. Mech. Eng. Rob. Res*, *2*, 379-384.
57. Rathod, M. K., & Banerjee, J. (2014). Experimental investigations on latent heat storage unit using paraffin wax as phase change material. *Experimental heat transfer*, *27*(1), 40-55.
58. Reyes, A., Mahn, A., & Vásquez, F. (2014). Mushrooms dehydration in a hybrid-solar dryer, using a phase change material. *Energy Conversion and management*, *83*, 241-248.
59. Reza, M. S., Bapary, M. A. J., Islam, M. N., & Kamal, M. D. (2009). Optimization of marine fish drying using solar tunnel dryer. *Journal of food processing and preservation*, *33*(1), 47-59.
60. Sablani, S. S., Rahman, M. S., Haffar, I., Mahgoub, O., Al-Marzouki, A. S., Al-Ruzeiqi, M. H., & Al-Belushi, R. H. (2003). Drying rates and quality parameters of fish sardines processed using solar dryers. *Agric Mar Sci*, *8*(2), 79-86.

61. Sachithananthan, K., Trim, D. S., & Speirs, C. I. (1986). A solar-dome dryer for drying fish. *FAO Fisheries Report (FAO)*, 329, 161-172.
62. Sain, P., Songara, V., Karir, R., & Balan, N. (2013, December). Natural convection type solar dryer with latent heat storage. In *2013 International Conference on Renewable Energy and Sustainable Energy (ICRESE)*, 9-14.
63. Saravanakumar, P. T., and K. Mayilsamy. (2010). Forced convection flat plate solar air heaters with and without thermal storage. *Journalof Scientific and Industrial Research*, 69(12), 966–968.
64. Seddegh, S., Wang, X., & Henderson, A. D. (2016). A comparative study of thermal behaviour of a horizontal and vertical shell-and-tube energy storage using phase change materials. *Applied Thermal Engineering*, *93*, 348-358.
65. Sengar, S. H., Khandetod, Y. P., & Mohod, A. G. (2009). Low cost solar dryer for fish. *African Journal of Environmental Science and Technology*, *3*(9).
66. Shalaby, S. M., & Bek, M. A. (2014). Experimental investigation of a novel indirect solar dryer implementing PCM as energy storage medium. *Energy conversion and management*, *83*, 1-8.
67. Shalaby, S. M., Bek, M. A., & El-Sebaii, A. A. (2014). Solar dryers with PCM as energy storage medium: A review. *Renewable and Sustainable Energy Reviews*, *33*, 110-116.
68. Sharma, V. K., Sharma, S., Ray, R. A., & Garg, H. P. (1986). Design and performance studies of a solar dryer suitable for rural applications. *Energy conversion and management*, *26*(1), 111-119.
69. Shringi, V., Kothari, S., & Panwar, N. L. (2014). Experimental investigation of drying of garlic clove in solar dryer using phase change material as energy storage. *Journal of Thermal Analysis and Calorimetry*, *118*(1), 533-539.
70. Smith Peter R. (2011). Planning and installing solar thermal systems." *Cross Street, London, England*, 82-103.
71. Swami, V. M., Autee, A. T., & Anil, T. R. (2018). Experimental analysis of solar fish dryer using phase change material. *Journal of Energy Storage*, *20*, 310-315.
72. Teklu, D. (2015). Determinant factors for wasted fish during harvesting at Amerti and Fichawa Reservoirs Oromia/Ethiopia. *Journal of FisheriesSciences. Com*, *9*(4), 12-15.

73. Tesfay S., & Teferi M. (2017). Assessment of fish post-harvest losses in Tekeze dam and Lake Hashenge fishery associations: northern Ethiopia. *Agriculture & Food Security*, *6*(1), 4.
74. Tigabu, Y. (2012). Fish Post Harvest Losses and Intervention Measure to Reduce Losses in Lake Hashengie, 2, 43-53.
75. Tiris, C., Tiris, M., & Dincer, I. (1995). Investigation of the thermal efficiencies of a solar dryer. *Energy conversion and management*, *36*(3), 205-212.
76. Tyagi, V. V., Pandey, A. K., Giridhar, G., Bandyopadhyay, B., Park, S. R., & Tyagi, S. K. (2012). Comparative study based on exergy analysis of solar air heater collector using thermal energy storage. *International journal of energy research*, *36*(6), 724-736.
77. Vyshak, N. R., & Jilani, G. (2007). Numerical analysis of latent heat thermal energy storage system. *Energy conversion and management*, *48*(7), 2161-2168.
78. Wang, S., & Hong, B. (2015). Optimum design of tilt angle and horizontal direction of solar collectors under Obstacle's shadow for building applications. *Journal of Building Construction and Planning Research*, *3*(2), 60-67.
79. Wang, W. W., Zhang, K., Wang, L. B., & He, Y. L. (2013). Numerical study of the heat charging and discharging characteristics of a shell-and-tube phase change heat storage unit. *Applied Thermal Engineering*, *58*(1-2), 542-553.
80. Youcef-Ali, S., Messaoudi, H., Desmons, J. Y., Abene, A., & Le Ray, M. (2001). Determination of the average coefficient of internal moisture transfer during the drying of a thin bed of potato slices. *Journal of food engineering*, *48*(2), 95-101.

APPENDIX A

Fish post-harvest loss estimation

The average fish post-harvest losses in Ethiopian lakes was estimated by interviewing fishermen at lake Ziway and based on data obtained from previous researches. Ethiopia is a country with large inland water bodies and high fish production potential. These water bodies have an estimated surface area of 7334 km^2 major lakes and reservoirs, 275 km^2 small water bodies and 7185 km long rivers and the annual fish production potential from those water bodies reaches up to 51,000 tons **(FAO, 2015).** The most commercially important fish species found in different lakes of Ethiopia are Nile tilapia (*Oreochromis niloticus*), African sharp tooth catfish (*Clarias gariepinus*), Nile perch (*Lates niloticus*), Barbs (*Barbus species*), Redbelly tilapia (*Tilapia zilli*) and Common carp (*Cyprinus carpio*) (Masresha *et al.*, 2017).

The daily fish harvesting potential of a single fisherman was estimated from both primary and secondary data sources. Primary data was collected by interviewing fishermen at lake Ziway which is one of the freshwater rift valleys of Ethiopia located 161km south of Addis Ababa. The surface area of lake Ziway is 440km^2 and its maximum depth is 8.9m. There are seven indigenous fish species in the lake comprising *Barbus paludinosus, Garra dembecha, Garra makiensis, Labeobarbus ethiopicus, Labeobarbus intermedius, Labeobarbus microterolepis* and *Oreochromis niloticus* (Golubtsov *et al.*, 2002; Getahun, 2010; Jacobus *et al.*, 2012).

Five willing groups of fishermen were asked questions about their fishing activities and the results are presented in Table A.1. Fishermen use wooden boats and nets to capture the fish. From Table A.1, it can be concluded that fishermen catch a maximum of 50 fishes and a minimum of 15 fishes per day. At times of maximum catch, 45 fishes were sold to customers during periods of high fish consumption and 30 fishes were sold during periods of low fish consumption. The remaining 5 and 20 fishes were discarded due to spoilage during high and low periods of fish consumption, respectively. The average weight of a single fish was 250g and the maximum mass of fishes discarded per day were 5kg.

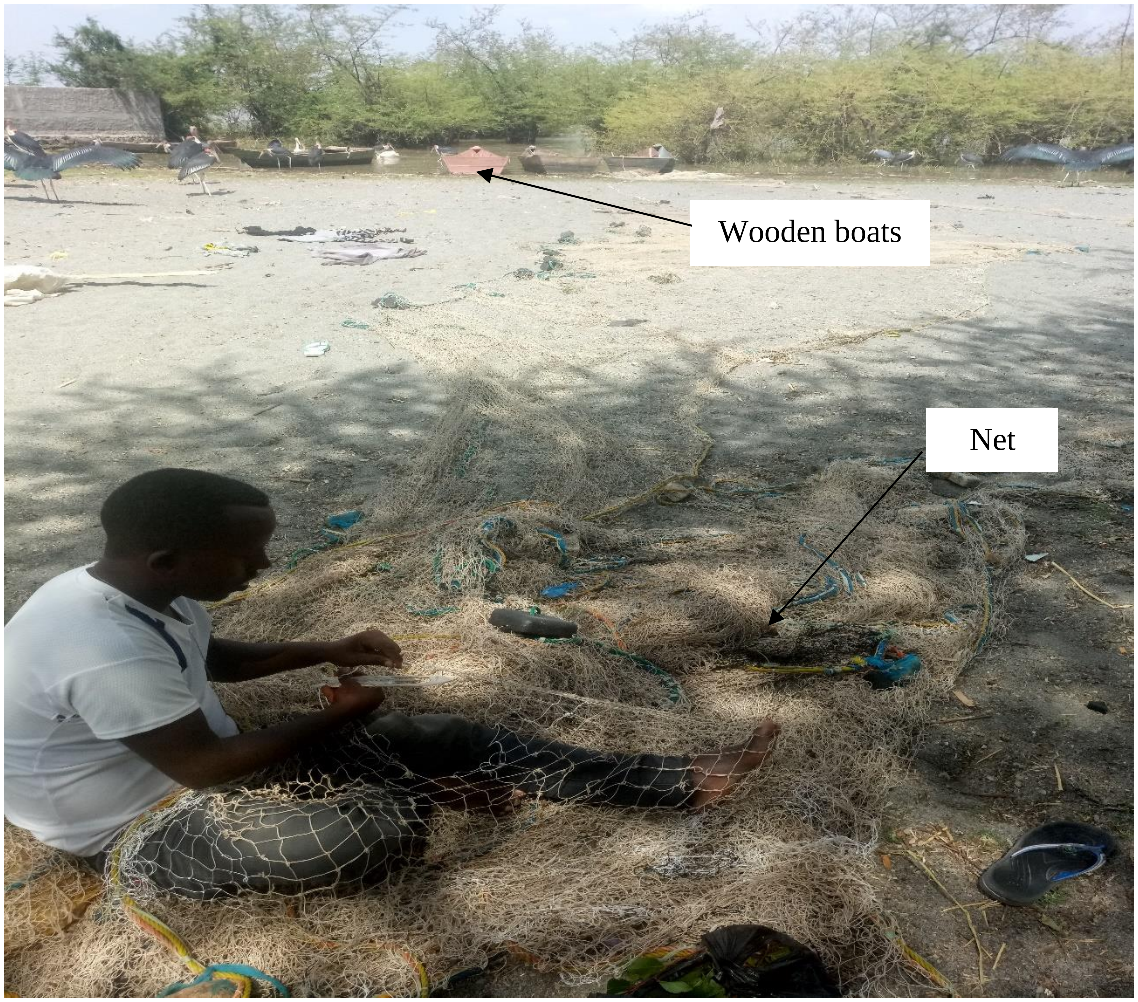

Figure A.1: Wooden boats and nets used by fishermen.

Table A.1: Post harvest losses at lake Ziway.

	Time of catch	Catch/day		Loss/day	
		Max.	Min.	Max.	Min.
Respondent 1	Morning, 5AM to 7:30AM	25	8	10	5
	Afternoon, 4:30PM to 6:30PM	20	9		
Respondent 2	Morning, 5:30AM to 7:30AM	30	10	20	10
	Afternoon, 4:30PM to 6:30PM	20	10		
Respondent 3	Morning, 5AM to 7AM	25	15	15	10
	Afternoon, 4:30PM to 6PM	25	5		
Respondent 4	Morning, 5:30AM to 7:30AM	25	10	15	5
	Afternoon, 4:30PM to 6:30PM	20	10		
Respondent 5	Morning, 5AM to 7:30AM	35	10	20	5
	Afternoon, 4:30PM to 6:30PM	15	5		

Secondary data was collected from previous researches and the results are presented in Table A.2. From Table A.2, it can be concluded that the average estimated fish catch in Ethiopia was 73 fishes per person per day. From the average 73 fish catches, the maximum number of fishes discarded were 25 and the minimum were 10 fishes per day.

Table A.2: Post harvest losses in some water bodies of Ethiopia.

Place	Catch/day		Loss/day		Reference
	Max.	Min.	Max.	Min.	
Denbi reservoir	50-60 (May-Sep.)	10-15 (Oct. and Apr.)	20	10	Mitku (2017)
Lake hayq	30	10	12	6	Tigabu (2012)
Tekeze	105	5	25	13	Solomon (2017)
Finchawa and amerti	108	25	10	-	Demeke (2015)

APPENDIX B

Design of shell and tube latent heat storage

The design of the shell and tube latent heat thermal energy storage system was done based on the procedure proposed by Shamsundar *et al*. (1992). The first step in the design process is selecting the PCM with the required melting temperature. The effectiveness is then estimated at the start of the discharging period when the PCM is completely liquid since the outlet temperature of the storage is higher at this stage than at any other time whereas at the latter instant of time there will be a buildup of solid which impedes heat transfer.

For a shell and tube latent heat thermal energy storage, effectiveness is defined as the ratio of the actual heat transfer to the heat transfer corresponding to not only infinite area but also infinite conductance in the PCM.

$$\varepsilon = \frac{T_f - T_i}{T_m - T_i} \quad \text{(B.1)}$$

Where, T_f and T_i are the outlet and inlet temperatures of air, respectively.

The number of transfer units (NTU) was expressed as:

$$\varepsilon_{max} = 1 - \exp\left(-NTU\right) \quad \text{(B.2)}$$

The minimum and maximum temperatures required for drying fish are 45℃ and 50℃, respectively. Substituting the values of T_{fmax} = 50°C, T_{fmin}=45°C, T_i=24°C and T_m=58°C into Eqn. B.1 gives ε_{max}=0.76, ε_{min}= 0.61 and NTU = 1.43.

Parameter β and Biot number B_i as a function of the inner and outer radius of the heat exchanger tubes, respectively, was determined as:

$$\beta = \frac{hR_i}{k_m} \quad \text{(B.3)}$$

$$B_i = \frac{hR_o}{k_m} \quad \text{(B.4)}$$

Where, h is convective heat transfer coefficient,

R_o and R_i are outer and inner radius of the heat exchanger tubes, respectively,

k_m is thermal conductivity of the PCM,

To estimate parameter β, the Nusselt number (Nu) should be first estimated depending upon the type of flow regime in the tube being either laminar or turbulent. If the fluid flow inside the tubes is considered as laminar and fully developed, the recommended assumption for Nu is 1.84. Nusselt number (Nu) is the ratio of convective to conductive heat transfer across the boundary.

$$N_u = \frac{hR_o}{k_a} \qquad \text{(B.5)}$$

Where, k_a is the thermal conductivity of air.

Parameter β can be written as $\beta = N_u \left(\frac{k_a}{k_m}\right)\left(\frac{R_i}{R_o}\right)$ (B.6)

Substituting the values of k_a= 0.0442W/m. K, k_m = 0.22W/m. K and N_u = 1.84 into Eqn. B.6 gives $\beta = 0.37$.

The outer radius of the tubes was determined as:

$$R_o = \left(\frac{k_m t(T_m - T_i)}{\tau_o \rho_{pf} L_{pf}}\right)^{0.5} \qquad \text{(B.7)}$$

Where, τ_o is the nondimensional time variable which was expressed as:

$$\tau_o = \left(\frac{F_o}{2\beta}\right) + \frac{1}{4}[(1 + F_o)\ln(1 + F_o) - F_o] \qquad \text{(B.8)}$$

F_o is the amount of PCM solidified at the tube inlet at the end of the discharge period and its value is usually between 0 and 10. Substituting the values of $F_o = 5.9$ and $\beta = 0.37$ into Eqn. B.8 gives $\tau_o = 9.83$ and $R_o = 8.3$mm. taking the ratio of the inner and outer radius of the tubes as 1.15, $R_i = 7.2$mm.

The number of tubes was determined from the length of the pipe as:

$$n_t = \left(\frac{NTU\dot{m}_a C_{pa}}{2\pi h R_i L}\right) \qquad \text{(B.9)}$$

h is the heat transfer coefficient of the air: $h = \frac{k_a Nu}{R_o}$ (B.10)

Substituting the values of Nu = 1.84, k_a=0.0442W/m.K, $\dot{m}_a$=0.01kg/s, C_{pa}=1.033kJ/kg.K, R_i= 7.2mm and R_o=8.3mm into Eqn. B.9 and B.10 gives n_t=5.

APPENDIX C

Thermocouple calibration

Thermocouples are sensors used to measure temperature by forming a junction between two wires of separate metals. One end of the junction is called the measurement “hot” junction and the other end is called the reference “cold” junction. When there is a temperature variation in the joint, voltage is created and this voltage can be converted into temperature with a thermocouple reference table or data logger. Thermocouples can be calibrated using a reference thermometer in a temperature calibration test by comparing both measurement values of a reference thermometer and other thermometers. The thermocouple used in this study is a K-type four channel thermocouple and a constant high temperature bath was used for the calibration. A laboratory standard thermocouple was used as a reference for the calibration and the results of the temperature measurement of both the reference and the K-type thermocouple is shown in Table C.1.

a. b.

Figure C.1: Thermocouples a) reference thermocouple (WL-362) and b) K-type thermocouple.

K-type thermocouple specifications

Serial number: HT-9815

Temperature range:0-800℃

Power supply: 9V

Weight: approx. 250g

Table C.1: Data from thermocouples during calibration.

Time	T_{w1} (WL-362) (°C)	T_{w2}(K-type thermocouple) (°C)	Uncertainty (%) $\frac{(Tw1-Tw2)}{Tw1}*100$
1	30.1	29.8	0.99668
3	35.6	35.4	0.5618
5	47.3	47.1	0.42283
7	57.1	56.8	0.52539
9	66.3	65.9	0.60332
11	72.6	72.1	0.68871
13	76.8	76.4	0.52083
15	79.8	79.5	0.37594
17	82.6	82.1	0.60533
19	84.3	83.9	0.4745
20	86.6	86.2	0.46189
22	88.1	87.8	0.34052
24	90.5	90.1	0.44199
26	91.3	90.9	0.43812
		Average uncertainty	0.53

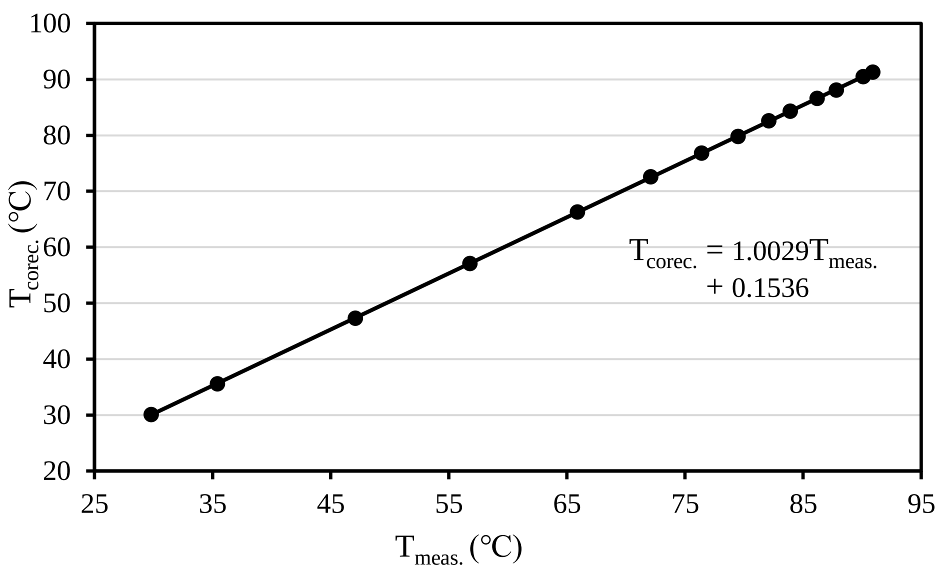

Figure C.2: Measured vs corrected temperature.